Calculation and automation of one-loop corrections to 2 to 2 fermion processes

Dissertation
zur Erlangung des Grades
Doktor der Naturwissenschaften (Dr. rer. nat.)
der Fakultät für Physik der Universität Bielefeld

vorgelegt von
Alejandro Lorca

February 18, 2005

Abstract

Complete perturbative one-loop quantum corrections for 2 to 2 fermion processes are presented. They are worked out within the electroweak standard model (EWSM) and quantum electrodynamics (QED) for typical linear collider energies.

Special attention is drawn to the organization of a fully automatic calculation of differential and integrated cross sections, where all the masses are exactly treated and soft-photon radiation is also analytically included. The computational strategy and algorithms are outlined according to the operational mode of the programs.

The first project in which I worked was an already existing FORTRAN program for top-quark production, TOPFIT, which has been upgraded [1] by reconsidering the strategy and programming of the one-loop amplitudes (see Sect. 4.2). The extension to generic fermion species $f\bar{f}$ in the final state has been completed. On a technical level, numerical stabilization and improvement of performance was observed. Dedicated comparisons were carried out for numerical agreement with the independent project FEYNARTS [2], with highly satisfactory results [3, 4]. Additionally, the main library of TOPFIT was combined with a Monte-Carlo package in order to provide the electroweak one-loop corrections to virtual top-pair decay to 6-fermions [5] .

The second project, *a*i̊TALC, has been fully developed as a LINUX package designed to automate loop calculations in two-fermion scattering processes [6] (see Sect. 4.3). Much more flexible and structured, it works on a free-based environment and partially contains existing programs: the Feynman graph generator DIANA [7] has been integrated and adapted with many new features for the specific 2 to 2 fermions case [8]. A complete one-loop utility has been written in FORM [9], in order to examine the symbolic amplitudes and push them into the numerical language FORTRAN77. For completeness, a framework for numerical computation has been created, incorporating the external LOOPTOOLS [10] package with the purpose of evaluating the loop integrals numerically. To this extent, the tests of technical precision have been excellent, saturating the available computational possibilities of standard FORTRAN compilers. *a*i̊TALC would not be very useful without the work spent on automation that, thanks to the MAKE environment, brings together the interoperability between the different modules. The final adaption to the UNIX standards of installation through AUTOCONF, licensing and documentation is also worth mentioning.

Finally, numerical applications are studied. For the final state fermion-pair we show production cross sections as well as angular distributions and asymmetries, predicted for the $e^+e^- \to t\bar{t}$, $c\bar{c}$, $b\bar{b}$, $\tau^+\tau^-$ reactions within the EWSM. Bhabha scattering ($e^+e^- \to e^+e^-$) is considered in more detail due to the increasing interest in supporting precise predictions for luminosity monitoring including necessarily the full electroweak corrections [11, 12, 13]. Other interesting fermion processes with flavour changing neutral currents ($e^+e^- \to b\bar{s}, t\bar{c}$) [14] and Møller scattering ($e^-e^- \to e^-e^-$) are also presented.

This work has become part of the European Linear Collider studies [15].

Declaration

I hereby declare that, in order to carry out my dissertation, I did not use other help or resources than those given in the Bibliography.

Alejandro Lorca

Contents

1 Introduction **1**

1.1 Motivation of the work 1

1.2 Outline 4

2 Description of the EWSM **5**

2.1 Lagrangian and bare fields 5

2.1.1 The Yang Mills Lagrangian 5

2.1.2 The fermionic piece 6

2.1.3 The Higgs Lagrangian 7

2.2 Rendering a physical model 7

2.2.1 Higgs-Kibble mechanism 7

2.2.2 Physical fields and parameters 8

2.2.3 Gauge invariance 10

2.2.4 Quantization 11

2.3 On-shell renormalization scheme 12

2.3.1 Counterterms 12

2.3.2 Renormalization conditions 14

3 Perturbative approach and radiative corrections **19**

3.1 S-matrix and scattering theory 19

3.1.1 Cross section in $2 \to 2$ processes 20

3.1.2 The matrix elements and form factors 22

3.1.3 Evaluation of the product of matrix elements 25

3.2 One-loop corrections 26

3.2.1 Opening path: from Feynman rules to numerics 27

3.2.2 Extraction of one-loop form factors 27

3.3 Bremsstrahlung contributions 29

3.3.1 Structure of the soft-photon radiation 29

3.3.2 Cancellation of infrared divergences 30

3.4 The $Z-$boson and its finite width 31

4 Computing **33**
4.1 New era in physics. The computer revolution . . . 33
4.1.1 Machine development . . . 33
4.1.2 Particle physics takes its chance . . . 34
4.2 The fortran code topfit . . . 35
4.2.1 Origin and first stage . . . 35
4.2.2 Upgrade to other fermion species . . . 35
4.3 The automated tool aitalc . . . 37
4.3.1 Introduction . . . 37
4.3.2 Technical requirements and configuration . . . 38
4.3.3 Makefile like an environmental language . . . 38
4.3.4 Feynman diagram generation: diana . . . 39
4.3.5 Algebra manipulation: library in form . . . 47
4.3.6 Getting numbers: the fortran code . . . 49
4.3.7 Examples including loop level . . . 51

5 Results **53**
5.1 Fermion-antifermion production . . . 53
5.1.1 Tree-level . . . 53
5.1.2 Loop-level . . . 55
5.1.3 Results . . . 57
5.2 Bhabha scattering . . . 66
5.2.1 In QED . . . 66
5.2.2 Within the EWSM . . . 69
5.2.3 Results . . . 70
5.3 Other $2 \to 2$ processes . . . 75
5.3.1 Møller scattering . . . 75
5.3.2 $e^+e^- \to t\bar{c}, b\bar{s}$ . . . 77

6 Conclusions and Outlook **81**

Acknowledgements **85**

A Parameters and constants **87**

B Conventions and Dirac algebra **89**
B.1 Metric and other tensors . . . 89
B.2 Dirac matrices . . . 90
B.3 Dirac equation and spinors . . . 91
B.4 Traces and contractions . . . 92
B.4.1 The problem with γ_5 . . . 93
B.4.2 Form convention . . . 93

C Dimensional regularization **95**
C.1 Wick's rotation . . . 95
C.2 The D-dimensional space . . . 97

D A_0, B_0, C_0, D_0 scalar integrals **99**
D.1 Working with A_0, B_0, C_0, D_0 integrals . . . 99
D.1.1 Definition . . . 99
D.1.2 Feynman parameters up to three-point function . . . 100
D.1.3 Compact expressions . . . 101
D.2 Calculation of A_0, B_0 and C_0 . . . 102
D.2.1 1-point function . . . 102
D.2.2 2-point function . . . 103
D.2.3 3-point function . . . 104
D.2.4 The 4-point function with complex mass . . . 107

E List of tables for aitalc **109**
E.1 Directory listing for any level . . . 109
E.2 Implemented models . . . 110
E.3 List of form procedures . . . 112
E.4 Settings for main.f . . . 115

Chapter 1

Introduction

1.1 Motivation of the work

High energy physics research tries to answer two basic questions: "what are the elementary constituents of Nature?" and "how do they interact?". Clearly, our picture of fundamental particles underwent a metamorphosis during the existence of science. The result is that we can hardly connect the original concepts and descriptions with today's knowledge and belief in quantum field theories and gauge symmetries.

The quantum theory of fields arose as the most successful framework in which we can jointly develop the quantum nature, visible at atomic scales and beyond, and the theory of special relativity. Further, the physical concepts of locality/causality and symmetry principles accommodate for the known fundamental interactions (strong, electromagnetic and weak), leaving gravity as the unique interaction still problematic to fit into a quantum formulation.

Nowadays the physics of accelerators is the only way to actively[1] perform experiments at short distances, deep inside of the nucleus structure. The analyses performed with the collected data at HERA, LEP, SLC, Tevatron and some low energy experiments excellently support the validity of the Standard Model (SM).

The combination of the many precise electroweak results have imposed strong constraints on the parameters of the model and ruled out other scenarios. An example on how important the theoretical predictions are, is pointed out by the LEP electroweak working group [16] regarding the determination of the number of neutrino species from the Z-boson width measurement ($N_\nu = 2.9841 \pm 0.0083$) and the SM value ($N_\nu = 3$): *"The theoretical error on the luminosity constitutes a large part of the uncertainties on N_ν and $\Delta\Gamma_{\text{inv}}$"*.

An equivalent observation is stated by Altarelli [17] when investigating the 3σ deviation in the precise NuTeV measurement [18] of $sin^2\theta_W$: *"There is growing evidence that the NuTeV anomaly could simply arise from an underestimation of the theoretical uncertainty in the QCD analysis needed to extract $sin^2\theta_W$."*.

Thus a deeper control of the theoretical predictions has to be worked out if we want to un-

[1] Highly energetic cosmic rays and other cosmological observations about early universe provide us also *passive* information in high energy physics.

derstand the significance of the present disagreements in N_ν, NuTeV data, $A_{\rm fb}^b$ asymmetry [16] or atomic parity violation in Cs [19].

With the advent of the next e^+e^- linear collider, the center-of-mass energies will rise up to several hundred GeV and the envisioned luminosity will be as high as 300 fb^{-1} [20]. Evidently, a new era of precision physics is approaching and hopefully new particles will be studied. The experimental precision which can be achieved at such a machine will by far exceed all current standards and will be a challenge to experimentalists and theoreticians alike.

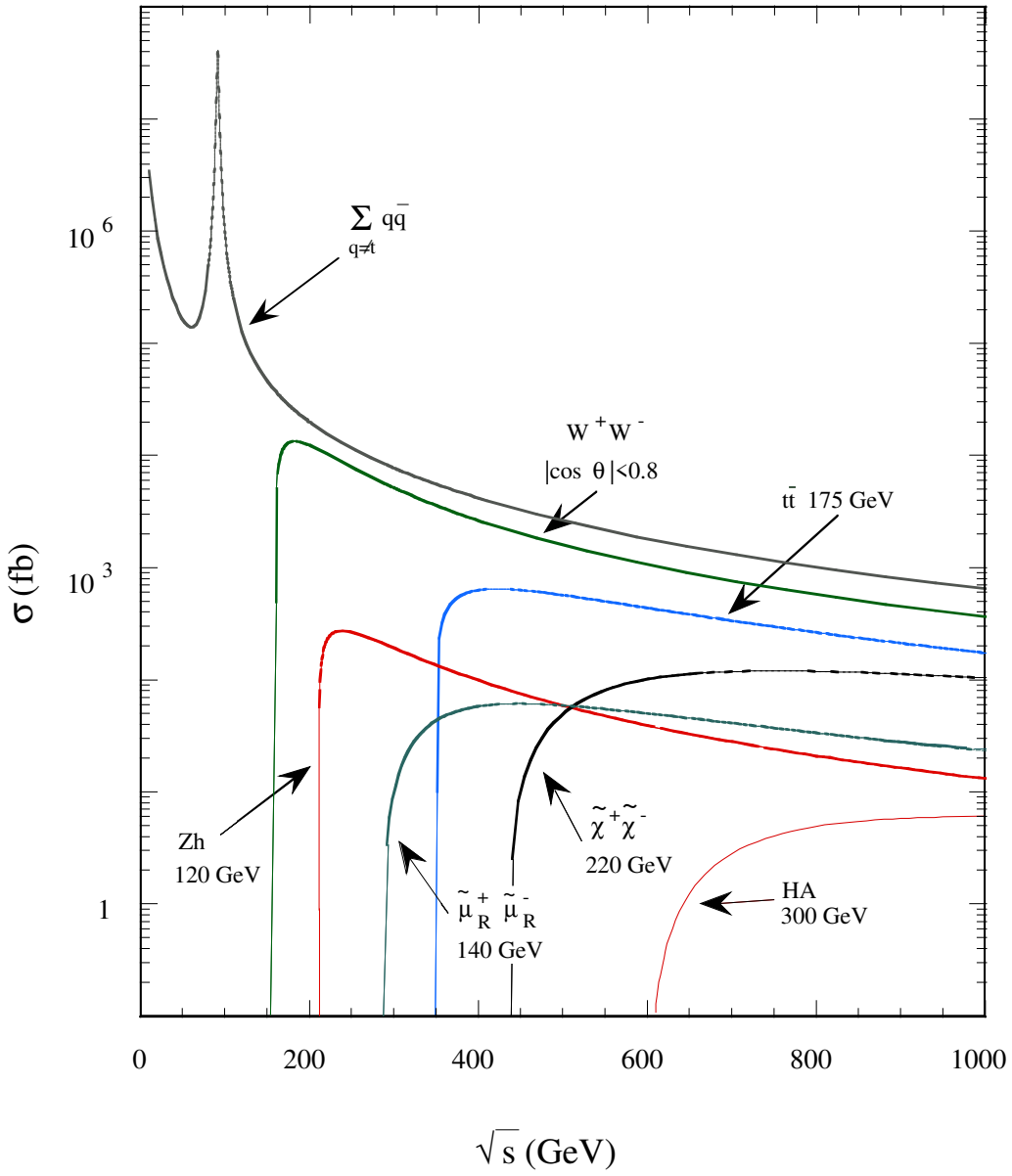

Figure 1.1: Integrated cross sections for different processes as expected for a linear collider [20].

As shown in Fig. 1.1, the expected cross sections for different production channels will be dominated by fermion-pair production. Thus it is natural to address the highest priority to the precise theoretical prediction for such processes, since they play a key role for

1. luminosity monitoring through small angle Bhabha scattering, $e^+e^- \to e^+e^-$,
2. measuring direct observables, with enough events to describe precise differential, integrated cross sections and forward-backward asymmetries,
3. establishing limits on *New Physics* as contact interaction between fermions, Z' bosons, leptoquarks, or graviton exchange in large extra dimensions,
4. quantifying backgrounds for many other processes from which we would like to extract a signal.

Based on the diagrammatic method introduced by Feynman in 1948 [21] and the smallness of the expansion parameter in terms of the coupling constant $\alpha \approx \frac{1}{137}$ in the electroweak model, the perturbative approach has been used extensively to predict physical observables. While the calculation of two-loop corrections to $2 \to 2$ fermion processes remains an open problem due to the multiple mass scales, the solution for the one-loop corrections was already worked out for the massless fermion case more than 25 years ago [22].

The methodology of Feynman diagrams is very simple and algorithmic, but tedious and susceptible to errors. In addition, the contributing diagrams grow enormously in number and complexity at every new level of the perturbation series. This is the reason why physicists have tried hard to systematize and automate the necessary steps to carry out the calculations: generation of diagrams, algebraic simplification and numerical evaluation.

Thanks to the recent progress in computer technologies and software applications, particle physics has greatly profited from an indeterminate number of tools and packages developed for the specific tasks mentioned above. In this sense we share very much the opinion expressed by other developers [23]. Globally speaking, we can state that the available calculational tools do not fulfill all our desired requirements[2]:

- Performing higher order corrections beyond leading order.
- Free-availability and free-based code (i.e. neither the tool nor its requirements have to be purchased).
- Comprehensibility, both in documentation and installation.
- Flexibility, being able to deal with different processes, theoretical models and to allow some modifications.

For this reason, a plan of the possibilities and structure of a tool that engages all the properties indicated above should be our starting point.

[2]We should allow possible recent exceptions, since there is much activity in the field as indicated in Sect. 4.1.2.

1.2 Outline

The structure of this thesis is as follows: first we review the methodology of one-loop calculations, introducing the electroweak model in Chap. 2 and the standard techniques for calculation of $O(\alpha)$ corrections in Chap. 3. In Chap. 4 we cover the major aim on a computational level, starting from the presentation of TOPFIT and following with the development of the complete tool *a*ĭTALC, with the intended characteristics lacking in other codes, and its description.

The results are presented in Chap. 5, devoted to performing mainly numerical predictions among a list of processes that will be of extreme interest for the present and future physics at colliders. Finally, conclusions are presented in Chap. 6 and a few Appendices complete the rest of the study.

Chapter 2

Description of the electroweak standard model

2.1 Approaching the model: Lagrangian and bare fields

The electroweak standard model (EWSM) was proposed in the sixties by Glashow [24], Weinberg [25] and Salam [26]. It describes the fundamental weak and electromagnetic interactions between quarks and leptons, derived from a local gauge principle with the gauge group

$$G = SU(2)_W \times U(1)_Y. \tag{2.1}$$

The classical Lagrangian of the EWSM can be split into several independent parts: the Yang-Mills part, the fermionic part and the Higgs part

$$\mathcal{L}_{\text{cl}} = \mathcal{L}_{\text{YM}} + \mathcal{L}_{\text{F}} + \mathcal{L}_{\text{H}}. \tag{2.2}$$

2.1.1 The Yang Mills Lagrangian

Gauge fields are the carriers of the electroweak interactions. They emerge as a requirement of local $SU(N)$ gauge symmetries acting on free matter. These fields consist of four vector bosons transforming under the adjoint representation of the group (2.1). The Lagrangian corresponding to the pure gauge fields is

$$\mathcal{L}_{\text{YM}} = -\frac{1}{4}\sum_{a=1}^{3}\left(\partial_\mu W_\nu^a - \partial_\nu W_\mu^a + g_2\epsilon^{abc}W_\mu^b W_\nu^c\right)^2 - \frac{1}{4}\left(\partial_\mu B_\nu - \partial_\nu B_\mu\right)^2. \tag{2.3}$$

where ϵ^{abc} represents the totally antisymmetric structure constants of the $SU(2)$ group, and the sum extends over the $2^2 - 1$ generators of the group.

A very useful construction is the *covariant derivative* since it provides the gauge interaction with the matter fields. It exhibits the non-simple nature of the group in terms of the two different

coupling constants, both for the weak hypercharge $U(1)_Y$ the and weak isospin $SU(2)_W$ group, g_1 and g_2 respectively:

$$D_\mu = \partial_\mu - \mathrm{i}g_2 \sum_{a=1}^{3} I_W^a W_\mu^a + \mathrm{i}g_1 \frac{Y_W}{2} B_\mu, \tag{2.4}$$

where I_W^a stands for the three generators of weak isospin and Y_W for the one of weak hypercharge. Then, the electric charge operator is defined via the Gell-Mann–Nishijima relation as

$$Q = I_W^3 + \frac{Y_W}{2}. \tag{2.5}$$

2.1.2 The fermionic piece

The matter fields which build up our world are associated with massless spin $\frac{1}{2}$ particles: leptons and coloured quarks. Left-handed fermions are grouped into doublets $\Psi_i'^L = (\psi_{i,+}'^L, \psi_{i,-}'^L)$ and right-handed fermions into singlets $\psi_i'^R$, according to the fundamental two-dimensional and one-dimensional representations of the $SU(2)_W$ group, respectively. A set of representation matrices for the doublets are connected with the Pauli matrices while the trivial representation stands for the singlets:

$$I_W^a = \frac{\tau^a}{2} \quad \text{for doublets,} \qquad I_W^a = 0 \quad \text{for singlets.} \tag{2.6}$$

The weak hypercharge Y_W of the fermions is fixed by imposing the correct charge in Eq. (2.5). For the fermions, the weak electroweak quantum numbers are given in Table 2.1.

	Doublets_L				Singlets_R			
	leptons		quarks		leptons		quarks	
	ν_L	l_L	u_L	d_L'	ν_R	l_R	u_R	d_R
I_W^3	$\frac{1}{2}$	$-\frac{1}{2}$	$\frac{1}{2}$	$-\frac{1}{2}$	0	0	0	0
Y_W	-1	-1	$\frac{1}{3}$	$\frac{1}{3}$	0	-2	$\frac{4}{3}$	$-\frac{2}{3}$
Q	0	-1	$\frac{2}{3}$	$-\frac{1}{3}$	0	-1	$\frac{2}{3}$	$-\frac{1}{3}$

Table 2.1: Fermions in the electroweak standard model and their quantum numbers. Neutrinos (ν_e,ν_μ,ν_τ) are represented by ν, negatively charged leptons (e^-,μ^-,τ^-) by l, up-type coloured quarks ($u_{r,g,b}$,$c_{r,g,b}$,$t_{r,g,b}$) by u and down-type ones ($d_{r,g,b}$,$s_{r,g,b}$,$b_{r,g,b}$) by d, which when primed represent the CKM rotated fields. Note that right-handed neutrinos are absent or have all quantum numbers zero in this model.

The Lagrangian reads

$$\mathcal{L}_\mathrm{F} = \sum_i \bar{\Psi}_i'^L \mathrm{i} \not{D} \Psi_i'^L + \sum_{i,\sigma} \bar{\psi}_{i,\sigma}'^R \mathrm{i} \not{D} \psi_{i,\sigma}'^R, \tag{2.7}$$

the sum over i standing for the collection of the three generations and σ for the two distinct isospin components and $\not{D} \equiv \gamma^\mu D_\mu$.

Note that so far we did not mention at all the property 'mass'. In the unbroken phase the theory is chiral and terms proportional to $\bar{\psi}\psi$ are strictly forbidden since they do not respect the group invariance.

2.1.3 The Higgs Lagrangian

The Higgs sector is required in order to allow for massive particles, thus breaking the chiral symmetry but preserving the $U(1)_{\text{em}}$ symmetry. The simplest choice consists of a complex $SU(2)_W$ doublet

$$\Phi = \begin{pmatrix} \phi^+ \\ \phi^0 \end{pmatrix}, \tag{2.8}$$

with weak hypercharge $Y_W = 1$. The Higgs field couples to the gauge fields and has also a self-coupling, resulting in the following Lagrangian:

$$\begin{aligned} \mathcal{L}_{\text{H}} &= \left(D_\mu \Phi\right)^\dagger \left(D^\mu \Phi\right) - \frac{\lambda}{4}(\Phi^\dagger \Phi)^2 + \mu^2 \Phi^\dagger \Phi \\ &\quad + \sum_{i,j} \left(g^-_{ij} \bar{\Psi}^L_i \psi^R_{j,-} \Phi + g^+_{ij} \bar{\Psi}^L_i \psi^R_{j,+} \Phi^c + \text{h.c.} \right), \end{aligned} \tag{2.9}$$

where the two terms in the Higgs potential $\lambda, \mu > 0$ and the second line describes the Yukawa couplings. Φ^c is the charge conjugate Higgs field

$$\Phi^c = \mathrm{i}\tau^2 \Phi^* = \begin{pmatrix} \phi^{0*} \\ -\phi^- \end{pmatrix}. \tag{2.10}$$

It should be stressed that fermionic fields appearing in Eq. (2.9) represent the mass eigenstates and not necessarily those of the electroweak interaction, which were denoted in Eq. (2.7) with a primed symbol. The rotation of the fields, once we choose the representatives for the field states, fixes the number of free parameters in the model. They are connected with the 17 free physical parameters in the on-shell scheme: 1 for the charge e, 3 for the boson masses m_Z, m_W, m_H, 9 for the fermion masses m_{f_i} and extra 4 for the parameters (3 angles plus 1 phase) in the 3×3 CKM matrix.

2.2 Rendering a physical model

2.2.1 Higgs-Kibble mechanism

The previous Lagrangian has been depicted in terms of bare quantities and even if the origin of spontaneous symmetry breaking was already introduced, no trace was seen about how this mechanism brings explicitly the mass terms for the gauge bosons. Let us see in this subsection how it works.

In Eq. (2.9), the terms λ, μ were chosen positive definite. One can see that this choice leads to a non-trivial minimum for the Higgs potential:

$$V(\Phi_{\min}) \equiv \frac{\lambda}{4}\Big(|\Phi_{\min}|^2\Big)^2 - \mu^2|\Phi_{\min}|^2 = -\frac{\mu^4}{\lambda}, \tag{2.11}$$

being satisfied with

$$|\Phi_{\min}|^2 = \frac{2\mu^2}{\lambda} = \frac{v^2}{2} \neq 0. \tag{2.12}$$

Still, the field doublet has three degrees of freedom. We can pick up a doublet of zero charge when applying Eq. (2.5) on it:

$$Q\Phi_0 = \left(\frac{\tau^3}{2} + \frac{Y_\Phi}{2}\right)\begin{pmatrix}\phi^+\\ \phi^0\end{pmatrix} = 0 \qquad \Rightarrow \qquad \phi^+ = 0, \tag{2.13}$$

and of course, both Eq. (2.12) and Eq. (2.13) are satisfied only up to a phase by a doublet that will be considered as the ground state

$$\Phi_0 = \begin{pmatrix}0\\ \frac{1}{\sqrt{2}}v\end{pmatrix}, \tag{2.14}$$

from which the Lagrangian is expanded in terms of the Higgs field (H) and the unphysical "would-be Goldstone bosons" ($\chi, \phi^\pm$)

$$\Phi = \begin{pmatrix}\phi^+\\ \frac{1}{\sqrt{2}}(v + H + \mathrm{i}\chi)\end{pmatrix}. \tag{2.15}$$

2.2.2 Physical fields and parameters

In the real world we find that the symmetry $SU(2)_W \times U(1)_Y$ has been broken into $U(1)_{\text{em}}$ and the physical particles acquire some mass, so we must identify the physical fields of the given theory. Soon we realize that the bosons mediating weak interactions should be massive, since their interactions are short ranged.

Under the previous assumptions on the Higgs mechanism, it is possible to rearrange the fields by introducing Eq. (2.15) into the Lagrangian Eq. (2.9). A key point is that the vacuum expectation value v induces some couplings of dimension mass.

The diagonalization of the mass matrices involves the known physical gauge boson and fermion fields. For the gauge bosons it suffices to check

$$\begin{aligned}\Delta\mathcal{L} &= \begin{pmatrix}0 & \frac{1}{\sqrt{2}}v\end{pmatrix}\left(g_2\frac{\tau^a}{2}W^a_\mu - g_1\frac{Y_\Phi}{2}B_\mu\right)\left(g_2\frac{\tau^b}{2}W^{b\mu} - g_1\frac{Y_\Phi}{2}B^\mu\right)\begin{pmatrix}0\\ \frac{1}{\sqrt{2}}v\end{pmatrix}\\ &= \frac{v^2}{8}\left(g_2^2(W^1_\mu)^2 + g_2^2(W^2_\mu)^2 + \Big(g_2W^3_\mu + g_1B_\mu\Big)^2\right),\end{aligned} \tag{2.16}$$

from which we can read off the masses (after diagonalization)

$$m_W = \frac{g_2}{2}v. \tag{2.17}$$

$$m_Z = \frac{\sqrt{g_1^2+g_2^2}}{2}v, \tag{2.18}$$

$$m_\gamma = 0, \tag{2.19}$$

Note that owing to the remaining $U(1)_{\rm em}$ symmetry, the mass matrix for the neutral gauge boson possesses a vanishing eigenvalue, representing the massless photon.

After the breaking we are left only with one good quantum number Q. Let us examine the charges of the gauge bosons: for the fields W_μ^a, owing to their vanishing hypercharge $Y_W = 0$, we get immediately the charge as the eigenvalues for the weak isospin operator I_W^3 in the adjoint representation ($\frac{\tau^3}{2}$ of Pauli matrices in B.17). With the help of the $SU(2)$ algebra we find

$$W_\mu^\pm = \frac{1}{\sqrt{2}}\left(W_\mu^1 \mp \mathrm{i}W_\mu^2\right), \tag{2.20}$$

$$\begin{pmatrix} Z_\mu \\ A_\mu \end{pmatrix} = \begin{pmatrix} c_{\rm W} & s_{\rm W} \\ -s_{\rm W} & c_{\rm W} \end{pmatrix}\begin{pmatrix} W_\mu^3 \\ B_\mu \end{pmatrix}. \tag{2.21}$$

and the definition of the weak mixing angle[1] $\theta_{\rm W}$

$$c_{\rm W} \equiv \cos\theta_{\rm W} = \frac{g_2}{\sqrt{g_1^2+g_2^2}}, \tag{2.22}$$

$$s_{\rm W} \equiv \sin\theta_{\rm W} = \frac{g_1}{\sqrt{g_1^2+g_2^2}}. \tag{2.23}$$

The rest of the mass identifications for the matter fields reads

$$m_{f,i} = \frac{1}{\sqrt{2}}U_{ij}^{f,L}g_{jk}^f U_{ki}^{f,R^\dagger}v, \tag{2.24}$$

$$m_H = \sqrt{2}\mu, \tag{2.25}$$

with the following physical fermion eigenvectors

$$f_i^L = U_{ij}^{f,L}f'^L_j, \tag{2.26}$$

$$f_i^R = U_{ij}^{f,R}f'^R_j. \tag{2.27}$$

In the quark sector, regarding the charged current for the weak interactions, an extra definition enters, relating the mass eigenstates of the distinct flavours with the eigenstates of the weak interaction. Defining the unitary quark-mixing matrix $\mathbf{V}$ as

$$V_{ij} \equiv U_{ik}^{u,L}U_{kj}^{d,L^\dagger}, \tag{2.28}$$

[1] Also called Weinberg angle.

it forms the charged current for hadrons [27,28] present on the vertex interaction between quarks and charged bosons

$$h_\mu^+ = \begin{pmatrix} \bar{u} & \bar{c} & \bar{t} \end{pmatrix} \gamma_\mu \frac{1}{2}(\mathbb{1} - \gamma_5) \begin{pmatrix} V_{ud} & V_{cd} & V_{td} \\ V_{us} & V_{cs} & V_{ts} \\ V_{ub} & V_{cb} & V_{tb} \end{pmatrix} \begin{pmatrix} d \\ s \\ b \end{pmatrix}. \tag{2.29}$$

For the neutral currents, the construction remains diagonal avoiding the flavour changing effect at tree-level.

Is interesting to rewrite finally the covariant derivative Eq. (2.4) in terms of the new mass eigenstates Eq. (2.20) and Eq. (2.21)

$$D_\mu = \partial_\mu - \mathrm{i}\frac{g_2}{\sqrt{2}}\left(W_\mu^+ I_W^+ + W_\mu^- I_W^-\right) - \mathrm{i}\frac{1}{\sqrt{g_2^2 + g_1^2}} Z_\mu \left(g_2^2 I_W^3 - g_1^2 \frac{Y_W}{2}\right) + \mathrm{i}\frac{g_2 g_1}{\sqrt{g_2^2 + g_1^2}} A_\mu \left(I_W^3 + \frac{Y_W}{2}\right). \tag{2.30}$$

with $I_W^\pm = I_W^1 \pm \mathrm{i} I_W^2$. Thus an identification of the last term with the electromagnetic coupling (e) in QED is straightforward,

$$\sqrt{4\pi\alpha} \equiv e = \frac{g_2 g_1}{\sqrt{g_2^2 + g_1^2}}, \tag{2.31}$$

and finally reparametrizes the interaction in terms of the two well-measured couplings e and $sin^2\theta_W$.

2.2.3 Gauge invariance

The Lagrangian (2.2) is invariant under the following infinitesimal transformation of fields [29]

$$W_\mu^a(x) \rightarrow W_\mu^a(x) + \frac{1}{g_2}\partial_\mu \delta\theta^a(x) + \epsilon^{abc} W_\mu^b(x) \delta\theta^c(x), \tag{2.32}$$

$$B_\mu(x) \rightarrow B_\mu(x) + \frac{1}{g_1}\partial_\mu \delta\theta^Y(x), \tag{2.33}$$

$$\Phi(x) \rightarrow \left(1 - \mathrm{i}\frac{1}{2}\delta\theta^Y(x) + \mathrm{i}\frac{\tau^a}{2}\delta\theta^a(x)\right)\Phi(x), \tag{2.34}$$

$$\Psi'^L_i(x) \rightarrow \left(1 - \mathrm{i}\frac{Y_i^L}{2}\delta\theta^Y(x) + \mathrm{i}\frac{\tau^a}{2}\delta\theta^a(x)\right)\Psi'^L_i(x), \tag{2.35}$$

$$\psi'^R_{i,\sigma}(x) \rightarrow \left(1 - \mathrm{i}\frac{Y_{i,\sigma}^R}{2}\delta\theta^Y(x)\right)\psi'^R_{i,\sigma}(x). \tag{2.36}$$

where θ^Y and θ^a are the parameters of the local gauge transformations corresponding to the groups $U(1)_Y$ and $SU(2)_W$, respectively.

We can equivalently write Eqs. (2.32–2.36) in terms of the physical fields and parameters introduced already in Sect. 2.2.2:

$$\begin{aligned}
W_\mu^\pm &\to W_\mu^\pm + \partial_\mu \delta\theta^\pm \\
&\quad \mp \mathrm{i}e\tfrac{1}{s_\mathrm{W}}\Big(W_\mu^\pm\left(s_\mathrm{W}\delta\theta^A - c_\mathrm{W}\delta\theta^Z\right) - \left(s_\mathrm{W}A_\mu - c_\mathrm{W}Z_\mu\right)\delta\theta^\pm\Big), && (2.37)\\
Z_\mu &\to Z_\mu + \partial_\mu\delta\theta^Z - \mathrm{i}e\tfrac{c_\mathrm{W}}{s_\mathrm{W}}\left(W_\mu^+\delta\theta^- - W_\mu^-\delta\theta^+\right), && (2.38)\\
A_\mu &\to A_\mu + \partial_\mu\delta\theta^A + \mathrm{i}e\left(W_\mu^+\delta\theta^- - W_\mu^-\delta\theta^+\right), && (2.39)\\
H &\to H + e\tfrac{1}{2s_\mathrm{W}c_\mathrm{W}}\chi\delta\theta^Z + \mathrm{i}e\tfrac{1}{2s_\mathrm{W}}\Big(\phi^+\delta\theta^- - \phi^-\delta\theta^+\Big), && (2.40)\\
\chi &\to \chi - e\tfrac{1}{2s_\mathrm{W}c_\mathrm{W}}(v+H)\delta\theta^Z + e\tfrac{1}{2s_\mathrm{W}}\Big(\phi^+\delta\theta^- - \phi^-\delta\theta^+\Big), && (2.41)\\
\phi^\pm &\to \phi^\pm \mp \mathrm{i}e\phi^\pm\Big(\delta\theta^A + \tfrac{s_\mathrm{W}^2 - c_\mathrm{W}^2}{2s_\mathrm{W}c_\mathrm{W}}\delta\theta^Z\Big) \pm \mathrm{i}e\tfrac{1}{2s_\mathrm{W}}(v+H\pm\chi)\delta\theta^\pm, && (2.42)\\
\psi_{i,\pm}^L &\to \psi_{i,\pm}^L - \mathrm{i}e\Big(q_{i,\pm}\delta\theta^A + \tfrac{s_\mathrm{W}}{c_\mathrm{W}}(q_{i,\pm} \mp \tfrac{1}{2s_\mathrm{W}^2})\delta\theta^Z\Big)\psi_{i,\pm}^L \\
&\quad + \mathrm{i}e\tfrac{1}{\sqrt{2}s_\mathrm{W}}\delta\theta^\pm v_{ij}^\pm \psi_{j,\mp}^L, && (2.43)\\
\psi_{i,\pm}^R &\to \psi_{i,\pm}^R - \mathrm{i}eq_{i,\pm}\Big(\delta\theta^A + \tfrac{s_\mathrm{W}}{c_\mathrm{W}}\delta\theta^Z\Big)\psi_{i,\pm}^R, && (2.44)
\end{aligned}$$

where we have used the definitions of

$$\begin{aligned}
\delta\theta^\pm &= \frac{1}{g_2}\left(\delta\theta^1 \mp \mathrm{i}\delta\theta^2\right), && (2.45)\\
\delta\theta^Z &= \frac{1}{g_1}s_\mathrm{W}\delta\theta^Y + \frac{1}{g_2}c_\mathrm{W}\delta\theta^3, && (2.46)\\
\delta\theta^A &= \frac{1}{g_1}c_\mathrm{W}\delta\theta^Y - \frac{1}{g_2}s_\mathrm{W}\delta\theta^3. && (2.47)
\end{aligned}$$

2.2.4 Quantization

Instead of quantizing the EWSM by incorporating Heisenberg commutation relations to the classical Hamiltonian, the quantization using Feynman's path integral approach brings some advantages: Lorentz invariance manifestly remains throughout the procedure (time does not play a predominant role as in the Hamiltonian), and the elimination of the unphysical degrees of freedom becomes very elegant thanks to the Faddeev-Popov method [30].

The procedure requires a new fixing Lagrangian term and an extra piece formed out of local Grassmann variables u^a and $\bar{u}^a$, known as the Faddeev-Popov ghosts,

$$\mathcal{L}_\mathrm{q} = \mathcal{L}_\mathrm{cl} + \mathcal{L}_\mathrm{fix} + \mathcal{L}_\mathrm{FP}, \tag{2.48}$$

with

$$\begin{aligned}
\mathcal{L}_\mathrm{fix} &= -\frac{1}{2\xi^A}(F^A)^2 - \frac{1}{2\xi^Z}(F^Z)^2 - \frac{1}{\xi^W}F^+F^-, && (2.49)\\
\mathcal{L}_\mathrm{FP} &= \bar{u}^\alpha(x)\frac{1}{\sqrt{\xi^\alpha}}\frac{\delta F^\alpha}{\delta\theta^\beta(x)}u^\beta(x), && (2.50)
\end{aligned}$$

the index α accounting for the different gauge fields ($\alpha = \pm, Z, A$) and F^α given by

$$F^\pm = \partial^\mu W^\pm_\mu \mp \mathrm{i} m_W \xi'^W \phi^\pm, \tag{2.51}$$

$$F^Z = \partial^\mu Z_\mu - m_Z \xi'^Z \chi, \tag{2.52}$$

$$F^A = \partial^\mu A_\mu. \tag{2.53}$$

There are several possibilities to pick up an explicit set of gauge parameters. We will use the choice

$$\xi'^\alpha = \xi^\alpha = 1, \tag{2.54}$$

which is the so-called *'t Hooft–Feynman gauge*. It greatly simplifies the perturbative calculations, since the longitudinal and transverse parts of the gauge-boson propagators coincide and the unphysical fields develop masses equal to the corresponding physical ones.

2.3 On-shell renormalization scheme

Renormalization of gauge theories is a difficult concept. Sketched in the seventies by Lee, Zinn-Justin [31, 32], Veltman and 't Hooft [33] it was proven to be adequate for gauge theories with spontaneous symmetry breaking [34, 35].

The idea behind the renormalization is to remove infinities by reparametrization of the original couplings and fields in the Lagrangian in terms of physical observables. This is required in quantum theories due to the fact that quantum corrections destroy the original relation between the parameters of the theory at tree-level and physical measurements.

There are several renormalization schemes that have been proposed. *MS* [36], $\overline{MS}$ [37], *star* [22,38], and *on-shell* [39,40,41,42,43,44] are some remarkable examples and they basically differ in the explicit input set of parameters used as physical reference. They all should provide the same answer for a physical prediction but, for a given order of perturbation theory, their answers differ by higher order contributions.

Here we adopt the on-shell renormalization scheme whose main ingredients are:

- use as input the masses of physical particles, the electron charge and the couplings of quark mixing matrix (this is of course very practical in explicit calculations), $m_W, m_Z, m_H, m_{f,i}, e, V_{ij}$,
- express the bare parameters and fields in terms of renormalized ones plus counterterms,
- establish the renormalization conditions in order to evaluate the finite parts of the counterterms.

2.3.1 Counterterms

In the following we are going to provide the explicit form for the counterterms, giving a flavour about how the renormalization procedure introduces new elements in the Lagrangian. A common

way to redefine the bare quantities is the multiplicative prescription, and the original Lagrangian from Eq. (2.48) gets a new form

$$\mathcal{L}(g,\Phi) = \mathcal{L}(Z_g g, Z_\Phi^{\frac{1}{2}}\Phi), \tag{2.55}$$

where the replacement is done on every parameter and field

$$g \to Z_g g, \qquad \Phi \to Z_\Phi^{\frac{1}{2}}\Phi. \tag{2.56}$$

In a perturbative fashion, the relations (2.56) between bare and physical quantities can be rewritten up to first order as

$$g_0 = \left(1+\delta Z_g\right) g, \qquad \Phi_0 = \left(1+\delta Z_\Phi^{\frac{1}{2}}\right)\Phi, \tag{2.57}$$

leading to the following standard structure for the Lagrangian:

$$\mathcal{L}(g_0,\Phi_0) = \mathcal{L}(g,\Phi) + \mathcal{L}_{\rm ct}(g,\Phi; Z_g, Z_\Phi^{\frac{1}{2}}). \tag{2.58}$$

The fact that we can reexpress the original bare Lagrangian in terms of a physical one plus a counterterm piece is a tremendous advantage. The physical one retains the same structure as the bare Lagrangian, so the whole set of Feynman rules are the same for both, and the counterterms play only a role through the so-called counterterm Lagrangian that contributes cancelling the ultraviolet divergences.

For the specific parameters of the electroweak Lagrangian, we have

$$\begin{aligned}
e_0 &= (1+\delta Z_e)e, && (2.59)\\
m^2_{W,0} &= m^2_W + \delta m^2_W, && (2.60)\\
m^2_{Z,0} &= m^2_Z + \delta m^2_Z, && (2.61)\\
m^2_{H,0} &= m^2_H + \delta m^2_H, && (2.62)\\
m^2_{f,i,0} &= m^2_{f,i} + \delta m^2_{f,i}, && (2.63)\\
V_{ij,0} &= V_{ij} + \delta V_{ij}, && (2.64)
\end{aligned}$$

and for the wave function renormalization

$$\begin{aligned}
W_0^\pm &= Z_W^{\frac{1}{2}} W^\pm = \left(1+\frac{1}{2}\delta Z_W\right) W^\pm, && (2.65)\\
\begin{pmatrix} Z_0 \\ A_0 \end{pmatrix} &= \begin{pmatrix} Z_{ZZ}^{\frac{1}{2}} & Z_{ZA}^{\frac{1}{2}} \\ Z_{AZ}^{\frac{1}{2}} & Z_{AA}^{\frac{1}{2}} \end{pmatrix}\begin{pmatrix} Z \\ A \end{pmatrix} = \begin{pmatrix} (1+\frac{1}{2}\delta ZZ) & \frac{1}{2}\delta Z_{ZA} \\ \frac{1}{2}\delta Z_{AZ} & (1+\frac{1}{2}\delta Z_{AA}) \end{pmatrix}\begin{pmatrix} Z \\ A \end{pmatrix}, && (2.66)\\
H_0^\pm &= Z_H^{\frac{1}{2}} H = \left(1+\frac{1}{2}\delta Z_H\right) H, && (2.67)\\
f^L_{i,0} &= Z_{ij}^{\frac{1}{2},f,L} f^L_j = \left(\delta_{ij}+\frac{1}{2}\delta Z_{ij}^{f,L}\right) f^L_j, && (2.68)\\
f^R_{i,0} &= Z_{ij}^{\frac{1}{2},f,R} f^R_j = \left(\delta_{ij}+\frac{1}{2}\delta Z_{ij}^{f,R}\right) f^R_j. && (2.69)
\end{aligned}$$

In the 't Hooft–Feynman gauge, the poles of the "would-be Goldstone" propagators ($\phi^{\pm}, \chi$) coincide with those of the physical sector ($W^{\pm}, Z$).

When inserting the above transformations (2.59–2.69) into Eq. (2.48), we get an expression with the form of Eq. (2.58). From there we can work out the Feynman rules. We will show next, how the counterterms are fixed and get their values. Otherwise the new parametrization would not have a direct physical meaning.

2.3.2 Renormalization conditions

The presented counterterms get their values by imposing renormalization conditions. In the on-shell scheme it has become customary to match the pole masses of the gauge bosons, Higgs boson and fermions with the corresponding physical masses. The electric charge is fixed by equaling the one measured in the Thomson limit.

There is also a second kind of renormalization conditions which have to do with the field counterterms. They allow to render physical fields finite, and a smart choice implies many simplifications on the specific form of the conditions for the physical parameters, apart from eliminating the wave-function renormalization for the external fields.

Conditions on Green Functions

Let us assume we have the following renormalized[2] one-particle irreducible components of the Green functions, that intuitively mean the inverse of the propagator

$\hat{\Gamma}^{VV'}_{\mu\nu}(p)$ = 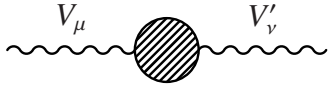

$= -\delta_{VV'} g_{\mu\nu}(p^2 - m_V^2)$

$$-\left(g_{\mu\nu} - \frac{p_\mu p_\nu}{p^2}\right)\hat{\Sigma}_T^{VV'}(p^2) - \frac{p_\mu p_\nu}{p^2}\hat{\Sigma}_L^{VV'}(p^2), \tag{2.70}$$

$\hat{\Gamma}^{HH}(p)$ = 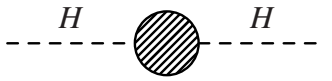

$= -(p^2 - m_H^2) + \hat{\Sigma}^{HH}(p^2),$ (2.71)

$\hat{\Gamma}^{f\bar{f}}_{ij}(p)$ = 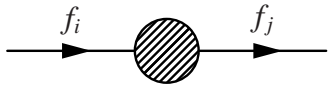

$= -\delta(\not{p} - m_{f,i})$

$$+\Big(\not{p}\mathbb{P}_L\hat{\Sigma}^{f,L}_{ij}(p^2) + \not{p}\mathbb{P}_R\hat{\Sigma}^{f,R}_{ij}(p^2) + m_{f,i}\mathbb{P}_L\hat{\Sigma}^{f,l}_{ij}(p^2) + m_{f,j}\mathbb{P}_R\hat{\Sigma}^{f,r}_{ij}(p^2)\Big), \tag{2.72}$$

with $VV' = WW, ZZ, ZA, AZ, AA$.

[2]From now on, we will denote with a hat (ˆ) to the renormalized quantities, in comparison to the unrenormalized ones (naked).

At this point we can then write the different conditions for the on-shell fields,

$$\mathfrak{Re}\,\hat{\Gamma}^{VV'}_{\mu\nu}(p)\varepsilon^{\nu}(p)\Big|_{p^2=m_V^2} = 0, \tag{2.73}$$

$$\mathfrak{Re}\,\hat{\Gamma}^{HH}(p)\Big|_{p^2=m_H^2} = 0, \tag{2.74}$$

$$\mathfrak{Re}\,\hat{\Gamma}^{f\bar{f}}_{ij}(p)u_j(p)\Big|_{p^2=m_{f,j}^2} = 0, \tag{2.75}$$

$$\lim_{p^2\to m_V^2}\frac{1}{p^2-m_V^2}\mathfrak{Re}\,\hat{\Gamma}^{VV'}_{\mu\nu}(p)\varepsilon^{\nu}(p) = -\varepsilon_{\mu}(p), \tag{2.76}$$

$$\lim_{p^2\to m_H^2}\frac{1}{p^2-m_H^2}\mathfrak{Re}\,\hat{\Gamma}^{HH}(p) = 1, \tag{2.77}$$

$$\lim_{p^2\to m_{f,i}^2}\frac{\not{p}+m_{f,i}}{p^2-m_{f,i}^2}\mathfrak{Re}\,\hat{\Gamma}^{f\bar{f}}_{ii}(p)u_i(p) = u_i(p), \tag{2.78}$$

where the vector fields are represented by the polarization vector ε^{μ} and the spin-$\frac{1}{2}$ fields by the spinors in momentum space u_i.

Tadpole renormalization

The definition of the *tadpole* is related to the vacuum expectation value v

$$t \equiv v\left(\mu^2 - \frac{1}{4}\lambda v^2\right). \tag{2.79}$$

We renormalize the one-point amputated renormalized Green function $\hat{\Gamma}$ for the Higgs field

$\hat{\Gamma}^H$ = 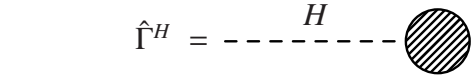 : $\delta t = -\Gamma^H(0)$ (2.80)

in terms of a tadpole counterterm. The advantage in doing so instead of renormalizing v is that there is no need to consider such diagrams in actual calculations.

Mass renormalization

For the mass counterterms recalling that the real parts of the poles given by the corresponding propagators equal the physical masses:

$$\delta m_W^2 = \mathfrak{Re}\,\Sigma_T^{WW}(m_W^2), \tag{2.81}$$

$$\delta m_Z^2 = \mathfrak{Re}\,\Sigma_T^{ZZ}(m_Z^2), \tag{2.82}$$

$$\delta m_H^2 = \mathfrak{Re}\,\Sigma^{H}(m_H^2), \tag{2.83}$$

$$\delta m_{f,i}^2 = \frac{m_{f,i}}{2}\mathfrak{Re}\left(\Sigma_{ii}^{f,L}(m_{f,i}^2) + \Sigma_{ii}^{f,R}(m_{f,i}^2) + \Sigma_{ii}^{f,l}(m_{f,i}^2) + \Sigma_{ii}^{f,r}(m_{f,i}^2)\right), \tag{2.84}$$

Σ being the unrenormalized self-energies and $\mathfrak{Re}$ indicating the real part.

Field renormalization

For the boson fields we have the following relations

$$\delta Z_{VV} = -\,\Re\mathrm{e}\,\frac{\partial\Sigma_T^{VV}}{\partial p^2}\bigg|_{p^2=m_V^2} \qquad (\text{for } V=W,Z,A), \tag{2.85}$$

$$\delta Z_{AZ} = -2\Re\mathrm{e}\,\frac{\Sigma_T^{AZ}(m_Z^2)}{m_Z^2}, \qquad \delta Z_{ZA} = 2\Re\mathrm{e}\,\frac{\Sigma_T^{AZ}(0)}{m_Z^2}, \tag{2.86}$$

$$\delta Z_H = -\,\Re\mathrm{e}\,\frac{\partial\Sigma_T^{H}}{\partial p^2}\bigg|_{p^2=M_H^2}, \tag{2.87}$$

$$\delta Z_{ii}^{f,Q} = -\Re\mathrm{e}\,\Sigma_{ii}^{f,Q}(m_{f,i}^2) - m_{f,i}^2\frac{\partial}{\partial p^2}\Re\mathrm{e}\,\left(\Sigma_{ii}^{f,L}+\Sigma_{ii}^{f,R}+\Sigma_{ii}^{f,l}+\Sigma_{ii}^{f,r}\right)\bigg|_{p^2=m_{f,i}^2}, \tag{2.88}$$

$$\delta Z_{ij}^{f,L} = \frac{2}{m_{f,i}^2-m_{f,j}^2}\Re\mathrm{e}\,\Big(m_{f,j}^2\Sigma_{ij}^{f,L}(m_{f,j}^2)+m_{f,i}m_{f,j}\Sigma_{ij}^{f,R}(m_{f,j}^2) \tag{2.89}$$

$$+m_{f,i}m_{f,j}\Sigma_{ij}^{f,l}(m_{f,j}^2)+m_{f,j}^2\Sigma_{ij}^{f,r}(m_{f,j}^2)\Big), \tag{2.90}$$

$$\delta Z_{ij}^{f,R} = \frac{2}{m_{f,i}^2-m_{f,j}^2}\Re\mathrm{e}\,\Big(m_{f,j}^2\Sigma_{ij}^{f,R}(m_{f,j}^2)+m_{f,i}m_{f,j}\Sigma_{ij}^{f,L}(m_{f,j}^2) \tag{2.91}$$

$$+m_{f,i}m_{f,j}\Sigma_{ij}^{f,r}(m_{f,j}^2)+m_{f,j}^2\Sigma_{ij}^{f,l}(m_{f,j}^2)\Big), \tag{2.92}$$

with $Q = L, R$ and $i \neq j$.

Charge renormalization

In order to finish the description, the rest of counterterm parameters have also to be expressed in terms of self-energies and their derivatives.

Charge renormalization is define through the normalization of the $ee\gamma$ vertex, being the explicit form

$$\delta Z_e = -\frac{1}{2}\delta Z_{AA} - \frac{s_{\mathrm{W}}}{c_{\mathrm{W}}}\delta Z_{ZA} = \frac{1}{2}\,\frac{\partial\Sigma_T^{AA}}{\partial p^2}\bigg|_{p^2=0} - \frac{s_{\mathrm{W}}}{c_{\mathrm{W}}}\frac{\Sigma_T^{AZ}(0)}{m_Z^2}. \tag{2.93}$$

Quark-mixing matrix renormalization

The renormalization of the quark-mixing matrix has a history with many success and missteps. Firstly proposed [45] it has been a long way for more than thirty years keeping the subject on the vogue (see discussions in [46, 47, 48]). Here we attach to the convention given at [29], and clarify possible violations when dealing with some flavour changing process via neutral currents

at one-loop. Then we could state the following counterterms for the CKM matrix:

$$\begin{aligned}\delta V_{ij} &= \mathfrak{Re}\Big(\frac{1}{m_{u,i}^2 - m_{u,k}^2}\Big(\tfrac{1}{2}(m_{u,k}^2 + m_{u,i}^2)\Sigma_{ik}^{u,L}(0) + m_{u,i}m_{u,k}\Sigma_{ik}^{u,R}(0) \\ &\quad + m_{u,i}m_{u,k}\Sigma_{ik}^{u,l}(0) + m_{u,k}^2\Sigma_{ik}^{u,r}(0)\Big)V_{kj} \\ &\quad - V_{ik}\frac{1}{m_{d,k}^2 - m_{d,j}^2}\Big(\tfrac{1}{2}(m_{d,j}^2 + m_{d,k}^2)\Sigma_{kj}^{d,L}(0) + m_{d,k}m_{d,j}\Sigma_{kj}^{d,R}(0) \\ &\quad + m_{d,k}m_{d,j}\Sigma_{kj}^{d,l}(0) + m_{d,j}^2\Sigma_{kj}^{d,r}(0)\Big)\Big). \end{aligned} \tag{2.94}$$

Chapter 3

Perturbative approach and radiative corrections

3.1 S-matrix and scattering theory

The scattering or decay of particles are physical phenomena with much more richness than the everlasting propagation of free fields. But the mathematical difficulties found on the exact analytical approach have lead physicists to think of interactions as a small perturbation to the free fields and apply, under this simplification, perturbation theory. At least for our model, a perturbative expansion in terms of α turns out to be a very successful idea, based on the smallness of the value ($\alpha \approx \frac{1}{137}$). This provides an exemplary decrease of the successive orders in the perturbative expansion.

Based on the interaction picture, Dyson worked out a solution for collision processes, called the scattering matrix or S-matrix expansion [49], which permits to extract the transition amplitude for a given process to any order of perturbation theory. Such mathematical background boosts the intuitive ideas of Feynman about diagrammatic representation [21] to a true calculating machinery.

The idea is to split the Lagrangian density (2.48), after inclusion of counterterms, into two main blocks: the first one describing the free fields while the second one containing the three- and four-particle interactions

$$\mathcal{L} = \mathcal{L}_0 + \mathcal{L}_I. \tag{3.1}$$

Considering a definite initial state at $t = -\infty$,

$$|\Phi(-\infty)\rangle = |i\rangle, \tag{3.2}$$

which corresponds as asymptotic limit to the solution of the free Hamiltonian derived from $\mathcal{L}_0$, the complete set of possible final states are related with the initial states through the S-matrix

$$|\Phi(\infty)\rangle = S\,|\Phi(-\infty)\rangle = S\,|i\rangle. \tag{3.3}$$

Thus the transition probability of the process to arrive at the final state $|f\rangle$, is given by the modulus square of the amplitude

$$\left|S_{fi}\right|^2 \equiv |\langle f|\Phi(\infty)\rangle|^2 = |\langle f|S\,|i\rangle|^2, \tag{3.4}$$

and the unitarity of the S-matrix reads

$$\sum_f \left|S_{fi}\right|^2 = 1. \tag{3.5}$$

The iterative solution to the equation of motion can be written in a covariant form

$$S = Te^{\mathrm{i}\int \mathrm{d}^4x\mathcal{L}_I(x)}, \tag{3.6}$$

where T means the time ordered product of the formal power series in $\mathcal{L}_I$. The evaluation of the different orders of the S-matrix, $\mathrm{S}_{fi}^{(i)}$, in momentum space leads to the Feynman diagrams as visual representation of the different terms in the Wick ordered expansion of the S-matrix. For convenience we define the invariant matrix element $\mathcal{M}_{fi}$ in connection with the S-matrix as

$$\langle f|S\,|i\rangle = \langle f|i\rangle + \mathrm{i}(2\pi)^4\delta^{(4)}(p_i - p_f)\mathcal{M}_{fi}. \tag{3.7}$$

From here we are then ready to set up the cross sections.

3.1.1 Cross section in $2 \to 2$ processes

Definition

Along this section, we will develop the formal theory in order to compute differential and total cross sections in the perturbative series of the electroweak coupling α. This includes soft-photon bremsstrahlung as well as one-loop amplitudes.

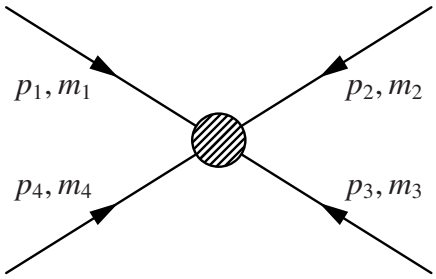

Figure 3.1: Definitions of kinematical variables. All momenta are incoming and clockwise indexed.

Our observables are the differential and total cross sections. In the center of mass frame and with the conventions given in Fig. 3.1, the differential cross section reads

$$\frac{\mathrm{d}\sigma}{\mathrm{d}\Omega} = \frac{1}{64\pi^2}\frac{|\mathbf{p}_f|}{|\mathbf{p}_i|E_{\mathrm{CM}}^2}\sum_{\mathrm{conf}}\left|\mathcal{M}_{fi}(s,\Omega)\right|^2, \tag{3.8}$$

where the invariant amplitude $\mathcal{M}$ contains all the frame-independent information about the process and the sum $\sum_{\text{conf}}$ deals with all the non-coherent indistinguishable possible final states $|f\rangle$. The r.h.s. of Eq. (3.8) contains three parts, the first is just a pure geometrical factor, the second one feels the balance of initial and final fluxes, and the last term contains the invariant probability transition between the initial and final states.

In the case in which the initial particles are not transversally polarized, there is a clear 2π-azimuthal symmetry around the beam direction[1]. The resulting amplitude is therefore invariant under changes along that angle ϕ and we can restrict our analyses to the one-dimensional differential cross section

$$\frac{\mathrm{d}\sigma}{\mathrm{d}\cos\theta} = \int_0^{2\pi} \mathrm{d}\phi \frac{\mathrm{d}\sigma}{\mathrm{d}\Omega} = \frac{1}{32\pi}\frac{\beta_f \beta_i^{-1}}{s}\sum_{\text{conf}} \left|\mathcal{M}_{fi}(s,\cos\theta)\right|^2, \tag{3.9}$$

θ being the angle between the incoming three-momentum $\mathbf{p}_1$ and the outgoing three-momentum $-\mathbf{p}_2$. The other quantities that appear are threshold functions of the final and initial states: $\beta_i = \beta_{14}$, and $\beta_f = \beta_{23}$, with

$$\beta_{jk} \equiv \frac{|\mathbf{p}_j| + |\mathbf{p}_k|}{\sqrt{s}} = \Theta(s - m_j^2 - m_k^2)\sqrt{1 - 2\frac{m_j^2 + m_k^2}{s} + \frac{\left(m_j^2 - m_k^2\right)^2}{s^2}}, \tag{3.10}$$

with s representing the initial energy squared in the centre of mass and Θ the usual step function that forbids beam energies lower than the initial or final energy at rest. Written so, the differential cross section is manifestly Lorentz invariant.

Later on, we will also need the other Mandelstam variables, so we introduce them all:

$$\begin{aligned}
s &\equiv (p_1 + p_4)^2 = E_{\text{CM}}^2, && (3.11)\\
t &\equiv (p_1 + p_2)^2 \\
&= -\frac{s}{2}\left((1 - \beta_i\beta_f\cos\theta) - \frac{1}{s}\sum_{j=1}^{4} m_j^2 + \frac{(m_1^2 - m_4^2)(m_2^2 - m_3^2)}{s^2}\right), && (3.12)\\
u &\equiv (p_1 + p_3)^2 \\
&= -\frac{s}{2}\left((1 + \beta_i\beta_f\cos\theta) - \frac{1}{s}\sum_{j=1}^{4} m_j^2 - \frac{(m_1^2 - m_4^2)(m_2^2 - m_3^2)}{s^2}\right). && (3.13)
\end{aligned}$$

Eq. (3.9) will be the starting point for building up other observables after integration, i.e. the total cross section and forward-backward asymmetry:

$$\begin{aligned}
\sigma &= \int_{-1}^{+1} \mathrm{d}\cos\theta \frac{\mathrm{d}\sigma}{\mathrm{d}\cos\theta}, && (3.14)\\
A_{\text{FB}} &= \frac{\sigma_{\text{F}} - \sigma_{\text{B}}}{\sigma_{\text{F}} + \sigma_{\text{B}}} = \frac{\int_0^{+1} \mathrm{d}\cos\theta \frac{\mathrm{d}\sigma}{\mathrm{d}\cos\theta} - \int_{-1}^{0} \mathrm{d}\cos\theta \frac{\mathrm{d}\sigma}{\mathrm{d}\cos\theta}}{\sigma}. && (3.15)
\end{aligned}$$

[1]Note that the final particles are always summed up under the different spin configuration states in $\sum_{\text{conf}}$ if there is no spin polarization analysis on the detected species.

Unpolarized amplitude

Being more specific, the processes we are interested in appear as a result of the e^+e^- interaction in high energy colliders. They contain four external fermions and, for an unpolarized amplitude, we have to average over possible initial spin configurations (σ_i), sum over the final ones (σ_f) and occasionally add incoherently the total number of colours (C_f) if we have quarks in the final state:

$$\sum_{\text{conf}} |\mathcal{M}_{fi}|^2 = \frac{1}{4} \sum_{\sigma_i=1}^{4} \sum_{\sigma_f=1}^{4} C_f |\mathcal{M}_{fi}|^2. \tag{3.16}$$

3.1.2 The matrix elements and form factors

The invariant transition amplitude can be expressed in terms of a standard basis of n matrix elements M_i, containing all the kinematical information of the scattering, and the form factors F_i, which account for the purely dynamical part.

$$\mathcal{M} = \sum_{i=1}^{n} M_i F_i = \begin{pmatrix} M_1 & M_2 & \cdots & M_n \end{pmatrix} \begin{pmatrix} F_1 \\ F_2 \\ \vdots \\ F_n \end{pmatrix}. \tag{3.17}$$

Represented by matrix multiplication, it is quite intuitive the construction of the amplitude square:

$$\begin{aligned} \sum_{\text{conf}} |\mathcal{M}|^2 &= \sum \mathcal{M}^* \mathcal{M} = \sum (MF)^* MF = \sum F^\dagger M^\dagger MF \\ &= \sum (F_1 \ \cdots \ F_n)^* \begin{pmatrix} M_1 \\ \vdots \\ M_n \end{pmatrix}^* (M_1 \ \cdots \ M_n) \begin{pmatrix} F_1 \\ \vdots \\ F_n \end{pmatrix} \\ &= (F_1{}^* \ \cdots \ F_n{}^*) \begin{pmatrix} \sum_{\text{conf}} M_1{}^* M_1 & \cdots & \sum_{\text{conf}} M_1{}^* M_n \\ \vdots & \ddots & \\ \sum_{\text{conf}} M_n{}^* M_1 & & \end{pmatrix} \begin{pmatrix} F_1 \\ \vdots \\ F_n \end{pmatrix} \\ &= \sum_{i,j=1}^{n} \langle \mathbb{M}_{i,j} \rangle F_i^* F_j, \end{aligned} \tag{3.18}$$

where the product of matrix elements $\langle \mathbb{M}_{i,j} \rangle \equiv \sum_{\text{conf}} M_i{}^* M_j$ is, in general, a much simpler scalar expression once we got rid of the spinor and tensor dependencies via trace theorems and Dirac equation. Therefore for the unpolarized case they only depend on our input parameter set: $\{s, m_j, \cos\theta\}$, $(j = 1, \ldots, 4)$.

The naïve set

Before we enter the technical description about how to reduce the amplitudes of an arbitrary diagram to the form given above, we have to set a specific choice of the basis for the matrix elements M_i. We define now our basis in the following way:

$$
\begin{aligned}
M_{1,k} &= \bar{w}(p_{i_1},\sigma_{i_1}) \quad \{\mathbb{1},\gamma_5\}\, w(p_{i_2},\sigma_{i_2}) \otimes \bar{w}(p_{i_3},\sigma_{i_3}) \quad \{\mathbb{1},\gamma_5\}\, w(p_{i_4},\sigma_{i_4}),\\
M_{2,k} &= \bar{w}(p_{i_1},\sigma_{i_1}) \quad \not{p}_{i_3}\{\mathbb{1},\gamma_5\}\, w(p_{i_2},\sigma_{i_2}) \otimes \bar{w}(p_{i_3},\sigma_{i_3}) \quad \{\mathbb{1},\gamma_5\}\, w(p_{i_4},\sigma_{i_4}),\\
M_{3,k} &= \bar{w}(p_{i_1},\sigma_{i_1}) \quad \{\mathbb{1},\gamma_5\}\, w(p_{i_2},\sigma_{i_2}) \otimes \bar{w}(p_{i_3},\sigma_{i_3}) \quad \not{p}_{i_1}\{\mathbb{1},\gamma_5\}\, w(p_{i_4},\sigma_{i_4}),\\
M_{4,k} &= \bar{w}(p_{i_1},\sigma_{i_1}) \quad \not{p}_{i_3}\{\mathbb{1},\gamma_5\}\, w(p_{i_2},\sigma_{i_2}) \otimes \bar{w}(p_{i_3},\sigma_{i_3}) \quad \not{p}_{i_1}\{\mathbb{1},\gamma_5\}\, w(p_{i_4},\sigma_{i_4}),\\
M_{5,k} &= \bar{w}(p_{i_1},\sigma_{i_1}) \quad \gamma^\mu\{\mathbb{1},\gamma_5\}\, w(p_{i_2},\sigma_{i_2}) \otimes \bar{w}(p_{i_3},\sigma_{i_3}) \quad \gamma_\mu\{\mathbb{1},\gamma_5\}\, w(p_{i_4},\sigma_{i_4}),\\
M_{6,k} &= \bar{w}(p_{i_1},\sigma_{i_1})\, \gamma^\mu \not{p}_{i_3}\{\mathbb{1},\gamma_5\}\, w(p_{i_2},\sigma_{i_2}) \otimes \bar{w}(p_{i_3},\sigma_{i_3}) \quad \gamma_\mu\{\mathbb{1},\gamma_5\}\, w(p_{i_4},\sigma_{i_4}),\\
M_{7,k} &= \bar{w}(p_{i_1},\sigma_{i_1}) \quad \gamma^\mu\{\mathbb{1},\gamma_5\}\, w(p_{i_2},\sigma_{i_2}) \otimes \bar{w}(p_{i_3},\sigma_{i_3})\, \gamma_\mu \not{p}_{i_1}\{\mathbb{1},\gamma_5\}\, w(p_{i_4},\sigma_{i_4}),\\
M_{8,k} &= \bar{w}(p_{i_1},\sigma_{i_1})\, \gamma^\mu \not{p}_{i_3}\{\mathbb{1},\gamma_5\}\, w(p_{i_2},\sigma_{i_2}) \otimes \bar{w}(p_{i_3},\sigma_{i_3})\, \gamma_\mu \not{p}_{i_1}\{\mathbb{1},\gamma_5\}\, w(p_{i_4},\sigma_{i_4}),\\
M_{9,k} &= \bar{w}(p_{i_1},\sigma_{i_1})\, \gamma^\mu\gamma^\nu\{\mathbb{1},\gamma_5\}\, w(p_{i_2},\sigma_{i_2}) \otimes \bar{w}(p_{i_3},\sigma_{i_3})\, \gamma_\mu\gamma_\nu\{\mathbb{1},\gamma_5\}\, w(p_{i_4},\sigma_{i_4}),
\end{aligned}
\tag{3.19}
$$

where w represents a fermion spinor (u or v) and each $M_{j,k}$ has 4 possible components labelled by k (running for the different $\mathbb{1}, \gamma_5$ combinations):

$$
\begin{aligned}
\text{for } k = 1 &\rightarrow \mathbb{1} \otimes \mathbb{1},\\
\text{for } k = 2 &\rightarrow \mathbb{1} \otimes \gamma_5,\\
\text{for } k = 3 &\rightarrow \gamma_5 \otimes \mathbb{1},\\
\text{for } k = 4 &\rightarrow \gamma_5 \otimes \gamma_5.
\end{aligned}
$$

The contracted momenta $\not{p}_{i_1}$ and $\not{p}_{i_3}$ correspond to the momentum of a spinor in the other chain[2]. By fermion chain we mean the collection of Dirac matrices sandwiched between two spinors. The symbol $\otimes$ stands for the product of the two fermion chains belonging to different spinor representations. Because of this, Dirac matrices of one chain do commute with the ones of the other chain.

Indeed, the given basis is general for any spinor combination. The labels $i_1, \ldots, i_4$ refer to any of the possibilities to construct a fermion chain. For instance, in the case of Bhabha scattering two possible constructions for fermion chains appear, one connecting the initial states and final states separately (called S-channel[3]) and the other in which there is no annihilation but just exchange of a neutral boson (T-channel), as shown in Fig. 3.2.

Thus, in case that there are more than one channel, each gets its independent set of basis elements according to the relevant spinors. As an example we reproduce here the contributing

[2]Contracted momentum of the spinors within the same chain are eliminated via Dirac equation.

[3]Here the denomination for the channels S, T and U has nothing to do with the S-matrix or T-matrix as mentioned in the literature.

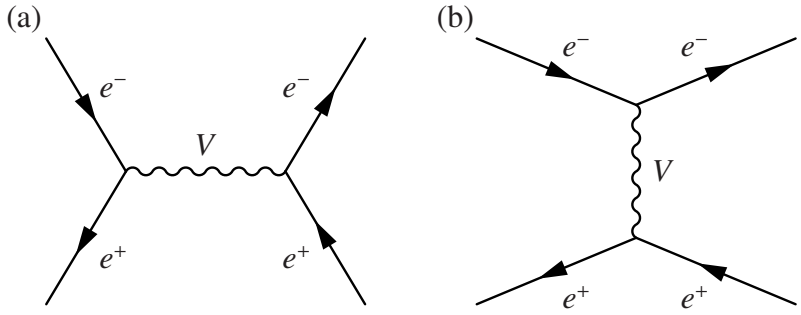

Figure 3.2: Feynman diagrams in Born approximation, with (a) S-channel exchange of neutral vector boson V; (b) T-channel. Note that the time direction goes from left to right and fermion lines pointing forward in time are particles (e^-) while pointing backward are antiparticles (e^+).

set of elements for the S-channel at tree-level:

$$\begin{aligned}
M^S_{1,1} &= \bar{v}(p_4,\sigma_4) \quad \mathbb{1} \quad u(p_1,\sigma_1) \otimes \bar{u}(-p_2,\sigma_2) \quad \mathbb{1} \quad v(-p_3,\sigma_3),\\
M^S_{1,4} &= \bar{v}(p_4,\sigma_4) \quad \gamma_5 \quad u(p_1,\sigma_1) \otimes \bar{u}(-p_2,\sigma_2) \quad \gamma_5 \quad v(-p_3,\sigma_3),\\
M^S_{5,1} &= \bar{v}(p_4,\sigma_4) \quad \gamma^\mu\mathbb{1} \quad u(p_1,\sigma_1) \otimes \bar{u}(-p_2,\sigma_2) \quad \gamma_\mu\mathbb{1} \quad v(-p_3,\sigma_3),\\
M^S_{5,2} &= \bar{v}(p_4,\sigma_4) \quad \gamma^\mu\mathbb{1} \quad u(p_1,\sigma_1) \otimes \bar{u}(-p_2,\sigma_2) \quad \gamma_\mu\gamma_5 \quad v(-p_3,\sigma_3),\\
M^S_{5,3} &= \bar{v}(p_4,\sigma_4) \quad \gamma^\mu\gamma_5 \quad u(p_1,\sigma_1) \otimes \bar{u}(-p_2,\sigma_2) \quad \gamma_\mu\mathbb{1} \quad v(-p_3,\sigma_3),\\
M^S_{5,4} &= \bar{v}(p_4,\sigma_4) \quad \gamma^\mu\gamma_5 \quad u(p_1,\sigma_1) \otimes \bar{u}(-p_2,\sigma_2) \quad \gamma_\mu\gamma_5 \quad v(-p_3,\sigma_3),
\end{aligned} \tag{3.20}$$

and another similar one for the T-channel with different spinor structure:

$$\begin{aligned}
M^T_{1,1} &= \bar{v}(p_4,\sigma_4) \quad \mathbb{1} \quad v(-p_3,\sigma_3) \otimes \bar{u}(-p_2,\sigma_2) \quad \mathbb{1} \quad u(p_1,\sigma_1),\\
&\vdots\\
M^T_{5,4} &= \bar{v}(p_4,\sigma_4) \quad \gamma^\mu\gamma_5 \quad v(-p_3,\sigma_3) \otimes \bar{u}(-p_2,\sigma_2) \quad \gamma_\mu\gamma_5 \quad u(p_1,\sigma_1).
\end{aligned} \tag{3.21}$$

These contain only a limited number of factors $M_{i,j}$ because no diagrams contribute at this level to the extended general structure (3.19).

Finally we can express the construction of the differential cross section in the following manner:

$$\begin{aligned}
\frac{\mathrm{d}\sigma}{\mathrm{d}\cos\theta} &= \frac{1}{32\pi}\frac{\beta_f\beta_i^{-1}}{s}\sum_{C_i,C_j}\sum_{i_1,j_1=1}^{9}\sum_{i_2,j_2=1}^{4} F^{C_i*}_{i_1,i_2}\langle \mathbb{M}^{C_i,C_j}_{i_1,i_2,j_1,j_2}\rangle F^{C_j}_{j_1,j_2}\\
&\equiv \frac{1}{32\pi}\frac{\beta_f\beta_i^{-1}}{s}\sum_{C_i,C_j}\sum_{i_1=1}^{9}\sum_{i_2=1}^{4} c_i c_j F^{C_i*}_{i_1,i_2} G^{C_j}_{i_1,i_2}.
\end{aligned} \tag{3.22}$$

where we have indicated a possible mix of channels $C_{i,j} = S, T$ or U and $c_{i,j}$ their respective Mandelstam variables s, t or u, and G defined as the effective form factor after multiplying with

the matrix elements. The set (3.19) accommodates any generic process involving four external fermions. It is still far from being optimal in a physical sense since there are no more than just 16 independent kinematical quantities, arising as the possible polarization states. Moreover the unpolarized case reduces this number further on. Then, why do we still use such a set with a maximum of $2 \times 9 \times 4 = 72$ configurations? The answer lays in our goal of global automation. It will be convenient to treat any possible contribution in terms of the same set. Automating the general case is easier even if in this case we are bound to sum large amounts of null contributions. They shall not disturb us much when applying the computational techniques to be mentioned in the next chapter.

3.1.3 Evaluation of the product of matrix elements

We have already mentioned that the calculation of the product of matrix elements $\langle \mathbb{M} \rangle$ requires very simple techniques. Decomposing the product into single elements we have

$$\begin{aligned} |\mathcal{M}|^2 &= \sum_{ij} F_i^* \langle \mathbb{M}_{i,j} \rangle F_j \\ &= \sum_{ij} \left(\bar{w}_1 \Gamma_{I_1}^{r_i} w_2 \otimes \bar{w}_3 \Gamma_{I_2,r_i} w_4 \right)^\dagger \left(\bar{w}_1 \Gamma_{J_1}^{r_j} w_2 \otimes \bar{w}_3 \Gamma_{J_2,r_j} w_4 \right) F_i^* F_j \\ &= \sum_{ij} \left(\bar{w}_4 \overline{\Gamma}_{I_2,r_i} w_3 \right) \left(\bar{w}_2 \overline{\Gamma}_{I_1}^{r_i} w_1 \right) \left(\bar{w}_1 \Gamma_{J_1}^{r_j} w_2 \right) \left(\bar{w}_3 \Gamma_{J_2,r_j} w_4 \right) F_i^* F_j, \end{aligned} \tag{3.23}$$

where $\Gamma_I^{r_i}$ symbolizes a possible set of the Dirac matrices with Lorentz index r_i and $\overline{\Gamma}$ is defined as

$$\overline{\Gamma} = \gamma^0 \Gamma^\dagger \gamma^0. \tag{3.24}$$

It is convenient to place all the non-barred spinors together with their barred partners and evaluate the appearing traces

$$|\mathcal{M}|^2 = \begin{cases} \sum_{ij} \ \mathrm{Tr}\left(w_1 \bar{w}_1 \Gamma_{J_1}^{r_j} w_2 \bar{w}_2 \overline{\Gamma}_{I_1}^{r_i} \right) \mathrm{Tr}\left(w_3 \bar{w}_3 \Gamma_{J_2,r_j} w_4 \bar{w}_4 \overline{\Gamma}_{I_2,r_i} \right) F_i^* F_j, & \text{(equal channels)} \\ \sum_{ij} \ \mathrm{Tr}\left(w_1 \bar{w}_1 \Gamma_{J_1}^{r_j} w_2 \bar{w}_2 \overline{\Gamma}_{I_1}^{r_i} w_3 \bar{w}_3 \Gamma_{J_2,r_j} w_4 \bar{w}_4 \overline{\Gamma}_{I_2,r_i} \right) F_i^* F_j, & \text{(mixed channels)} \end{cases} \tag{3.25}$$

by means of the Dirac equation, completeness relation for spinors and properties of the trace of γ matrices[4].

Just to give a flavour of how straightforward the calculations become, we reproduce some of the matrix elements required in Bhabha scattering. Here the degeneracy of external masses permits to represent all the kinematics only in terms of the Mandelstam variables defined in

[4] See Eqs. (B.21–B.22), Eqs. (B.25–B.26) and Eqs. (B.38–B.43) given in the appendix.

Eqs. (3.11–3.13)

$$\begin{aligned}
\langle \mathbb{M}^{S,S}_{1,1,1,1} \rangle &= \mathrm{Tr}\left(\frac{1}{4} \sum_{\sigma_4,\sigma_1} \mathbb{1} v(p_4,\sigma_4)\bar{v}(p_4,\sigma_4)\ \mathbb{1} u(p_1,\sigma_1)\bar{u}(p_1,\sigma_1) \right) \times \\
&\quad \mathrm{Tr}\left(\sum_{\sigma_2,\sigma_3} \mathbb{1} u(-p_2,\sigma_2)\bar{u}(-p_2,\sigma_2)\ \mathbb{1} v(-p_3,\sigma_3)\bar{v}(-p_3,\sigma_3) \right) \\
&= \frac{1}{4}\mathrm{Tr}\left((\not{p}_4 - m_e)(\not{p}_1 + m_e) \right) \mathrm{Tr}\left((-\not{p}_2 + m_e)(-\not{p}_3 - m_e) \right) \\
&= (-m_e^2 + p_4 \cdot p_1)(-4m_e^2 + 4p_2 \cdot p_3) = (s - 4m_e^2)^2 = 2tu + t^2 + u^2, \qquad (3.26) \\
\langle \mathbb{M}^{S,T}_{5,2,5,2} \rangle &= \langle \mathbb{M}^{S,T}_{5,2,5,3} \rangle = \langle \mathbb{M}^{S,T}_{5,3,5,2} \rangle = \langle \mathbb{M}^{S,T}_{5,3,5,3} \rangle \\
&= 2su + 2tu, \qquad (3.27) \\
\langle \mathbb{M}^{T,T}_{5,1,5,1} \rangle &= 2tu + 2ts - 2us + 3t^2 + u^2 + s^2, \qquad (3.28)
\end{aligned}$$

and so one.

3.2 One-loop corrections

Order by order, the modulus square of the amplitude is formed from the interference of different levels of the perturbative expansion

$$\begin{aligned}
|\mathcal{M}|^2 &= \left(\mathcal{M}^{(0)} + \mathcal{M}^{(1)} + \ldots \right)^* \left(\mathcal{M}^{(0)} + \mathcal{M}^{(1)} + \ldots \right) \\
&= \mathcal{M}^{(0)*}\mathcal{M}^{(0)} + \mathcal{M}^{(0)*}\mathcal{M}^{(1)} + \mathcal{M}^{(1)*}\mathcal{M}^{(0)} + \ldots \\
&= \underbrace{\left|\mathcal{M}^{(0)}\right|^2}_{O(\alpha^2)} + \underbrace{2\mathfrak{Re}\left(\mathcal{M}^{(0)*}\mathcal{M}^{(1)} \right)}_{O(\alpha^3)} + \underbrace{\left|\mathcal{M}^{(1)}\right|^2 + 2\mathfrak{Re}\left(\mathcal{M}^{(0)*}\mathcal{M}^{(2)} \right)}_{O(\alpha^4)} + \ldots \qquad (3.29)
\end{aligned}$$

The first term corresponds to the leading order or the so called Born or 'classical' result. In this thesis we consider the $O(\alpha)$ correction to the first term, which is due to the interference between the tree and the one-loop levels. Also the simplest photonic radiation affects this order and we will consider it at a later moment. The last explicit term corresponds to the next to next to leading order and contains one-loop squared amplitudes, together with the interference between tree and two-loop levels. Complete two-loop contributions in $2 \to 2$ fermion processes are still a non-solved issue for the massive case, and we will not discuss them here.

The perturbative expansion of the amplitude will ultimately be connected with the expansion in the mediating dynamical forces, so it only concerns the form factors. One can rewrite Eq. (3.17) in a perturbative fashion

$$\mathcal{M} = \sum_{i=1}^{n} M_i \left(F_i^{(0)} + F_i^{(1)} + \ldots \right), \qquad (3.30)$$

where different orders of the perturbation are labelled with a superscript: (0) for tree-level, (1) for one-loop and so one.

3.2.1 Opening path: from Feynman rules to numerics

Once the tools are presented, we are in the position to calculate the form factors for a given process. The strategy is well defined and follows closely [44].

1. Sketch all the diagrams we have in the process.
2. Apply the Feynman rules to each of them.
3. Decompose the individual amplitudes according to Eq. (3.19).
4. Collect the results, sum them all up and evaluate numerically the resulting expression.

All these tasks are indeed rather straightforward to be implemented in computers. The need for automation, even if not strictly coming from the tree-level, is clear when higher-loop orders are to be evaluated. For these, many more than a couple of diagrams and few lines result from the calculation. Furthermore some of the procedures are long, repetitive and not enlightening when executed more than once; commuting γ matrices, applying completeness relation for spinors or evaluating traces are examples one may think of.

We considered that the main difficulties arising at the loop-level are:

- the number of diagrams grows too fast even for simple models in comparison with the tree-level,
- one-loop amplitudes require the treatment of several products of γ matrices and loop integrals,
- many and large analytical expressions need effective and systematic processing,

and for them the use of Feynman diagram generators, computer algebra and an environment which controls the calculation is very welcome. In the next chapter it is described how we implemented a tool being able to structure and automate the whole calculation.

3.2.2 Extraction of one-loop form factors

In the following we describe some steps in transforming the amplitudes at one-loop from an abstract symbolic level to numerically evaluable expressions. This procedure composes the core of the analytical work.

By applying the Feynman rules we meet mathematical expressions like

$$\mathcal{M}_{\text{diagram}} = c \int_{-\infty}^{\infty} \frac{\mathrm{d}^4 q}{(2\pi)^4} \frac{\bar{w}_1 \Pi_I^r(q - k_i; m_i) w_2 \otimes \bar{w}_3 \Pi_{J,r}(q - k_i; m_i) w_4}{N_0 \dots N_{l-1} \dots N_t}, \tag{3.31}$$

where c is a combinatorial coefficient, the integral represents the quantum loop (with integration momentum labelled q), the Π's are chains of product of Dirac matrices with different tensor structure (up to rank 3 in $2 \to 2$ fermion processes) depending on the specific momenta of

the internal lines $q - k_i$ and masses m_i. The product in the denominator consists of internal propagators, given generically as

$$N_i = \begin{cases} (q-k_i)^2 - m_i^2 + \mathrm{i}\varepsilon, & \text{for } i < l \quad \text{(belonging to the loop)}, \\ k_i^2 - m_i^2 + \mathrm{i}\varepsilon, & \text{for } i \geq l \quad \text{(outside the loop)}. \end{cases} \tag{3.32}$$

The following is a description of possible management of Eq. (3.31):

1. **Reduce the Πs to a minimal set**: The set of 16 Dirac matrices $\{\mathbb{1}, \gamma^\mu, \sigma^{\mu\nu}, \gamma^\mu\gamma_5, \gamma_5\}$ given in Eq. (B.9) in App. B.2, spans the 16-dimensional space of the 4×4 complex matrices forming a basis. It is possible to reduce any matrix, like Π_I^r, to a linear combination of the basis. This reduction introduces antisymmetric ϵ tensors as well as extra γ_5s.

2. **Trace possible fermion loops**: In case of dealing with loop insertions in bosonic self-energies, closed fermion loops will appear. They have no topological connection with the external fermions and can be traced out, removing the potential third chain Π.

3. **Perform projection to scalar functions**: A simplification of the tensor integrals can be applied by reducing them to scalar expressions by means of internal momenta decomposition as in [44]. An alternative representation in terms of external momenta was firstly derived in [50]. We prefer the first choice since it contains only independent momenta and we can easily evaluate numerically the loop integrals with [10, 51] or eventually reduce them to scalar master integrals A_0, B_0, C_0 and D_0 given in [52].

4. **Apply on-shell conditions and Dirac equation**: Up to now, the expressions in terms of internal momenta are not yet really useful since it makes sense to express them in terms of kinematical invariants. After this step only Mandelstam variables and masses appear. Moreover, those $\not{p}$ appearing in a fermion chain sandwiched from a side with $w(p)$ or $\bar{w}(p)$ must be further eliminated by applying the Dirac equation on momentum space with Eqs. (B.21−B.22) or the equivalent Gordon identities.

5. **Returning to 4-dimensions**: This is required because step 1 left $[D-4]$ terms leading to finite contributions when encountering UV-divergent scalar integrals. After this feature has been considered we are safe to bring back the physical limit

$$[D-4] \to 0. \tag{3.33}$$

   The appearence of those $[D-4]$ factors is natural in dimensional regularization and occurs in the manipulation with ϵ tensors via Eqs. (B.30−B.33) and in the application of Chisholm identities given in Eqs. (B.34−B.37).

6. **Bring Dirac chains to the Eq. (3.19) basis**: Since no more contractions are to take place, one can reorder the Dirac chains in the expression to match the required basis. Scalar expressions accompanying each of the matrix elements are known as the one-loop form factors $F_i^{(1)}$ which finally can be evaluated numerically.

3.3 Bremsstrahlung contributions

Radiative corrections have to include the diagrams with photon emission from external charged particles. The reason is that real detectors cannot resolve photons with lower energy than a given threshold, resulting in experimentally undistinguishable events. Taking into account such processes with *soft photons* is also theoretically welcome, since they are by themselves unphysical[5] but correctly cancel the divergences arising in the evaluation of the infrared divergent one-loop integrals of the *pure* process [53]. Adding the possible processes with one emitted photon (denoted with a subscript γ) we have for the observed amplitude an equivalent to Eq. (3.29)

$$\begin{aligned} |\mathcal{M}|^2 &= \left(\mathcal{M}^{(0)} + \ldots\right)^* \left(\mathcal{M}^{(0)} + \ldots\right) + \left(\mathcal{M}_\gamma^{(0)} + \ldots\right)^* \left(\mathcal{M}_\gamma^{(0)} + \ldots\right) + \ldots \\ &= \underbrace{\left|\mathcal{M}^{(0)}\right|^2}_{O(\alpha^2)} + \underbrace{2\Re\mathfrak{e}\left(\mathcal{M}^{(0)*}\mathcal{M}^{(1)}\right) + \left|\mathcal{M}_\gamma^{(0)}\right|^2}_{O(\alpha^3)} + O(\alpha^4). \end{aligned}$$

To illustrate the phenomenon, Fig. 3.3 shows the most general case in Bhabha scattering where the emission comes from all possible legs in the different channels.

There is a natural limit concerning how hard in energy a *soft* photon can be, and it has to do with the validity of the soft-photon approximation. Whenever the applicability of the soft-photon approach is not admissible anymore, we have unavoidably to switch our description to the theory of hard emission in which the emitted photon has already taken enough energy out of the process, so that it requires an exact 3-body particle state description in the final phase space integration. Analytical methods with fourfold integrals have been proposed for QED [54] and later extended for electroweak interactions [55], numerical techniques are Monte-Carlo integrations [56,57,58] or phase space slicing [59] (and references therein) and they deal successfully with hard photons. Anyway, hard-photon emission is a subject more related with a multi-leg analysis than with the focus of this thesis. For this reason we will just present here the treatment of the soft-photon bremsstrahlung.

3.3.1 Structure of the soft-photon radiation

The structure of the photon emission is simplified and treated in many textbooks closely following [60], and here we shall just mention the more significant results for a single radiated photon. Let $\mathcal{M}$ be the original diagram still without emission. Then we can express the invariant amplitude for the same diagram with just one photon emission out of an incoming fermion as

$$\mathcal{M}_{\text{soft}} = -eQ_f \frac{\varepsilon \cdot p}{k \cdot p} A(p)u(p) = -eQ_f \frac{\varepsilon \cdot p}{k \cdot p}\mathcal{M}, \tag{3.34}$$

where ε is the photon polarization vector, k its momentum and Q_f the charge of the radiating fermion. Here we have already introduced the soft-photon approximation by dropping terms proportional to k in the numerator. Then the differential cross section is given by

$$\frac{\mathrm{d}\sigma^{(\text{soft})}}{\mathrm{d}\cos\theta} = -\frac{\mathrm{d}\sigma^{(0)}}{\mathrm{d}\cos\theta}\frac{e^2}{(2\pi)^3}\int_{|\mathbf{k}|\le\Delta E}\frac{\mathrm{d}^3k}{2\sqrt{k^2+\lambda^2}}\sum_{i,j}\frac{\pm p_i\cdot p_j Q_i Q_j}{(p_i\cdot k)(p_j\cdot k)}, \tag{3.35}$$

[5] No experiment is able to isolate processes with only soft-photon emission.

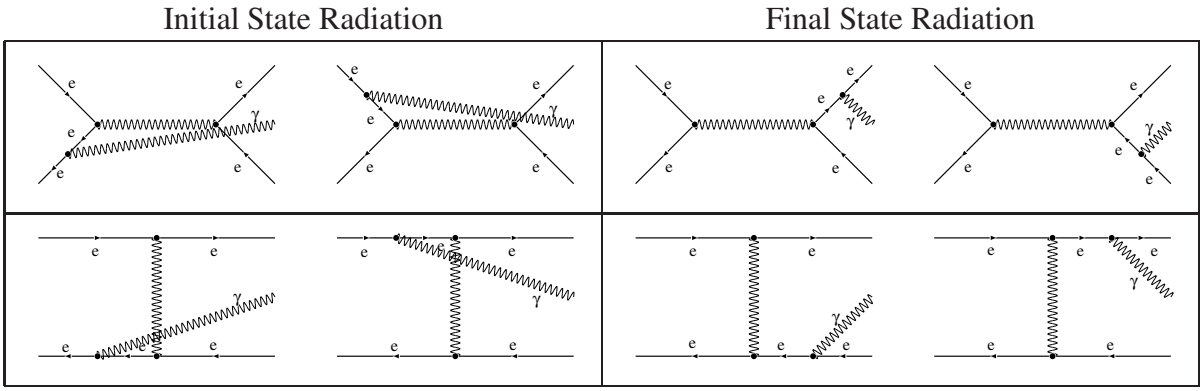

Figure 3.3: Feynman diagrams for the possible initial and final state radiation (ISR and FSR respectively) for Bhabha scattering at both S- and T-channels (upper and lower row respectively).

with the $\pm$ sign standing in the case of incoming/outgoing fermion. Note that this formula is indeed proportional to the Born cross section of the original process, so it corresponds to an ideal emission which does not modify the kinematical structure of the original process. The integral over the photon three-momentum was already worked out in [52], given in terms of the parameter λ representing the *photon mass*. This formulation is equivalent to the dimensional regularization scheme where the cut-off is regulated by ϵ (see Eq. (C.9)) as generally discussed in [61].

3.3.2 Cancellation of infrared divergences

The following contributions do cancel the infrared divergences exactly:

- ISR or FSR from same leg with the counterterms from fermion field renormalization,
- ISR or FSR from different legs with vertices,
- Interference between ISR and FSR with boxes.

These cases may be visually understood with the help of Feynman diagrams. For example in the last item the cancellation reads graphically

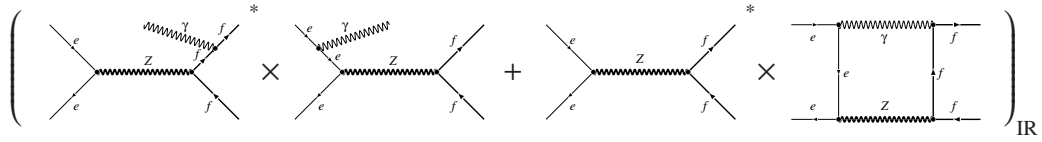

independently whether the boson mediating the interaction is dressed with some width or not. This idea helps to fix the case when treating massive unstable gauge bosons inside a loop as it will be shown next.

3.4 The $Z-$boson and its finite width

Unstable elementary particles have worried physicists in the quest for adapting them to the framework of quantum field theories. Some of the first ideas about their treatment on the pole representation were pioneered in [62] and, during LEP era, other analyses went further for $O(\alpha)$ precision for the Z and W bosons [63, 64, 65, 66, 67]. These and many other studies contributed to our today's understanding of resonances and instability.

For our studies with neutral currents, the resonant effects appear at the Z-boson resonance. The reason is that already at the lowest order, the propagators diverge in the limit $\sqrt{s} \to m_Z$ if the Z-boson width is not taking into account, breaking the predictive power of perturbation theory. A resummation to all orders of the vacuum-polarization effects, called *Dyson summation*, restores a finite amplitude and leads to finite results with predictive power.

The Z-peak resonance was exhaustively studied at LEP-I with precise measurements of the electroweak sector. Here we will refer to the Z-boson exclusively, but the same applies for other unstable bosons like the W or Higgs. The problem arises when we proceed with strict one-loop calculation. On the resonance, the inverse propagator vanishes, and we have to account for 2-loop effects if the intention is to keep at least $O(\alpha)$ accuracy. Furthermore, it was found [63] that on-shell masses disagree with pole masses beyond one-loop, giving for the Z-boson a measurable difference of about 34 MeV. Thus the renormalization of unstable bosons in the pole-scheme has to be treated carefully.

Several schemes about how to implement the resummation have been proposed and compared [68, 69]. Here we stick to the most immediate approach, the *fixed-width scheme*. Even if it is not free of some theoretical inconsistencies, namely break-down of gauge invariance and non-expected imaginary parts for T- or U-channel propagators, it will prove to render finite corrections and serve as example for the implementation that, to some extent, is similar to the other schemes.

The fixed-width proposal adds a constant complex term $\mathrm{i}m_Z\Gamma_Z$ to the propagator that displaces the position of the mass pole. This substitution accounts for a resummation to all orders of the vacuum-loops arising in the self-energies, and goes beyond $O(\alpha)$. Moreover, unlike fermionic loops, bosonic loop resummations break gauge invariance so that we have to consider the results only approximate arguing that the gauge violations are suppressed to the next order of perturbation theory. On the other hand, more elaborated schemes like the fermion-loop scheme [68] can be safely introduced as dealing with gauge invariance in a more consistent approach.

Adding the constant width Γ_Z to the boson propagator,

$$\frac{1}{s - m_Z^2} \to \frac{1}{s - m_Z^2 + \mathrm{i}\Gamma_Z m_Z}, \tag{3.37}$$

accounts properly for the resummation of the self-energies and therefore provides a finite behaviour on-resonance, retaining the gauge invariance for the $U(1)_{\mathrm{em}}$ and behaving properly at large energies. The algorithm to use is the following:

- Apply substitution (3.37) on Feynman Rules.
- Discard self-energy diagrams already resummed in the contribution to Γ_Z, to avoid double counting.
- Consider the divergent loop integrals with complex mass arguments.

The last point on the algorithm needs a detailed view. While one-loop integrals are often calculated with real arguments of momenta and masses, the mathematical calculation of the integrals can be extended to complex arguments. Unlike for the real case, the appearence of finite imaginary parts simplifies the calculation due to the eventual displacement of singularities from the real axis, where the integration is performed[6].

As pointed out in Eq. (3.36), whenever the dressing of the propagator is done at tree-level, the cancellation of infrared singularities from the soft-photon approximation contribution requires also equivalent treatment of the internal massive propagator in the loop diagram. The explicit calculation for a generic diagram of the form sketched in Fig. 3.4 was carried out in [70] and is also presented in the last part of App. D.2.4.

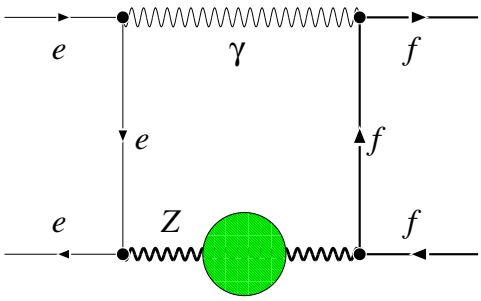

Figure 3.4: Example of a loop diagram in which one of the internal virtual propagators contains a finite imaginary part.

The other integrals, which do not contain a loop composed in terms of an unstable gauge boson and a photon propagator, are finite at the Z-peak and do not need to be calculated within the fixed-width scheme. In this sense we will be minimal, including complex arguments for the unstable bosons only if the result of loop integrals diverges at the considered peak.

[6] See App. D and the Feynman parametrization.

Chapter 4

Computing

4.1 New era in physics. The computer revolution

4.1.1 Machine development

The few decades of friendship between computer technology and physics have been undoubtedly an enormous enrichment for both. Such an experience has brought present-day experimental and theoretical physicists into debt with computing that has been already repaid many times over by making fundamental contributions to advances in hardware, software and systems technologies.

The human beings have always considered their fingers as the most immediate tool to count and represent counted entities. This gave origin to the decimal numerical system. Still on prehistoric times the use of external objects, such as pebbles (in Latin *calculus*), helped to represent simple sums. It was in civilized cultures when the first machine played a role in abstract counting; the abacus, being the most sophisticated mechanical aid for counting. In its classical form it consists of a wooden frame with several rods piercing wooden beads that slide freely on them.

It was not until the XVII century, when Blaise Pascal built the first automatic calculator (1642). It had gears simulating the add and subtraction operations in the abacus. Some decades later, Gottfried Leibniz improved this machine to multiply, divide and extract square roots. The application of mechanical systems to the textile production was achieved by Joseph Marie Jacquard, who designed an automatic loom using perforated wooden sheets that guided the nails weaving complex patterns. It can be considered as the first mechanical programmed machine.

The idea of using perforated cards as encoding languages developed further on by some other contributors. Charles Babbage and Augusta Ada Byron invented and programmed the 'differential machine' and the 'analytic machine' (1832-34), which even if not totally constructed, were considered as the predecessors of the modern computers.

Special mention is deserved to Konrad Zuse. Born in Berlin, he developed and built the first binary digital computer in the world, Z1 (1938), during pre-war times, independently of Babbage's ideas. The world war II irrupted in his life and his work on a second machine. Finally some of Zuse's computers were destroyed in bombing raids near the end of the war and some others were eventually relocated for security and employed for years. Secretly working at that time and founded by the British government, Alan Turing built a programmable vacuum-tube

digital machine 'Colossus', used for decrypting the secret Nazi messages encoded by 'Enigma' and more complicated systems.

Following this walk through the history of the machine development, the first stored-program electronic computer, ENIAC (1946) was built at the Moore School of the University of Pennsylvania. ENIAC, a major triumph for vacuum-tube technology, was originally designed for the calculation of gun-firing tables and could add 5000 numbers in one second. The machine was nevertheless large and expensive and turned off nine years later because the US Army could no longer justify the expense of operating and maintaining it.

Also in the late 40s, three scientists at Bell Telephone Laboratories, William Shockley, Walter Brattain, and John Bardeen move on by demonstrating their new invention of the point-contact transistor amplifier. The name transistor is short for 'transfer resistance'. This new solid-state technology was born to lead the sector after a critical phase of decisions in large electronic companies and overtook the vacuum-tubes for economical and size reasons.

The performance of the transistor used in computing followed during many years an exponential growth with time. The related law, noticed by Gordon Moore, related the chip functionality with both, the research activities and the increasing fields of application in the market. It predicts that the transistor eventually will reach the frontier between classical solid-state statistics and quantum effects. This is expected to happen soon depending on research brilliance and decisions of corporate executives; perhaps in twenty years from now. New technologies and calculation possibilities shall come.

It is therefore revealing the small look back and forth on time to see how much this technology evolution has challenged our life-style in general and the methods of science in particular.

4.1.2 Particle physics takes its chance

Let's refresh how the quantum field theory got benefit out of the computing progress. Pioneering projects were undertaken by individuals who took a challenging step in research: the introduction of the newest available technologies at that time. One of them, Hans Kaiser, worked at the former Institute für Hochenergiephysik in Zeuthen with the 'Lochkarten' machine. Much more popular became Veltman's Schoonschip [71], designed to facilitate the algebra for gamma matrices. At that time, in the early seventies, numerical approaches were investigated to extract non-perturbative solutions in discrete space-time to models such as QCD, leading to what later has been named *lattice* gauge theories.

Ever since, codes for collider physics had become world-spread and public available such as CompHEP [72] or the experimentalists' favourite Zfitter [73]. Those projects worked on the tree-level approximation or were designed as numerical static codes with multitude of flags and approximations. On the one hand, a more integrated view has been developed during the last decades in FeynArts FormCalc [2] and LoopTools [10] (based itself on FF [51]), packages that work jointly using the commercial Mathematica environment. On the other hand, several Feynman graph generators with analyzing tools as Grace [74] or Madgraph [75] have been recently displayed being able to handle multi-particle final states. Even an on-line project with Java technology was launched recently under the SanC [76] denomination.

In the next sections, we want to present the description of the codes which have been part of the doctoral activities carried out. The first contribution was within the started TOPFIT project [1], while the second one covered the full design, develop and documentation of a new tool, *a*i̊TALC.

4.2 The FORTRAN code TOPFIT

4.2.1 Origin and first stage

The project TOPFIT was born with the intention to provide numerical and semi-analytical predictions to the $t\bar{t}$ production at e^+e^- Linear Colliders. The final code, appeared as a FORTRAN compilation of files.

Developed during the years 2001-2002, the initial running versions incorporated the $O(\alpha)$ electroweak corrections, in two blocks, one for the gauge independent weak sector and the other for the whole set. They also include soft photon emission and hard photon analytical integration for the three-particle final state.

Even if the calculations were performed with the help of DIANA, no trace of the use of this tool was left after the analytical decompositions of the one-loop amplitudes were done. Just compact expressions were implemented in the FORTRAN code.

Some external tests were then performed by executing intended comparisons with other researching groups and their tools. We can mention here the efforts on reaching numerical agreement [77, 78, 79]:

- up to 7 digits against the GRACE project [74] regarding the $O(\alpha)$ corrections and per mill agreement on the hard-bremsstrahlung part after integration,
- up to 8 digits against the FEYNARTS project [2],
- up to 8-10 digits against SANC (former CALCPHEP) [76] project, as reported by their comparisons.

To finish up the studies on top-quark, the TOPFIT collaboration presented their work in terms of both analytical and numerical results [80].

4.2.2 Upgrade to other fermion species

It should be pointed out that for the purpose of this thesis, it was desirable to reconvert minimally TOPFIT to deal with other fermion species in the final state. But this possibility was evaluated and turned out to be not so easily accessible, as jokingly shown in the art-like design drafts Fig. 4.1. The main problems arose because the code was intrinsically designed with explicit use of top-quark quantum numbers and there was not a strict control of the input parameter set and technical performance.

A reconstruction program was planned leading to major changes:

1. The extra direct-box loop diagram, appearing as a crossed-box for the top-quark case, was calculated and programmed to allow for different weak-isospin fermions with $I_W^3 = -\frac{1}{2}$.

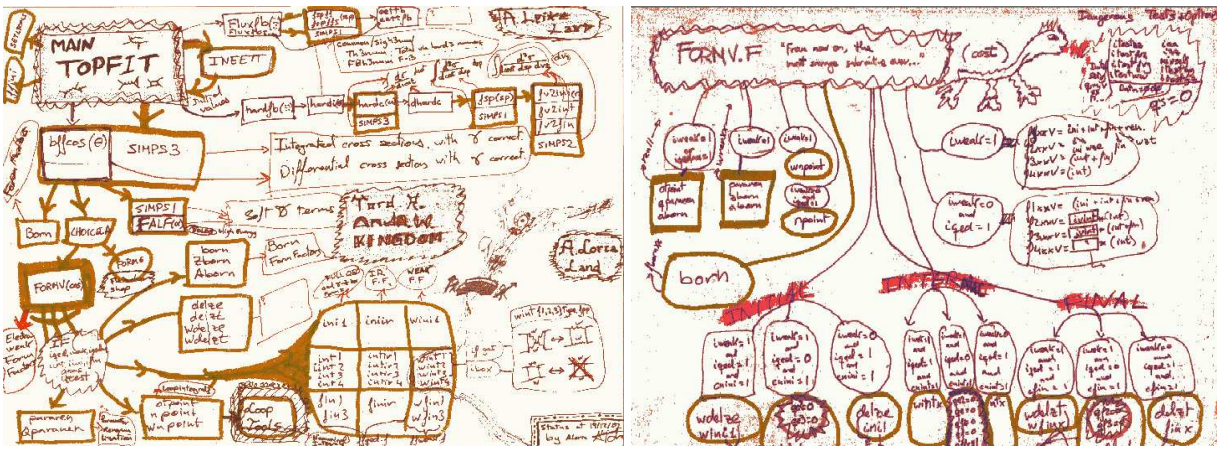

Figure 4.1: Initial hand-made design for the study and improvement of TOPFIT program and its subroutine `formv`.

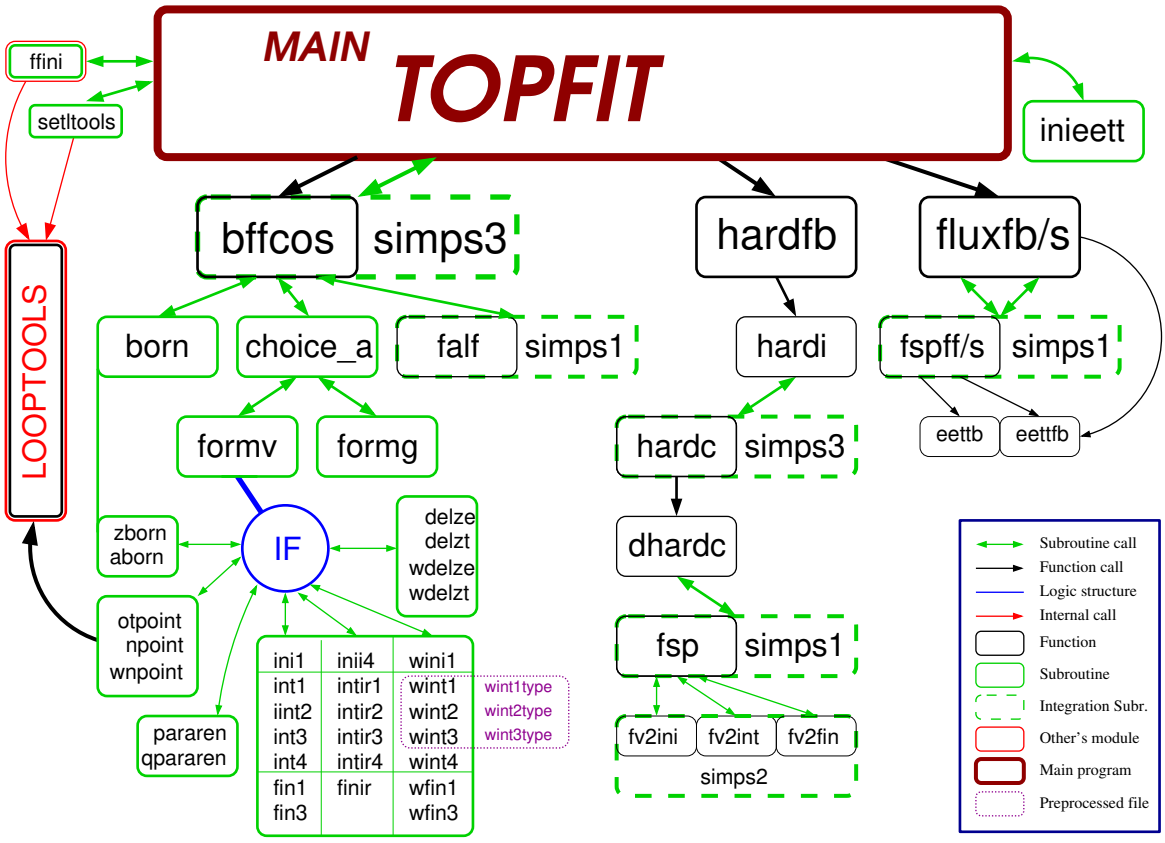

Figure 4.2: Logical flow chart structure for TOPFIT version 0.92.

2. Top-quark quantum numbers were explicitly included in terms of generic couplings, which allows for the generic case. Cross-checking of the rest of the contributions was done and the flip of signs in triple-boson vertex ZWW and γWW was corrected.

3. The FORTRAN structure was fully revised, moving all the initialization parameters to a single subroutine, adapting many pieces of code to standards of double precision and establishing the logical hierarchy given in Fig. 4.2.

The final version 0.92 was successfully built and is used throughout in Sect. 5.1, where we present our results for $f\bar{f}$ production.

Besides these results, the constituent library with the corrections has been proven to be a profitable independent block in the study of related reactions. It was added to the Monte Carlo program EETT6F in order to account for the higher order electroweak corrections to the decay of top-quarks into 6 fermions in the final state [5]. Such a work may improve precision predictions for standard model processes at linear colliders and help the understanding of the decay of heavy unstable particles and their treatment.

4.3 The automated tool *aï*TALC

4.3.1 Introduction

*aï*TALC is designed as a tool to perform automated perturbative calculations of cross sections in high energy physics.

The main goal is to create numerical programs directly from Feynman rules. It is actually developed for few known models like the electroweak standard model and QED, and the limit of application is, for the moment, the $2 \to 2$ particles reactions involving only external fermions.

The user is expected to cook his or her own process within a set of basic and/or advanced ingredients. As a reward to such effort comes the output of *aï*TALC: Fast and reliable FORTRAN code with differential and integrated cross sections, analytical expressions for the transition amplitude and nice drawings of the individual Feynman graphs.

The tool was intended to integrate only free-of-charge packages existing on the market. As the calculation proceeds, in a modular fashion, it profits from an adaptation of the DIANA package [7] (based itself on the QGRAF [81] code) for the generation and analysis of Feynman graphs, the FORM [9] language when dealing analytically with the large expressions in the amplitudes and, finally, the LOOPTOOLS [10] library (also integrating the FF package [51]) for the numerical calculation of the loop integrals.

Last but not least, this tool owns its birth to qualitative evolution of the static FORTRAN code TOPFIT previously reported, intended for the calculation of top-pair production. Some of the features then available such as the hard-photon bremsstrahlung or separate weak-QED contributions were discarded in pro of a full automation, higher technical precision and flexibility for many other processes.

4.3.2 Technical requirements and configuration

We present a list of the necessary conditions to install and run *aï*TALC on a computer.

System compulsory requirements:

- A computer under LINUX[1] operating system with standard
  - GNU MAKE utility,
  - C compiler,
  - FORTRAN77 compiler (with preprocessing ability).

Suggested optional features:

- CPU speed ≥ 333 MHz,
- RAM Memory ≥ 128 MB,
- at least from 1.5 to 10 MB[2]free space on disk for installation.

The package is licensed under the GNU General Public License, contains a documented tutorial and can be found at the web page `http://www-zeuthen.desy.de/theory/aitalc`.

An often underestimated issue is the installation, that proceeds conforming to the standards of the UNIX packages. The operations include a customization of your system settings via `configure` and the later extraction of individual packages (if needed) and examples. This process is also controlled by a `make` instruction.

4.3.3 Makefile like an environmental language

Automation requires effective intercommunication and a smart way to organize the tasks. This second concept has been widely exploited through the Makefile environment, being its conceptual organization a pro in order to build the different sections of the calculation and provide a chain-dependency between files and modules. The Makefile environment accomplishes

- the simplification of user interface,
- building the sections `tree`, `loop` and `fortran`,
- running the driver process file,
- writing the intermediate information DIANA → FORM, → FORTRAN in a row,
- compiling the numerical program leading to the final results,

in a modular fashion. The execution is carried out sequentially following the control flow structure sketched in Fig. 4.3.

[1]Installation on other UNIX systems might be possible if there are already some modules present. The package has been successfully built in SOLARIS for testing purposes.

[2]The fewer modules you have already installed the larger the size for including them. Another extra 30 MB will be needed when building the three examples proposed.

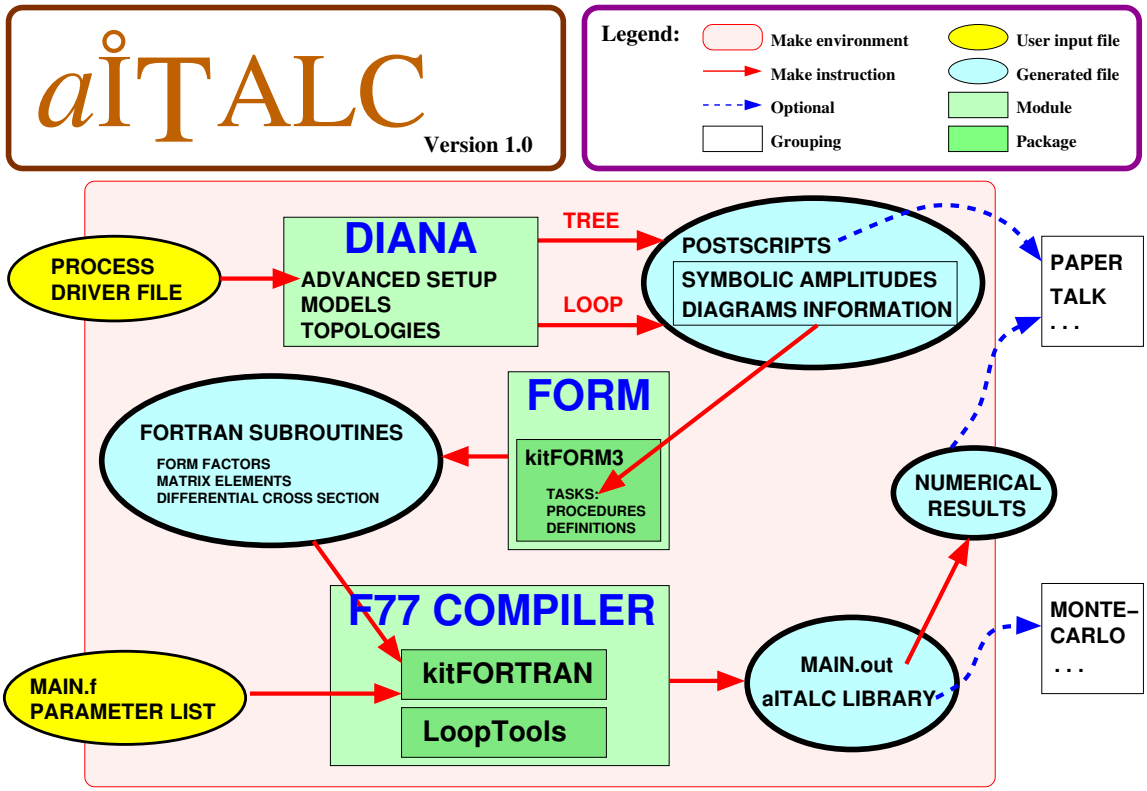

Figure 4.3: Logical flow chart structure for *a*ITALC.

Despite of the simplicity, the idea of calculating a process by a `make` instruction has another major advantage: reproducibility, being understood as the ability to recreate once and again similar processes for testing or cross-checking purposes. On the contrary, the customization of a specific process turns out to be spread among different parts: driver file, add-on files for neglecting the default ones and specific commands in the main FORTRAN programs.

We will dedicate the next parts to a deeper discussion of how each module addresses its tasks and the description of the *modus operandi*.

4.3.4 Feynman diagram generation: DIANA

Let us introduce some basic concepts about DIANA. If we are thinking of some process, a very intuitive approach is to draw some Feynman diagrams to get a feeling and support the calculation which comes later.

Such a task is very likely to be implemented with the help of computers since it is basically a combinatorial problem. Once we define a model, the external particles, and the level of loops, the problem can be solved. Indeed, DIANA will do it for us.

Status of version 2.35 and adaptation to *a*ℓTALC

For the sake of clarity, we will briefly comment which have been the major modifications and extensions performed in DIANA to adapt it to the requirements of *a*ℓTALC and the intention of this thesis.

- Named, sorted and reshaped topologies. In many cases it will be helpful to load some predefined topologies for simple processes containing up to 1-loop or 5-legs and the full set of appearing topologies being already prepared (for 2legs1loops, {3,4}legs{0,1}loops and 5legs0loops) with a visual aspect nicer than the default construction, a given name related with legs-channel-degeneracy-looptype information and fixed momenta distribution obeying symmetry properties. The arrangement of momenta follows a clockwise indexing with notation for external momenta p_i, integration loop-momenta q and internal momenta decomposition k_i (e.g. Fig. 4.4).

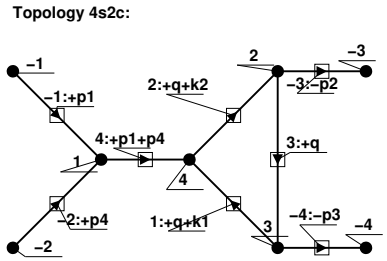

Figure 4.4: Example of momenta distribution in topology 4s2c

All the topologies can be found in the `diana/topologies/` folder, accessible with the instruction `\Begin(topology,4legs1loops.top)`, which appears by default in the driver file.

- Algorithm for topology clustering. The idea of topology clustering offers the possibility to organize the later processing of diagrams according to certain topology classes. As soon as the diagrams are invoked in a successive order of topologies it can be recognized which is the first and the last diagram within the same class. For example, if our intention is to further calculate with FORM such information is then stored into initialization values for dollar variables (`$`), allowing a flexible use in `#do` loops. This is what the output looks like:

```
#define topologiesnames "4s2c,4s4b,4s3b"
#$first4s3b =91;
#$last4s3b =114;
#$first4s4b =67;
#$last4s4b =90;
#$first4s2c =1;
#$last4s2c =66;
```

- Fermionic current analysis. Since much information related to external fermions can be extracted generically for all the diagrams, some functions were developed to decide whether a diagram belongs to the fermion channel "S","T" or "U" without analyzing the topology itself, just comparing the indices given to external fermion lines. Also new variables are set, telling us to which fermion line-index belongs any external particle and giving a suitable definition of external momenta required in the evaluation of matrix elements. This feature is particularly useful when several channels are in connection as shown in Fig. 3.2 for Bhabha scattering.

- Fermion color implementation. Many of the calculations carried out with DIANA were related to electroweak processes, it has been fruitful to simplify the models without color indices for quarks. Nevertheless, when tracing fermion loops or summing over final states, it becomes mandatory to check which color the fermions carry in the process. By telling DIANA which of the prototypes in our model file are with `color=3` (u,d are the prototypes for our quarks in the model file), a pair of variables is defined for each diagram concerning internal fermion loops and the color is added to each of the external fermions. For instance, a quark loop in a self-energy of any propagator mediating lepton-lepton scattering will lead to:

```
#define FERMIONLOOP "1"
#define COLORFACTOR "3"
...
#define color1 "1"
#define color2 "1"
#define color3 "1"
#define color4 "1"
```

- Model implementation. The model `EWSM.model` was undertaken from a less elaborated standard model file for DIANA developed by several contributors in the Theory groups at Bielefeld University and DESY Zeuthen. It has been completed[3] with all the fermion generations, the unphysical fields of the Higgs sector and the counterterm parameters in Feynman rules, as appear in Table E.3. The `QED.model` was specially created for simplicity, containing the minimal amount of fields and coupling, as shown in Table E.2.

- Inclusion of counterterm diagrams. This was a challenging subject; to reproduce counterterm diagrams which, possessing the same topological structure as the tree-level, have to be firstly considered at $O(\alpha)$, and therefore generated at loop-level. The implementation mimics high-number vertex interaction: of 5 particles for a vertex counterterm and 4 particles for propagators. A closed counterterm loop joins two extremes of a so-called counterterm propagator. The strategy was tested and successfully reproduced the required counterterms at the one-loop calculations.

[3]To the extent that $2 \to 2$ fermion processes are concerned.

- Improvement of postscript output. Through the file `diana/prg/particleaspect.prg` one may define the aspect of the propagator lines, counterterms and particle symbols appearing in the postscript-like files.

Basic driver file: Input

The driver file (e.g. `process.ini`) serves as basic input. It contains primarily:

- physical model,
- incoming and outgoing particles,
- process control flags and options.

These items are crucial for the determination of the DIANA "create" file that will serve as main user input stream for DIANA at each level, i.e. `tree` or `loop`. Only the number of loops is left to be arranged and written by the `Makefile` on the "create". For example, it is compulsory to check and agree with the five lines

```
...
SET _processname=muon_production
...
\Begin(model,EWSM.model)
...
ingoing le(;p1),Le(;p4);
outgoing lm(;-p2),Lm(;-p3);
...
options=notadp,onshell;
...
```

in `process.ini` before creating any process. For the case of μ-pair production, as considered in the previous lines, the full driver file is shown in the Fig. 4.5. Only one remark at this point: special care is needed with the momentum definitions. They all should be assigned to be incoming and clockwise indexed (e.g. `p1` addressed to be the first incoming particle, `-p2` to be the first outgoing one and so on), and making room with a blank field for the Lorentz index if required, i.e. for spin-1 particles `(index;vector)`. The reason is based on a concordance with the predefined topologies by *aî*TALC. Not following the convention used in the examples may lead to errors.

As it can be easily realized, the comment character is `*` and the `** MODIFY HERE! **` sentences indicate where some modifications are accepted. Regarding the flags for the initial settings, the topology editor (TEDI) can be launched at running time by uncommenting the line: `*SET _TOPOLOGYEDITORNAME="tedi"`.

process.ini Page 1/2

```
**********************************************************************
** Driver file for Diana 2.35 <process.ini>                         **
** This file is part of aITALC                                      **
** Copyright (C) 2004 Alejandro Lorca <alejandro.lorca@desy.de>     **
**                                                                  **
** Please, modify the file with your taste, mainly after the        **
** MODIFY HERE! sentence.                                           **
**********************************************************************

* DIANA RUNNING SETTINGS
**====================================================================
** MODIFY HERE! **
SET _processname=muon_production

** To assign direction in loop momenta and naked integration line
*SET _MARK_LOOP="YES"
** Next means remember loop momenta
*SET rlm = "rlm"

** Next (YES/NO) avoid/load
** generic topology tables and internal abstract momenta
SET _NO_TABLES="YES"
*SET _NO_TABLE_MOMENTA="NO"
*--------------------------------------------------------------------
** To be adjusted by autoconf
SET _DIANANAME=diana35
** if you want to edit the topologies:
*SET _TOPOLOGYEDITORNAME=tedi

only interpret
\openlanguage(create.tml)
\MINVERSION(2.35)
*--------------------------------------------------------------------

\Begin(program)

* MODEL TYPE
**====================================================================
** MODIFY HERE! **
*\Begin(model,QED.model)
\Begin(model,EWSM.model)
\End(model)
**--------------------------------------------------------------------

* DESCRIPTION OF OUR PROCESS (INGOING AND OUTGOING PARTICLES)
**====================================================================
\Begin(process)
** MODIFY HERE! **
ingoing le(;p1),Le(;p4);
outgoing lm(;-p2),Lm(;-p3);
** To be adjusted in the Makefile
loops=N;
\End(process)
```

process.ini Page 2/2

```
**--------------------------------------------------------------------
\loopmomenta(q)
\zeromomentum(zero)
* For the topology tables
*\token(bridge,b)
*\token(chord,k)
*\token(loop,q)
**--------------------------------------------------------------------
\include(runningrestrictions.prg)

* LOADING/CREATION OF TOPOLOGIES
**====================================================================
** When creating a topology from the scratch, please save it into
** a file and rerun Diana with that topology file.
**--------------------------------------------------------------------
** To be adjusted with the Makefile
*\tables(4legsNloops.tab)
\Begin(topology,4legsNloops.top)
\End(topology)
**--------------------------------------------------------------------
\Begin(qgrafoptions)
** MODIFY HERE! **
*options=;
options=notadp,onshell;
\End(qgrafoptions)
**--------------------------------------------------------------------

* POSTSCRIPT FLAGS AND OPTIONS
**====================================================================
\Begin(header)
**--------------------------------------------------------------------
** MODIFY HERE! **
SET MakePs = "!"
SET MakeInfo = "!"
SET MakeEps  = "!"
SET MakeInfoEps  = "!"
**--------------------------------------------------------------------
debug off
forced execute
extra call
messages disable
\End(header)
**--------------------------------------------------------------------

* TML LANGUAGE
**====================================================================
\include(thetmlstuff.prg)
**--------------------------------------------------------------------
\indices(mu1,mu2,mu3,mu4,mu5,mu6,mu7,mu8,mu9,mu10,mu11,mu12)
\vectors(p,p1,p2,p3,p4,p5,p6,k,k1,k2,k3,k4,k5,k6,q,q1,q2,zero)
**--------------------------------------------------------------------
\End(program)
```

Figure 4.5: Snapshot for `process.ini` driver file.

Implemented models

Once the driver file is fully set up, DIANA is able to offer some of the information to QGRAF and, by looking at the allowed couplings given in the model file, create the possible diagrams appearing at each level. The available model files by the moment are `QED.model` and `EWSM.model`. A summary of them is given in Table E.2 and Table E.3.

Both of these models share basic properties according to their phenomenological content. We can distinguish between the following sections:

- Propagator definitions, with general structure
  [Particle , Antiparticle ; Prototype ; Function (Prop-label , arguments) *factor ; Mass^2 .]
  - Boson, e.g. `[Wm,Wp ;W; VV(num,ind:1 ,ind:2 ,vec, 2)*i_ ;MMW]`
  - Fermion, e.g. `[le,Le;l; FF(num,fnum,vec, Mle)*i_; MMle]`
  - Ghost, e.g. `[ghZ,GhZ; Z ; SS(num,1)*i_; MMZ]`
- Vertex definitions, as
  [Interacting particles ; ; Function (arguments) *factor]

in which at later point, the specific Feynman rules will act. They are to some extent part of the model but, from a computational point of view, they belong to the module controlled by FORM programs and therefore encoded in a procedure (`ctfeynmanrules`), based in the counterterm description worked out in [43,44] but in the vector-axial basis ($V-A$) instead of left-right ($L-R$).

Topology editor

TEDI is designed to allow the user ultimate flexibility on topology naming, shaping and even defining momenta. It was developed together with DIANA as a helping tool for the topological issues of the Feynman diagrams. It requires the X window server running in the system and the windows and tab structure renders a very intuitive use, as it is shown in Fig. 4.6. Furthermore, help and printing facilities are also embedded in the program.

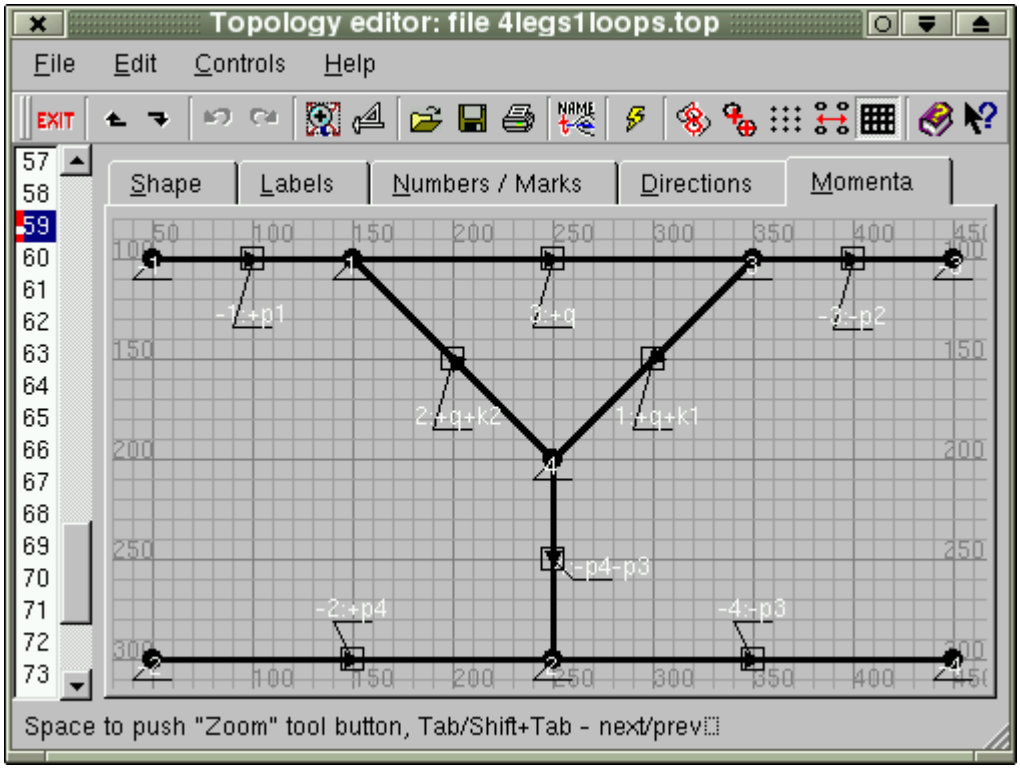

Figure 4.6: Snapshot for the momenta tab in TEDI.

The content of the five tabs has to do with

- Shape: handles with the aesthetics of the Feynman diagrams. Here the user can reshape the different legs and loops of the topology according to an optimized algorithm or to his own taste. Aligning to grid is also possible by adapting the alignment distance and toggling the key points between nodes for each object.

- Labels: External legs, internal propagators and vertices are given a label in DIANA. The location of this label might be varied with respect to the graph to avoid illegible superpositions.

- Numbers/Marks: Every line has an index that is negative for external legs and positive for internal propagators. Working this tab one can assure to give the highest index values to a loop or to fixed-momenta lines.

- Directions: The sign of the momentum flow in each internal line can be flipped by clicking on the arrow with the right-button mouse.

- Momenta: Alternative symbols can be arranged for the momenta attribute.

Apart from these main five features, a bar on the left scrolls between the different topologies that were generated for the specific process.

A deeper discussion of the possibilities of TEDI is out of the focus of a standard *aï*TALC description. Indeed it has been chosen that the default running of any of the examples does not require the topology editor at any moment. We will close this summary with the Fig. 4.7 in order to give the user an impression of the standard graphical output of TEDI.

Advanced setup

But what about if we want to exclude some couplings or modify some aspect of the diagrams?

After the installation of *aï*TALC it is also possible to use DIANA[4] as an independent package. For our present purpose, we will show shortly the tested modifications that can be performed at this level.

Once the example has been run, inside of the `tree/` directory (also the `loop/` directory in other examples) it is possible to select some files to be considered instead of the default ones coming from the following directory: `$AITALCHOME/diana/prg/`. This is automatically done by placing those files on the `examples/muon_production/` directory and remaking the process. When the process has to be run for a second time, the instructions read '`make clean`' and then '`make`' again.

We do not suggest to copy and modify any other file from `diana/prg/` since they are mostly functions using advanced DIANA declarations, but the following files are welcome to be modified:

- `particleaspect.prg`: Defines what every propagator and particle label looks like in the `.ps` and `.eps` files. The syntax is not described (just a couple of comments), but intuitive. The field label `CT` is assigned to counterterms.

- `runningrestrictions.prg`: Fields or couplings can be excluded here, as before uncommenting or replacing where desired[5].

[4] This extends also to FORM and LOOPTOOLS.

[5] Warning: As soon as you may discard some fields or couplings, be aware that the renormalization of parameters and fields is fixed and complete within each model and does not know about your intentions, so performing a consistency check of the results is mandatory.

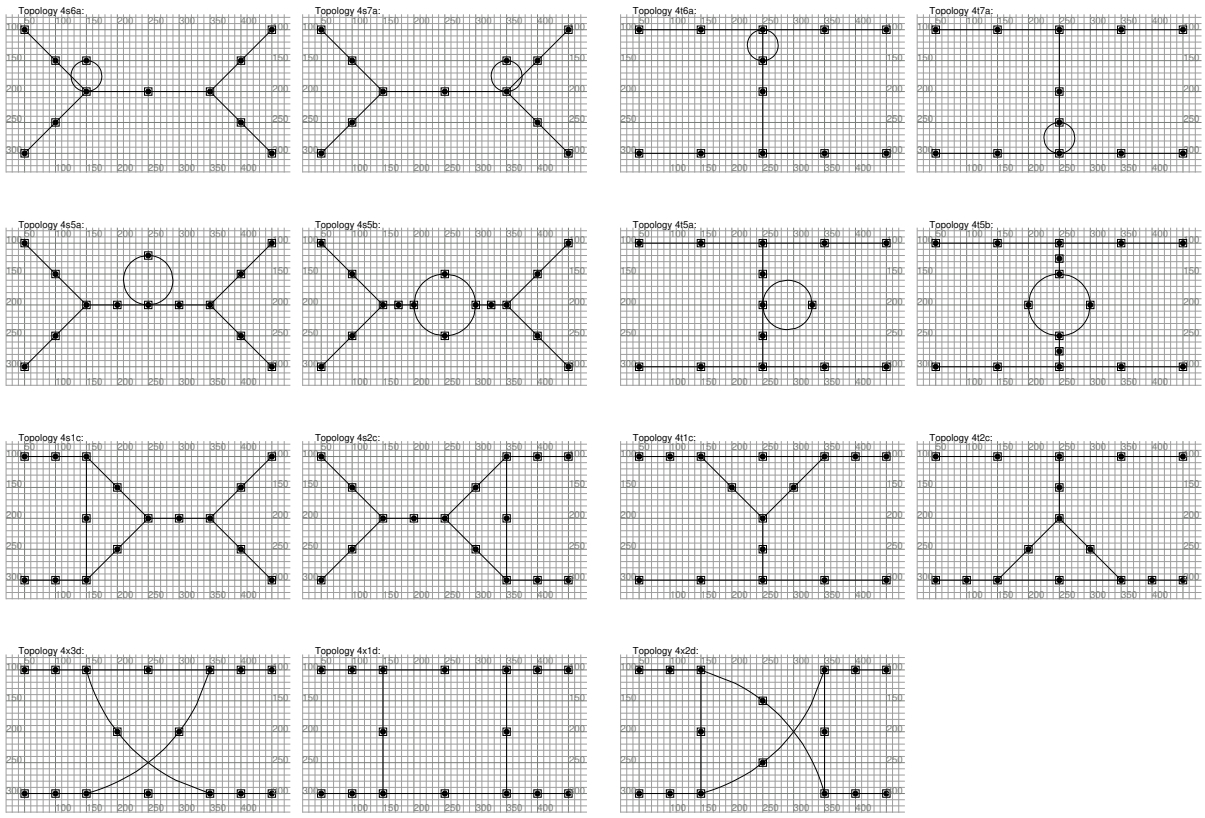

Figure 4.7: Collection of topologies given by TEDI for Bhabha scattering at one-loop level. Tadpoles on vertices account for counterterm diagrams.

What do we get?

Let's have a look inside a level directory (e.g. `tree` or `loop`): The organizer file is called `Makefile`. It has the instructions to create, organize and fill the different directories by given commands under the MAKE environment. This means that in order to build the process, only a `make` instruction is needed and nothing else is necessary but waiting while monitoring the abundant screen messages. Depending on the process, modifications, hardware and compiler the time for each module varies from seconds till several minutes[6]. At the beginning and end of each module, time stamps are placed in the `Makefile.log` file listed at Table E.1.

At this stage, the directory also offers FORM processed files that we will discuss later. By the moment we can concentrate in just two aspects:

1. **Graphical representation**. The global files `$processname.ps` and `$processnameInfo.ps` summarize all the Feynman graphs appearing in the process. Inside the `EPS/` (and `EPSInfo/`) directories one may find `.eps` files with all individual diagrams (and momenta-label def-

[6] If large files are to be compiled, occasionally the system might overload. Everything taking longer than half an hour is suspicious of going awry.

inition). Fig. 4.8 represents the two types of output for a single vertex diagram for the t-channel exchange in Bhabha scattering.

2. **Diagram info**. As it comes out of DIANA, the file `$processname.in` contains the required information about both, global process and individual diagrams. Besides a compulsory expression for the amplitude, specially useful for the FORM routines are the preprocessed variables defined for each diagram. Below we show the connection between Fig. 4.8 and their corresponding output in `$processname.in`.

```
*--#[ n11:
****(qgraf number 11)
**** (diagram 11)

#define imm1 "MMle"                #define DIAGRAM "11"
#define q1 "-q-k1"                 #define COUNTER "11"
#define loopline1 "1"              #define LINE "4"
#define imm2 "MMle"                #define FERMIONLOOP "0"
#define q2 "-q-k2"                 #define TOPOLOGY "4t1c"
#define loopline2 "1"              #define CHANNEL "t"
#define imm3 "MMA"                 #define SKELETON "1"
#define q3 "+q"                    #define LOOPTYPE "c"
#define loopline3 "1"              #define LOOPTYPENUMBER "3"
#define imm4 "MMA"                 #define PROTOTYPE "llaa"
#define q4 "+p4+p3"                #define FERMIONCHANNEL "T"
#define loopline4 "0"              #define l1 "1"
#define k1 "(+p2)"                 #define l2 "2"
#define k2 "(-p1)"                 #define l3 "1"
                                   #define l4 "2"
...

*---------------------------------------
g [Amplitude,11] =
       (-1)*F(3,1,mu2,1,0,1)*(-i_)*e*Qle*FF(1,1,-q-k1,Mle)*i_*
       F(4,1,mu4,1,0,1)*(-i_)*e*Qle*FF(2,1,-q-k2,Mle)*i_*
       F(1,1,mu1,1,0,1)*(-i_)*e*Qle*F(2,2,mu3,1,0,1)*(-i_)*e*Qle*
       VV(3,mu1,mu2,+q,0)*i_*VV(4,mu3,mu4,+p4+p3,0)*i_;

*--#] n11:
```

4.3.5 Algebra manipulation: library in FORM

Such module acts as a bridge connecting the world of the purely symbolic representation of the Feynman diagrams, directly read off the Lagrangian, and the experimental view of a numerical

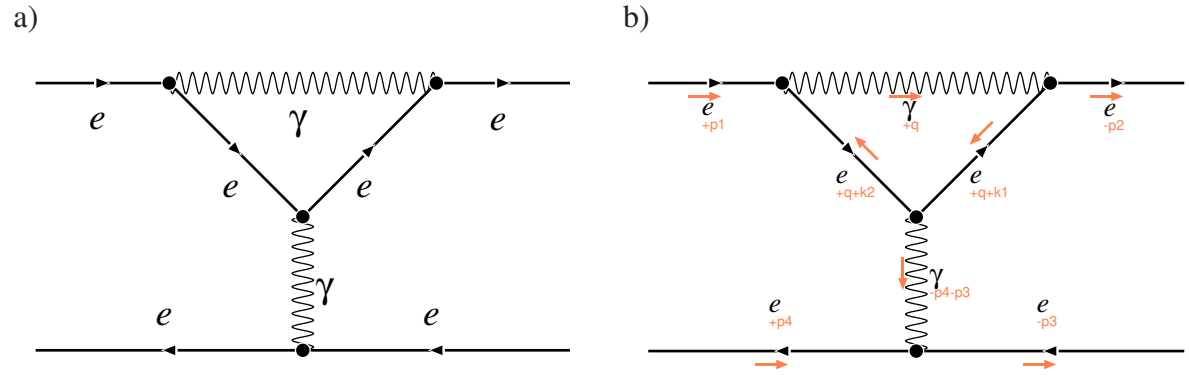

Figure 4.8: Encapsulated postscript diagrams for a typical diagram in Bhabha scattering. a) Simple diagram from `EPS/` directory, b) also with momenta distribution from `InfoEPS/`.

problem for the scattering of real particles.

As soon as DIANA has finished one of the levels, a complete description of the process falls into our hands, but still in an encoded language. Different FORM programs will prepare the amplitudes in order to render numerically evaluable expressions. Tracing, commuting γ matrices, applying the Dirac equation to external fermions or introducing the Mandelstam variables is part of the physical achievement at this module.

There are basically two kind of programs: The main routines and the procedures. We describe the four routines:

- `do_amplitude.frm`: Struggles with the most important analytical simplifications given in Sect. 3.2.2 for the individual amplitude from each diagram, extracting out the form factors in the basis of matrix elements from Eq. (3.19).

- `joinkinematics.frm`: Defines how the differential cross section should be composed in terms of fermion currents (`S`, `T` or `U`), the normalization of the incoming flux in the cross section formula, soft photon emission and the definition of the Mandelstam variables.

- `joinmm.frm`: The standard set of matrix elements is considered by this program giving, as output, the multiplication of any two elements appearing in the amplitude decomposition, as seen in Sect. 3.1.3.

- `joinff.frm`: Once all the diagrams were considered, this part pastes together the form factor contributions sorted out by topologies. The final translation into FORTRAN code is also done at this step.

`#procedures` without end

One of the most important principles in any calculation is the correctness of the expression after every step. By using procedures with a clear physical or mathematical intention, we ensure a systematic processing for the Feynman amplitudes and an easy way to eliminate potential bugs.

The listing of the procedures is long, and the description of each of them is shortly presented in Table E.4.

We would like here to draw the attention to one option regarding the neglect of the external masses of particles (e.g. light fermion masses). This can be achieved including an adapted `Neglectedmasses.inc` file into the main directory, together with the driver file `process.ini`.

Coming back to our listing of the directory given in Table E.1, we find in the files `do_amplitude.log` and `joinmm.log` information about the individual evaluation of each diagram and the kinematical factors corresponding to the product of matrix elements, respectively. Also, extra functions related with soft photon emission, flux factors and Mandelstam variables can be found in `joinkinematics.log`. As an intermediate step, individual amplitudes are stored in the `FF$processaname/` directory.

4.3.6 Getting numbers: the FORTRAN code

Up to now the expressions that were generated involve a large amount of analytical work. It is desirable to execute them and evaluate the parameters, loop integrals and finally retrieve finite form factors, clustered by topologies. They, jointly with the matrix elements, answer the question of how large is the cross section for a given process.

Considering the `fortran` module, its structure can be outlined as follows:

- `main.f, parameterlist.hf`: they both give the user access to modify the output structure of the program and the explicit values of the model respectively. In the `main.f` file we find many settings as logical flags, input of kinematics and output control.
- KITFORTRAN: consists of the full set of FORTRAN subroutines and functions needed to compile the `main.f` program. We can divide them into two categories, according to the role they play during running time.
  - **Global** are those that were fixed at installation time and considered to be process independent. They are stored at `$AITALCHOME/fortran/src`
  - **Local** are written at running time by the `tree` and `loop` modules and depend explicitly on the physical application. They are located at `$processname/fortran/src`.
- LOOPTOOLS: this library is called with the purpose of calculating the numerical value of the loop integrals.

Understanding and controlling the output

If after all, the desired scattering reaction was calculated, it is no waste of time to shortly outline an explanation on the results and how to adapt them to the user's needs.

In the table of cross section distributions (given always in pb) shown in Table 4.1 as an example, the first column corresponds to the beam energy ($\sqrt{s}$ = `sqrtsman`) given in GeV, the second one to the $\cos\theta$ (`cost`), θ being the angle between the three-momenta $\mathbf{p_1}$ and $-\mathbf{p_2}$. Later on we have successively the columns of differential cross sections (`dcs`) for the Born

approximation (Born), the interference terms of the tree and loop levels (loop) and the soft photonic corrections (soft). These three columns (third ,fourth and fifth) are summed into the sixth column (B+l+s) resulting into the finally corrected cross section. The last column loop^2 returns back the result concerning the one-loop squared terms in the perturbative approach. The maximum energy fraction that the soft photon may gain out of $\sqrt{s}$ is limited by the variable setfracomega.

```
#=============================================================================================
# aITALC Version 1.2 (17.01.2005) by A.Lorca -- T.Riemann
#---------------------------------------------------------------------------------------------
#sqrtsman   cost  dcs(Born)     dcs(loop)     dcs(soft)     dcs(B+l+s)    dcs(loop^2)
 0.5000E+03 -.900 0.9458936E-01 0.7074202E-02 -.1137770E-01 0.9028587E-01 0.9789278E-03
 0.5000E+03 -.500 0.8929449E-01 0.1142066E-01 -.1603201E-01 0.8468314E-01 0.1158249E-02
 0.5000E+03 0.000 0.1503198E+00 0.2280391E-01 -.3291616E-01 0.1402075E+00 0.1880510E-02
 0.5000E+03 0.500 0.2865049E+00 0.6366626E-01 -.7403504E-01 0.2761361E+00 0.4732650E-02
 0.5000E+03 0.900 0.4495681E+00 0.1596106E+00 -.1428113E+00 0.4663674E+00 0.1499405E-01
#=============================================================================================
#Energy given in GeV, Cross sections in pb, setfracomega= 0.1000000
```

Table 4.1: Output main.log for a complete μ-pair production example in the EWSM

If the calculation is correct, all the columns should be constant[7] under variation of the ultraviolet (UV) parameter (one can check this by turning on the flag luvcheck). The same check for the infrared (IR) behaviour (lricheck) will change the explicit values in columns loop and soft, but the sum should still be invariant! The last column may also suffer from IR variation since it is not compensated by double soft photon emission. Those loop^2 numbers are crucial when they become the leading order in, for instance, flavour changing neutral current processes, or just as an estimator of the order of magnitude for the error in the next level of perturbation theory. When integrated cross sections are under study, the integration region is limited by the setlimcost variable, the ics and fba being defined as

$$\texttt{ics} \;=\; \sigma_{\rm tot} = \int_{-\texttt{setlimcost}}^{\texttt{setlimcost}} \mathrm{d}\cos\theta\, \texttt{dcs} \tag{4.1}$$

$$\texttt{fba} \;=\; \frac{\sigma_{\rm fw}-\sigma_{\rm bw}}{\sigma_{\rm tot}} = \int_{0}^{\texttt{setlimcost}} \mathrm{d}\cos\theta\, \frac{\texttt{dcs}}{\texttt{ics}} - \int_{-\texttt{setlimcost}}^{0} \mathrm{d}\cos\theta\, \frac{\texttt{dcs}}{\texttt{ics}}. \tag{4.2}$$

$$\tag{4.3}$$

The integration algorithm is based on a Richardson extrapolation to the Romberg integration [82] with four steps. The estimated error is supplied in short forms in extra columns. If it does not suffice or with the intention of checking, the same subroutine with eight steps (ICS8) can be called instead of the faster ICS. A complete survey of variables is presented in Table E.5.

[7]Warning: as a result of numerical variation, the round off of intermediate results will modify the last digits in the results. Such variation increases at the collinear cases due to cancellations.

A luxurious possibility: quadruple precision

Not every compiler[8] allows for extended or quadruple precision. This is a feature beyond of the ANSI FORTRAN77. Even if *aï*TALC contains some code's implementations beyond the ANSI syntax, they are quite common (e.g. using underscore, or double complex), so decent compilers won't complain.

But on high level computation, or simply as comparison, switching on the quadruple precision could stabilize numerical results or render amazing agreement with other calculations.

4.3.7 Examples including loop level

To finish this descriptive section, we would like to present the examples available with the distribution.

The package is delivered with three examples that the user is expected to run without further considerations. Located at the directory `examples/` we have the following processes:

- μ-pair production at tree level: $e^-e^+ \to \mu^-\mu^+$
- Bhabha scattering in QED: $e^-e^+ \to e^-e^+$
- Flavour changing through neutral current example: $e^-e^+ \to b\bar{s}$

under the directory names of `muon_production`, `Bhabha_QED` and `leLe.bS`.

With the purpose of giving a flavour of timings expected for the execution, all the examples were studied on two different machines, representing today's typically available computers. The results are shown in Table 4.2. There we can see that when the size of the produced FORTRAN code begins to be large (i.e. more than ~200KB for a single subroutine to be compiled), then the compiling time for the GNU compiler gets extremely long, in comparison with the magnitude of the other processes.

	`muon_production`		`leLe.bS`		`bhabha_QED`	
Module	Desktop	Laptop	Desktop	Laptop	Desktop	Laptop
`tree`	9”	3”	4”	1”	30”	9”
`loop`	–	–	2’20”	52”	37”	12”
`fortran`	15”	4”	4:35’56”	33”	26”	8”
Total	24”	7”	4:38’20”	1’26”	1’33”	29”

Table 4.2: Typical timings for the different modules. The technical specifications for system Laptop are: Intel Centrino 1.5GHz cpu, 512MB RAM, Intel `icc` and `ifort` version 8.1 compilers. For Desktop: Intel Pentium III 853MHz cpu, 256MB RAM, GNU `gcc` and `g77` version 3.3.3 compilers.

[8]The use of quadruple precision has been positively tested under INTEL FORTRAN compiler (see `http://www.intel.com/software/products/compilers/flin/noncom.htm`).

Chapter 5

Results

5.1 Fermion-antifermion production

Two-fermion production processes, such as

$$e^+e^- \to f\bar{f}\,(\gamma) \qquad f \neq e^-, \tag{5.1}$$

play a dominant role at typical linear collider energies as foreseen by [20] and shown in Fig. 1.1.

In the late seventies the one-loop correction to μ-pair production was calculated for the first time [50], where the muons and electrons were considered to be massless. Ever since, fermion-pair production processes attracted much attention during the LEP era. Dedicated experimental analyses have been performed and yearly updated by the electroweak working group at CERN [16], and compared against theoretical predictions given by tools like [83] or [73].

The resulting cross section after applying the method of Sect. 3.1.1, and neglecting throughout terms proportional to the electron mass is

$$\frac{\mathrm{d}\sigma}{\mathrm{d}\cos\theta} = \frac{1}{32\pi}\frac{\beta_f}{s}C_f \sum_{i_2=1}^{4} s^2 \left(F^{(0)\,*}_{5,i_2} G^{(0)}_{5,i_2}(1+\xi_{\mathrm{soft}}) + 2\Re\mathrm{e}\left(F^{(0)\,*}_{5,i_2} G^{(1)}_{5,i_2}\right) + \ldots \right), \tag{5.2}$$

where C_f is the multiplicative factor accounting for the fermion colour in the final state (1 for leptons, 3 for quarks) and ξ_{soft} is the soft photon contribution to the cross section after factorizing the part that is proportional to the Born term. The evaluation of the form factors, F_i and $G_i \equiv \langle \mathbb{M}_{i,j} \rangle F_j$ are our next concerns.

5.1.1 Tree-level

The reaction (5.1), when considered at the tree-level of perturbation theory, is represented by four Feynman diagrams, which we divide into two categories as shown in Fig. 5.1. The important diagrams, from a quantitative point of view, which mediate the interaction are photon and Z-boson, appearing in a). The other two diagrams are very much suppressed since the coupling for the Higgs-fermion vertex is proportional to the fermion mass as shown in Eq. (2.24), which is quite small in comparison with those of the weak scale.

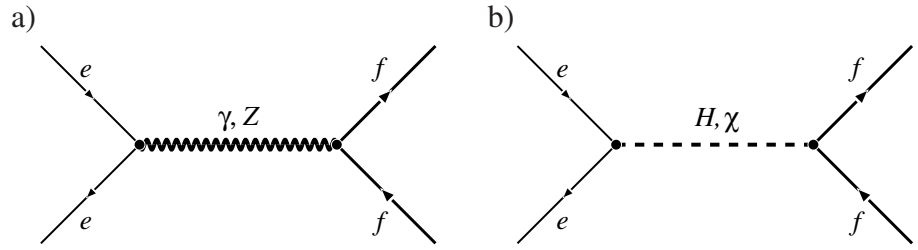

Figure 5.1: Feynman diagrams contributing at tree-level for fermion-pair production. a) Via vector boson interaction, b) Higgs-like mediation.

The form factors $F^{(0)}_{i_1,i_2}$ are extracted from the diagrams a) in Fig. 5.1 and are calculated according to the definition of the basis of matrix elements in Eq. (3.19). Since in this case no mixing of different channels occurs, we skip the superscript S indicated elsewhere. Then

$$F^{(0)}_{5,1} = \mathrm{i}e^2\left(+V_eV_f\frac{1}{s-m_Z^2}+Q_eQ_f\frac{1}{s}\right), \tag{5.3}$$

$$F^{(0)}_{5,2} = \mathrm{i}e^2\left(-V_eA_f\frac{1}{s-m_Z^2}\right), \tag{5.4}$$

$$F^{(0)}_{5,3} = \mathrm{i}e^2\left(-A_eV_f\frac{1}{s-m_Z^2}\right), \tag{5.5}$$

$$F^{(0)}_{5,4} = \mathrm{i}e^2\left(+A_eA_f\frac{1}{s-m_Z^2}\right), \tag{5.6}$$

with Q, V, A, accounting for the charge, weak vector coupling and weak axial coupling of the fermions to the photon and Z-boson.

The effective form factors $G^{(0)}_{i_1,i_2}$ read on this level:

$$G^{(0)}_{5,1} = +\left(3+2\frac{t+u}{s}+\frac{(t-u)^2}{s^2}\right)F^{(0)}_{5,1}+2\frac{t-u}{s}F^{(0)}_{5,4}, \tag{5.7}$$

$$G^{(0)}_{5,2} = +\left(3+2\frac{t+u}{s}+\frac{(t-u)^2}{s^2}\right)F^{(0)}_{5,2}+2\frac{t-u}{s}F^{(0)}_{5,3}, \tag{5.8}$$

$$G^{(0)}_{5,3} = -\left(1+2\frac{t+u}{s}-\frac{(t-u)^2}{s^2}\right)F^{(0)}_{5,3}+2\frac{t-u}{s}F^{(0)}_{5,2}, \tag{5.9}$$

$$G^{(0)}_{5,4} = -\left(1+2\frac{t+u}{s}-\frac{(t-u)^2}{s^2}\right)F^{(0)}_{5,4}+2\frac{t-u}{s}F^{(0)}_{5,1}. \tag{5.10}$$

Note that since the form factors contain a factor $\sim 1/s$ in the propagator, the cross-section of Eq. (5.2) falls off as $\sim 1/s$ beyond the Z-resonance for increasing energy, as expected.

5.1.2 Loop-level

Because our interest is the one-loop corrections to the above process, a representation in terms of Feynman diagrams is given in detail. The diagrams are grouped according to their topological structures. Understanding by f' the isospin partner for the final fermion state f, by f_i the collection of $\{e, \mu, \tau, u, c, t, d, s, b\}$ and ν_i for $\{\nu_e, \nu_\mu, \nu_\tau\}$ we have:

- Counterterms (designed to absorb the ultraviolet divergences)

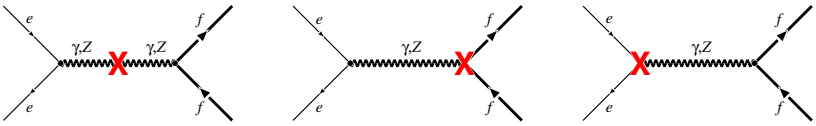

- One-point self-energies

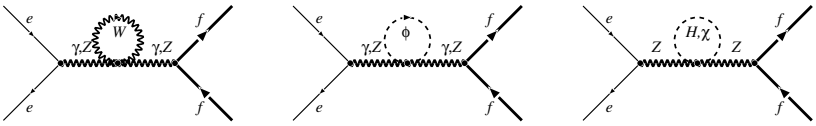

- Two-point self-energies

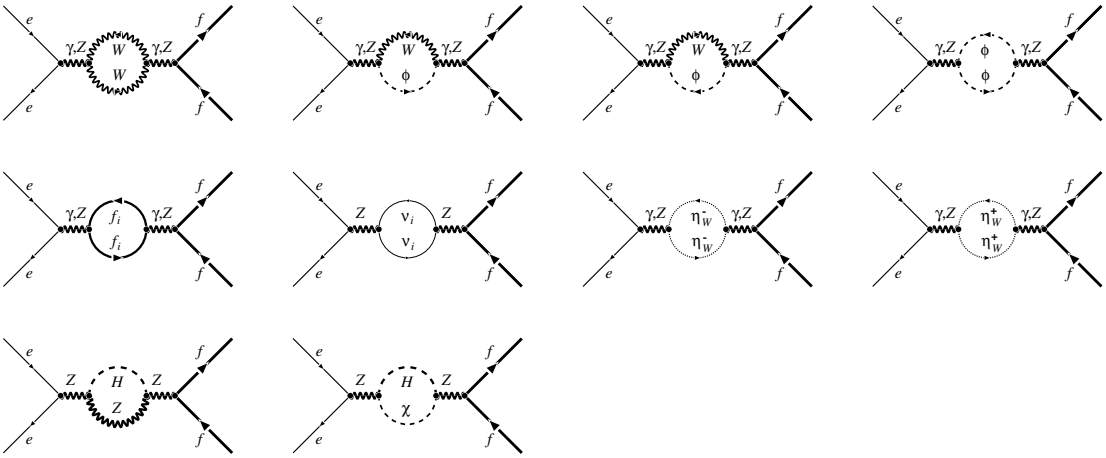

- Vertices

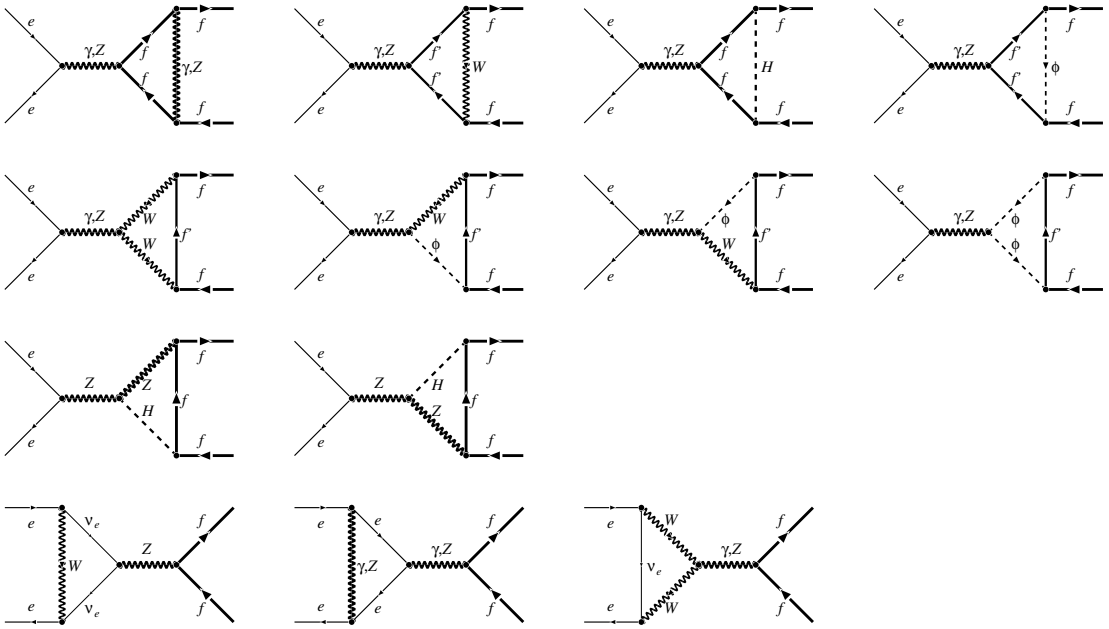

- Boxes

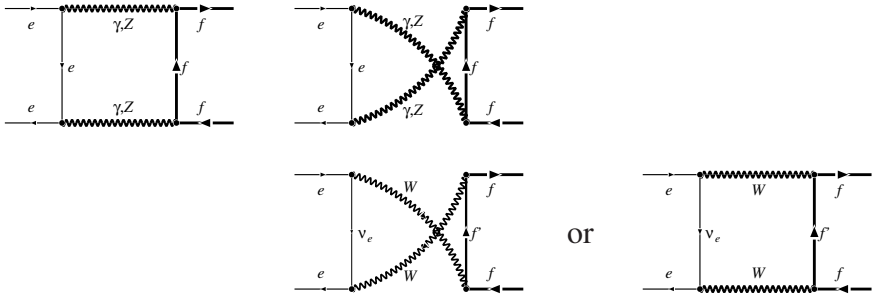

In the case of WW exchange either the crossed box diagram contributes for the case of production of isospin $\frac{1}{2}$ fermions (as neutrinos or up-type quarks) or the direct one for the case of isospin $-\frac{1}{2}$ (charged leptons or down-type quarks).

The decomposition of the effective form factors $G^{(1)}$ in terms of the standard ones $F^{(1)}$ reads

$$\begin{aligned}
G^{(1)}_{5,1} &= +\left(3+2\tfrac{t+u}{s}+\tfrac{(t-u)^2}{s^2}\right)F^{(1)}_{5,1}+2\tfrac{t-u}{s}F^{(1)}_{5,4} \\
&\quad +\left(1+2\tfrac{t+u}{s}+\tfrac{(t-u)^2}{s^2}\right)\left(\tfrac{t-u}{4}F^{(1)}_{4,1}+m_f F^{(1)}_{2,1}+\tfrac{s}{4}F^{(1)}_{4,4}\right)+2m_f\left(F^{(1)}_{7,4}-F^{(1)}_{7,1}\right), \qquad (5.11)\\
G^{(1)}_{5,2} &= +\left(3+2\tfrac{t+u}{s}+\tfrac{(t-u)^2}{s^2}\right)F^{(1)}_{5,2}+2\tfrac{t-u}{s}F^{(1)}_{5,3} \\
&\quad +\left(1+2\tfrac{t+u}{s}+\tfrac{(t-u)^2}{s^2}\right)\left(\tfrac{t-u}{4}F^{(1)}_{4,2}+m_f F^{(1)}_{2,2}+\tfrac{s}{4}F^{(1)}_{4,3}\right)+2m_f\left(F^{(1)}_{7,3}-F^{(1)}_{7,2}\right), \qquad (5.12)\\
G^{(1)}_{5,3} &= -\left(1+2\tfrac{t+u}{s}-\tfrac{(t-u)^2}{s^2}\right)F^{(1)}_{5,3}+2\tfrac{t-u}{s}F^{(1)}_{5,2} \\
&\quad +\left(1+2\tfrac{t+u}{s}+\tfrac{(t-u)^2}{s^2}\right)\left(\tfrac{t-u}{4}F^{(1)}_{4,3}+\tfrac{s}{4}F^{(1)}_{4,2}\right)+2m_f\left(F^{(1)}_{7,3}-F^{(1)}_{7,2}\right), \qquad (5.13)\\
G^{(1)}_{5,4} &= -\left(1+2\tfrac{t+u}{s}-\tfrac{(t-u)^2}{s^2}\right)F^{(1)}_{5,4}+2\tfrac{t-u}{s}F^{(1)}_{5,1} \\
&\quad +\left(1+2\tfrac{t+u}{s}+\tfrac{(t-u)^2}{s^2}\right)\left(\tfrac{t-u}{4}F^{(1)}_{4,4}+\tfrac{s}{4}F^{(1)}_{4,1}\right)+2m_f\left(F^{(1)}_{7,4}-F^{(1)}_{7,1}\right). \qquad (5.14)
\end{aligned}$$

The individual contribution of each diagram is obtained directly from the application of the techniques given in Sect. 3.2.2. The direct-box WW contribution was not present in the original TOPFIT and was added for the $b\bar{b}$-production. Therefore we present here, as an example of particular interest, the corresponding non-zero form factors

$$\begin{aligned}
F^{(1)}_{2,1} = -F^{(1)}_{2,3} &= \mathrm{i}\frac{e^4}{16\pi^2}\frac{1}{4s_{\mathrm{W}}^4}m_f\left(D_{22}+D_2\right), \qquad (5.15)\\
F^{(1)}_{2,2} = -F^{(1)}_{2,4} &= \mathrm{i}\frac{e^4}{16\pi^2}\frac{1}{4s_{\mathrm{W}}^4}m_f\left(2D_{12}+D_{22}+2D_1+D_2\right), \qquad (5.16)\\
F^{(1)}_{4,1} = F^{(1)}_{4,4} = -F^{(1)}_{4,2} = -F^{(1)}_{4,3} &= \mathrm{i}\frac{e^4}{16\pi^2}\frac{1}{4s_{\mathrm{W}}^4}\left(D_{12}+D_{22}+D_{23}+D_1+D_2+D_3\right), \qquad (5.17)\\
F^{(1)}_{5,1} = F^{(1)}_{5,4} = -F^{(1)}_{5,2} = -F^{(1)}_{5,3} &= \mathrm{i}\frac{e^4}{16\pi^2}\frac{1}{4s_{\mathrm{W}}^4}D_{00}, \qquad (5.18)
\end{aligned}$$

with the following internal arguments in the loop functions given in LOOPTOOLS notation for the 4-point function

$$D_j \equiv D_j(m_e^2, m_f^2, m_f^2, m_e^2, t, s; m_{\nu_e}^2, m_W^2, m_{f'}^2, m_W^2). \qquad (5.19)$$

The rest of the contributions is not shown because the expressions are lengthy and would occupy many pages. For this we recall that they are easily obtained with *a*i̊TALC and placed on-line in the web address [84].

5.1.3 Results

In this section we present the numerical results of the electroweak one-loop calculation of fermion-pair production. We performed a fixed-order calculation, i.e. no higher-order corrections such as photon exponentiation have been taken into account.

We compared the numbers obtained from the calculation outlined in this thesis with the results of a calculation with FEYNARTS [2], FORMCALC and LOOPTOOLS [10]. For the numerical

evaluation we assume the input values [78, 77, 80] described in Table A.1, and moreover the following restrictions to the calculations:

- diagonal CKM matrix (no couplings between different quark generations),
- neglect of terms $\propto m_e$ on form factors,
- no width for gauge bosons.

This has been discussed in detail in [77, 80] and calculated for realistic applications by dedicated Monte-Carlo programs for 2- to 6-fermion production [85, 86].

In the following we show the numerical results obtained by both calculations for various final-state fermions. The processes are sampled at typical LC energies of 500 GeV and 1 TeV. The following differential cross-sections are compared:

$\left.\frac{\mathrm{d}\sigma}{\mathrm{d}\cos\theta}\right|_{\mathrm{B}}$: Born cross-section.

$\left.\frac{\mathrm{d}\sigma}{\mathrm{d}\cos\theta}\right|_{\mathrm{B+w}}$: Born plus interference of tree with one-loop virtual weak corrections. The running of the electromagnetic coupling is included here[1].

$\left.\frac{\mathrm{d}\sigma}{\mathrm{d}\cos\theta}\right|_{\mathrm{B+w+q+s}}$: The QED + soft photon emission (with $E^{\max}_{\gamma_{\mathrm{soft}}} = \sqrt{s}/10$) is added to the previous contributions.

The Topfit calculations have been done explicitly with the modified code [1].

In Tables 5.1–5.8 we present the differential cross-sections for two generic values of $\sqrt{s}$. The first column sets the scattering angle, the second column corresponds to the tree-level calculation and serves mainly to check that we are actually comparing the same observables under the same restrictions and input. The other columns show the corrected Born with the weak (third column) and also QED+soft contributions (in fourth column). Last column is reserved for the package used.

Compared to [78], the agreement between our calculations has improved by three orders of magnitude. This has been achieved thanks to a closer contact between both groups and a more methodical programming in the Fortran code Topfit. The agreement is now up to 11 digits of technical precision. It is worth to note the effort required for setting up such kind of comparisons: agreement on the same input parameter set, the same conventions when neglecting small quantities, avoiding misunderstandings about what does actually 'weak' or 'QED' mean.

Fig. 5.2 reproduces graphically the cross section distributions at 500 GeV and 1 TeV for the production of the different fermion-pair cases. The curves for the Born level and the corrected cross section to $O(\alpha)$ ('All $O(\alpha^3)$' in the legend) correspond to the second and fourth columns of Tables 5.1–5.8. The 'Born+weak' curve reflects the same weak corrections as the third column but without the running of the electromagnetic coupling. A first glance to these figures indicates that the quantum corrections generically reduce the expected Born cross section by some percent, even if this effect becomes unclear at the edges of $\cos\theta$-axis (the beam line). The fermion masses

[1] This is not the case for the plots, where no running is included into the weak contributions.

in final state play an important role for the $t\bar{t}$ case, as seen in plot (d) when comparing versus (c) where the $c\bar{c}$ production is shown. We have to keep in mind that this difference does not arise from the values in the quantum numbers.

Other two plots are presented in Fig. 5.3, trying to emphasize the magnitude of the corrections with increasing energy for the $t\bar{t}$ and $b\bar{b}$ production. The figure on top shows the expected integrated cross section, for the whole phase space ($0^\circ \leq \theta \leq 180^\circ$). Continuous lines represent the calculation at Born level while the others, dotted and dash-dotted lines, account for the corrections with two different cuts on the maximum energy available for the soft-photon, which is related with the acollinearity of the two-fermions in the final state. The lines diverge slowly with growing energy magnifying the relevance of quantum corrections by means of Sudakov logarithms. The lower graph, scans the expected forward-backward asymmetry, defined in Eq. (3.15), up to 1 TeV. Note the phenomenological implications of the Z-boson threshold, inverting the asymmetry for the b quarks and also leading to the well-known resonance on the integrated cross section. For the top, the threshold energy for production is above the Z mass leading to positive asymmetries.

$e^+e^- \to \tau^+\tau^-(\gamma)$, $\sqrt{s} = 500$ GeV				
$\cos\theta$	$\left[\frac{d\sigma}{d\cos\theta}\right]_B$ /pb	$\left[\frac{d\sigma}{d\cos\theta}\right]_{B+w}$ /pb	$\left[\frac{d\sigma}{d\cos\theta}\right]_{B+w+q+s}$ /pb	Tool
−0.9	$0.94591\,02171\,86329 \cdot 10^{-1}$	$0.10860\,60371\,92303$	$0.92419\,02671\,14061 \cdot 10^{-1}$	TOPFIT
−0.9	$0.94591\,02171\,86327 \cdot 10^{-1}$	$0.10860\,60371\,93233$	$0.92419\,02671\,18656 \cdot 10^{-1}$	FA+FC
−0.5	$0.89298\,53117\,79858 \cdot 10^{-1}$	$0.10025\,68354\,16001$	$0.86699\,48248\,65248 \cdot 10^{-1}$	TOPFIT
−0.5	$0.89298\,53117\,79856 \cdot 10^{-1}$	$0.10025\,68354\,16428$	$0.86699\,48248\,69477 \cdot 10^{-1}$	FA+FC
0.0	$0.15032\,16827\,75192$	$0.16418\,09556\,08258$	$0.14359\,79492\,08648$	TOPFIT
0.0	$0.15032\,16827\,75192$	$0.16418\,09556\,07903$	$0.14359\,79492\,08618$	FA+FC
0.5	$0.28649\,90174\,53525$	$0.31504\,05045\,07441$	$0.28258\,86777\,59811$	TOPFIT
0.5	$0.28649\,90174\,53525$	$0.31504\,05045\,06135$	$0.28258\,86777\,59161$	FA+FC
0.9	$0.44955\,18970\,14604$	$0.50904\,21673\,78790$	$0.47648\,29191\,20038$	TOPFIT
0.9	$0.44955\,18970\,14604$	$0.50904\,21673\,76612$	$0.47648\,29191\,19623$	FA+FC

Table 5.1: Differential cross-sections for selected scattering angles for τ production at 500 GeV. Born, Born+weak, and Born+weak+QED+soft are given on different columns. The first number represents the result of the TOPFIT project while the second stands for FEYNARTS+ FORMCALC calculation.

$e^+e^- \to \tau^+\tau^-(\gamma)$, $\sqrt{s} = 1$ TeV				
$\cos\theta$	$\left[\frac{d\sigma}{d\cos\theta}\right]_B$ /pb	$\left[\frac{d\sigma}{d\cos\theta}\right]_{B+w}$ /pb	$\left[\frac{d\sigma}{d\cos\theta}\right]_{B+w+q+s}$ /pb	Tool
−0.9	$0.24337\,58691\,13477 \cdot 10^{-1}$	$0.27641\,21664\,58412 \cdot 10^{-1}$	$0.23440\,03881\,68909 \cdot 10^{-1}$	TOPFIT
−0.9	$0.24337\,58691\,13477 \cdot 10^{-1}$	$0.27641\,21664\,60671 \cdot 10^{-1}$	$0.23440\,03881\,70852 \cdot 10^{-1}$	FA+FC
−0.5	$0.22648\,34522\,34421 \cdot 10^{-1}$	$0.25087\,88401\,11477 \cdot 10^{-1}$	$0.21435\,50246\,92009 \cdot 10^{-1}$	TOPFIT
−0.5	$0.22648\,34522\,34421 \cdot 10^{-1}$	$0.25087\,88401\,12536 \cdot 10^{-1}$	$0.21435\,50246\,93075 \cdot 10^{-1}$	FA+FC
0.0	$0.37338\,94309\,20687 \cdot 10^{-1}$	$0.40075\,04507\,03072 \cdot 10^{-1}$	$0.34538\,81564\,13972 \cdot 10^{-1}$	TOPFIT
0.0	$0.37338\,94309\,20687 \cdot 10^{-1}$	$0.40075\,04507\,02276 \cdot 10^{-1}$	$0.34538\,81564\,13421 \cdot 10^{-1}$	FA+FC
0.5	$0.70698\,59649\,23715 \cdot 10^{-1}$	$0.76863\,25654\,09100 \cdot 10^{-1}$	$0.68181\,23407\,81333 \cdot 10^{-1}$	TOPFIT
0.5	$0.70698\,59649\,23714 \cdot 10^{-1}$	$0.76863\,25654\,06057 \cdot 10^{-1}$	$0.68181\,23407\,78805 \cdot 10^{-1}$	FA+FC
0.9	$0.11082\,80391\,95421$	$0.12645\,00486\,28998$	$0.11773\,76209\,15053$	TOPFIT
0.9	$0.11082\,80391\,95421$	$0.12645\,00486\,28487$	$0.11773\,76209\,14679$	FA+FC

Table 5.2: Idem as Table 5.1 at 1 TeV.

$e^+e^- \to b\bar{b}(\gamma)$, $\sqrt{s} = 500$ GeV				
$\cos\theta$	$\left[\frac{d\sigma}{d\cos\theta}\right]_B$ /pb	$\left[\frac{d\sigma}{d\cos\theta}\right]_{B+W}$ /pb	$\left[\frac{d\sigma}{d\cos\theta}\right]_{B+W+q+s}$ /pb	Tool
−0.9	$0.35947\,21020\,03927 \cdot 10^{-1}$	$0.42347\,36269\,56878 \cdot 10^{-1}$	$0.37629\,38061\,51582 \cdot 10^{-1}$	TOPFIT
−0.9	$0.35947\,21020\,03927 \cdot 10^{-1}$	$0.42347\,36269\,50374 \cdot 10^{-1}$	$0.37629\,38061\,44883 \cdot 10^{-1}$	FA+FC
−0.5	$0.52846\,99142\,94595 \cdot 10^{-1}$	$0.55564\,40895\,92051 \cdot 10^{-1}$	$0.49542\,16119\,64096 \cdot 10^{-1}$	TOPFIT
−0.5	$0.52846\,99142\,94594 \cdot 10^{-1}$	$0.55564\,40895\,84646 \cdot 10^{-1}$	$0.49542\,16119\,57136 \cdot 10^{-1}$	FA+FC
0.0	0.13444 84372 56821	0.13513 90019 99522	0.12117 62087 02347	TOPFIT
0.0	0.13444 84372 56821	0.13513 90019 97996	0.12117 62087 00907	FA+FC
0.5	0.28324 62378 51991	0.29122 72277 53244	0.26454 12363 95596	TOPFIT
0.5	0.28324 62378 51991	0.29122 72277 50185	0.26454 12363 92671	FA+FC
0.9	0.45066 58537 60950	0.48256 44834 85869	0.44708 31668 19343	TOPFIT
0.9	0.45066 58537 60950	0.48256 44834 81057	0.44708 31668 15091	FA+FC

Table 5.3: Idem as Table 5.1 for $b\bar{b}$ production at 500 GeV.

$e^+e^- \to b\bar{b}(\gamma)$, $\sqrt{s} = 1$ TeV				
$\cos\theta$	$\left[\frac{d\sigma}{d\cos\theta}\right]_B$ /pb	$\left[\frac{d\sigma}{d\cos\theta}\right]_{B+W}$ /pb	$\left[\frac{d\sigma}{d\cos\theta}\right]_{B+W+q+s}$ /pb	Tool
−0.9	$0.85256\,94949\,38769 \cdot 10^{-2}$	$0.98313\,19956\,72613 \cdot 10^{-2}$	$0.86113\,09362\,51944 \cdot 10^{-2}$	TOPFIT
−0.9	$0.85256\,94949\,38768 \cdot 10^{-2}$	$0.98313\,19956\,58270 \cdot 10^{-2}$	$0.86113\,09362\,37511 \cdot 10^{-2}$	FA+FC
−0.5	$0.12689\,55586\,65297 \cdot 10^{-1}$	$0.12711\,32506\,71243 \cdot 10^{-1}$	$0.11163\,82185\,03862 \cdot 10^{-1}$	TOPFIT
−0.5	$0.12689\,55586\,65297 \cdot 10^{-1}$	$0.12711\,32506\,69579 \cdot 10^{-1}$	$0.11163\,82185\,02235 \cdot 10^{-1}$	FA+FC
0.0	$0.32532\,44660\,76073 \cdot 10^{-1}$	$0.31258\,65157\,55267 \cdot 10^{-1}$	$0.27674\,41895\,03390 \cdot 10^{-1}$	TOPFIT
0.0	$0.32532\,44660\,76072 \cdot 10^{-1}$	$0.31258\,65157\,51750 \cdot 10^{-1}$	$0.27674\,41894\,99947 \cdot 10^{-1}$	FA+FC
0.5	$0.68639\,85356\,49626 \cdot 10^{-1}$	$0.69302\,03325\,89997 \cdot 10^{-1}$	$0.62501\,12097\,14961 \cdot 10^{-1}$	TOPFIT
0.5	$0.68639\,85356\,49626 \cdot 10^{-1}$	$0.69302\,03325\,82884 \cdot 10^{-1}$	$0.62501\,12097\,07973 \cdot 10^{-1}$	FA+FC
0.9	0.10923 62308 06567	0.12127 77274 48650	0.11240 86957 39236	TOPFIT
0.9	0.10923 62308 06567	0.12127 77274 47528	0.11240 86957 38153	FA+FC

Table 5.4: Idem as Table 5.1 for $b\bar{b}$ production at 1 TeV.

$e^+e^- \to c\bar{c}(\gamma)$, $\sqrt{s} = 500$ GeV				
$\cos\theta$	$\left[\frac{d\sigma}{d\cos\theta}\right]_B$ /pb	$\left[\frac{d\sigma}{d\cos\theta}\right]_{B+w}$ /pb	$\left[\frac{d\sigma}{d\cos\theta}\right]_{B+w+q+s}$ /pb	Tool
−0.9	$0.78403\,69156\,96992 \cdot 10^{-1}$	$0.91244\,84607\,87569 \cdot 10^{-1}$	$0.83668\,39315\,90920 \cdot 10^{-1}$	TOPFIT
−0.9	$0.78403\,69156\,96992 \cdot 10^{-1}$	$0.91244\,84607\,99371 \cdot 10^{-1}$	$0.83668\,39316\,04269 \cdot 10^{-1}$	FA+FC
−0.5	0.10411 12875 82399	0.11650 15689 39071	0.10590 20427 16561	TOPFIT
−0.5	0.10411 12875 82399	0.11650 15689 39412	0.10590 20427 16692	FA+FC
0.0	0.24770 82888 45901	0.26255 80017 68786	0.23448 15990 25778	TOPFIT
0.0	0.24770 82888 45900	0.26255 80017 67528	0.23448 15990 23961	FA+FC
0.5	0.51515 25192 73431	0.53094 95526 19036	0.46371 41775 17198	TOPFIT
0.5	0.51515 25192 73431	0.53094 95526 15566	0.46371 41775 12847	FA+FC
0.9	0.81827 79086 13557	0.83043 43356 61887	0.70026 97050 29472	TOPFIT
0.9	0.81827 79086 13556	0.83043 43356 56199	0.70026 97050 21870	FA+FC

Table 5.5: Idem as Table 5.1 for $c\bar{c}$ production at 500 GeV.

$e^+e^- \to c\bar{c}(\gamma)$, $\sqrt{s} = 1$ TeV				
$\cos\theta$	$\left[\frac{d\sigma}{d\cos\theta}\right]_B$ /pb	$\left[\frac{d\sigma}{d\cos\theta}\right]_{B+w}$ /pb	$\left[\frac{d\sigma}{d\cos\theta}\right]_{B+w+q+s}$ /pb	Tool
−0.9	$0.20476\,82671\,10479 \cdot 10^{-1}$	$0.23804\,15350\,74367 \cdot 10^{-1}$	$0.21460\,20354\,03294 \cdot 10^{-1}$	TOPFIT
−0.9	$0.20476\,82671\,10479 \cdot 10^{-1}$	$0.23804\,15350\,77280 \cdot 10^{-1}$	$0.21460\,20354\,06337 \cdot 10^{-1}$	FA+FC
−0.5	$0.26302\,86046\,48394 \cdot 10^{-1}$	$0.29192\,27449\,28377 \cdot 10^{-1}$	$0.26283\,52825\,19898 \cdot 10^{-1}$	TOPFIT
−0.5	$0.26302\,86046\,48394 \cdot 10^{-1}$	$0.29192\,27449\,29292 \cdot 10^{-1}$	$0.26283\,52825\,20679 \cdot 10^{-1}$	FA+FC
0.0	$0.61063\,66375\,83921 \cdot 10^{-1}$	$0.63092\,30352\,27478 \cdot 10^{-1}$	$0.55698\,44755\,91055 \cdot 10^{-1}$	TOPFIT
0.0	$0.61063\,66375\,83920 \cdot 10^{-1}$	$0.63092\,30352\,24633 \cdot 10^{-1}$	$0.55698\,44755\,87819 \cdot 10^{-1}$	FA+FC
0.5	0.12635 58682 75626	0.12548 22393 89320	0.10778 82066 27453	TOPFIT
0.5	0.12635 58682 75626	0.12548 22393 88519	0.10778 82066 26582	FA+FC
0.9	0.20057 22407 70464	0.19463 36446 48183	0.16019 87823 32139	TOPFIT
0.9	0.20057 22407 70464	0.19463 36446 46866	0.16019 87823 30647	FA+FC

Table 5.6: Idem as Table 5.1 for $c\bar{c}$ production at 1 TeV.

$e^+e^- \to t\bar{t}(\gamma)$, $\sqrt{s} = 500$ GeV				
$\cos\theta$	$\left[\frac{d\sigma}{d\cos\theta}\right]_B$ /pb	$\left[\frac{d\sigma}{d\cos\theta}\right]_{B+w}$ /pb	$\left[\frac{d\sigma}{d\cos\theta}\right]_{B+w+q+s}$ /pb	Tool
−0.9	0.10883 91940 76039	0.12425 90371 32943	0.11408 40955 77861	TOPFIT
−0.9	0.10883 91940 76039	0.12425 90371 33664	0.11408 40955 78964	FA+FC
−0.5	0.14227 50693 93371	0.15684 83718 76069	0.14308 12051 65511	TOPFIT
−0.5	0.14227 50693 93371	0.15684 83718 76250	0.14308 12051 65581	FA+FC
0.0	0.22547 04640 33559	0.24026 68040 30724	0.21718 80097 67412	TOPFIT
0.0	0.22547 04640 33559	0.24026 68040 30032	0.21718 80097 66323	FA+FC
0.5	0.35466 64703 33217	0.36888 65069 94389	0.32933 72739 51692	TOPFIT
0.5	0.35466 64703 33217	0.36888 65069 92599	0.32933 72739 49095	FA+FC
0.9	0.49114 37157 67761	0.50333 75116 05520	0.44290 81673 51494	TOPFIT
0.9	0.49114 37157 67761	0.50333 75116 02681	0.44290 81673 46094	FA+FC

Table 5.7: Idem as Table 5.1 for $t\bar{t}$ production at 500 GeV.

$e^+e^- \to t\bar{t}(\gamma)$, $\sqrt{s} = 1$ TeV				
$\cos\theta$	$\left[\frac{d\sigma}{d\cos\theta}\right]_B$ /pb	$\left[\frac{d\sigma}{d\cos\theta}\right]_{B+w}$ /pb	$\left[\frac{d\sigma}{d\cos\theta}\right]_{B+w+q+s}$ /pb	Tool
−0.9	$0.22785\,42327\,32090 \cdot 10^{-1}$	$0.25521\,28532\,98051 \cdot 10^{-1}$	$0.23101\,70508\,05040 \cdot 10^{-1}$	TOPFIT
−0.9	$0.22785\,42327\,32090 \cdot 10^{-1}$	$0.25521\,28533\,00748 \cdot 10^{-1}$	$0.23101\,70508\,07714 \cdot 10^{-1}$	FA+FC
−0.5	$0.29782\,13110\,31861 \cdot 10^{-1}$	$0.31863\,48943\,59857 \cdot 10^{-1}$	$0.28823\,01902\,00931 \cdot 10^{-1}$	TOPFIT
−0.5	$0.29782\,13110\,31861 \cdot 10^{-1}$	$0.31863\,48943\,60711 \cdot 10^{-1}$	$0.28823\,01902\,01653 \cdot 10^{-1}$	FA+FC
0.0	$0.61180\,06742\,25039 \cdot 10^{-1}$	$0.61591\,61295\,77963 \cdot 10^{-1}$	$0.54950\,88904\,88739 \cdot 10^{-1}$	TOPFIT
0.0	$0.61180\,06742\,25038 \cdot 10^{-1}$	$0.61591\,61295\,75474 \cdot 10^{-1}$	$0.54950\,88904\,85894 \cdot 10^{-1}$	FA+FC
0.5	0.11774 69498 88318	0.11404 76860 51226	$0.99417\,00898\,39905 \cdot 10^{-1}$	TOPFIT
0.5	0.11774 69498 88318	0.11404 76860 50527	$0.99417\,00898\,32292 \cdot 10^{-1}$	FA+FC
0.9	0.18112 20970 86446	0.17134 61927 22790	0.14426 23325 41248	TOPFIT
0.9	0.18112 20970 86446	0.17134 61927 21645	0.14426 23325 40061	FA+FC

Table 5.8: Idem as Table 5.1 for $t\bar{t}$ production at 1 TeV.

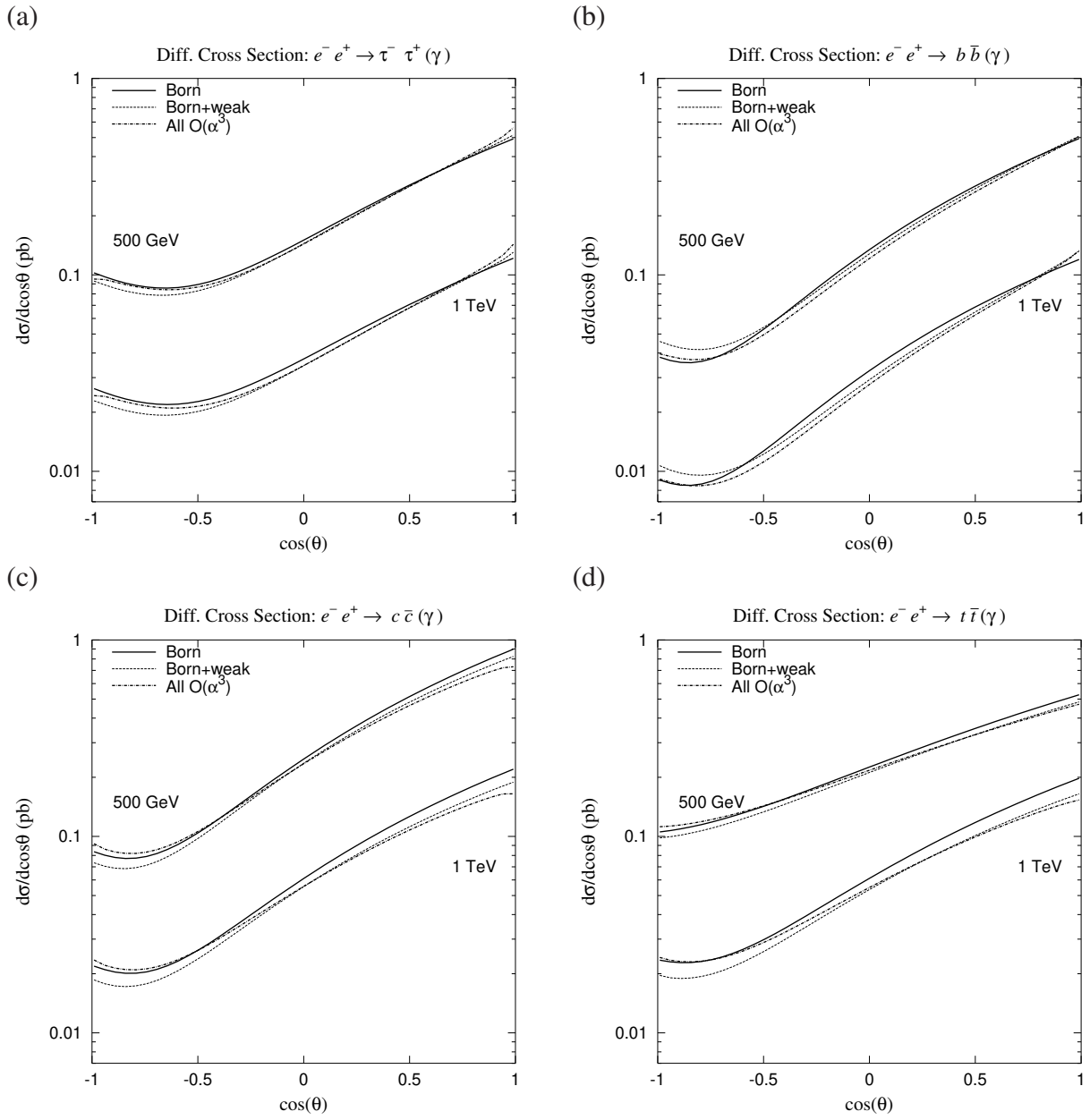

Figure 5.2: Comparison of differential cross-sections at 500 GeV and 1 TeV for (a) $\tau^+\tau^-$ production, (b) $b\bar{b}$, (c) $c\bar{c}$ and (d) $t\bar{t}$. Continuous line stands for Born, others as shown in legend for weak corrected (without running coupling) and corrected up to all $O(\alpha)$, i.e. Born+weak+QED+soft.

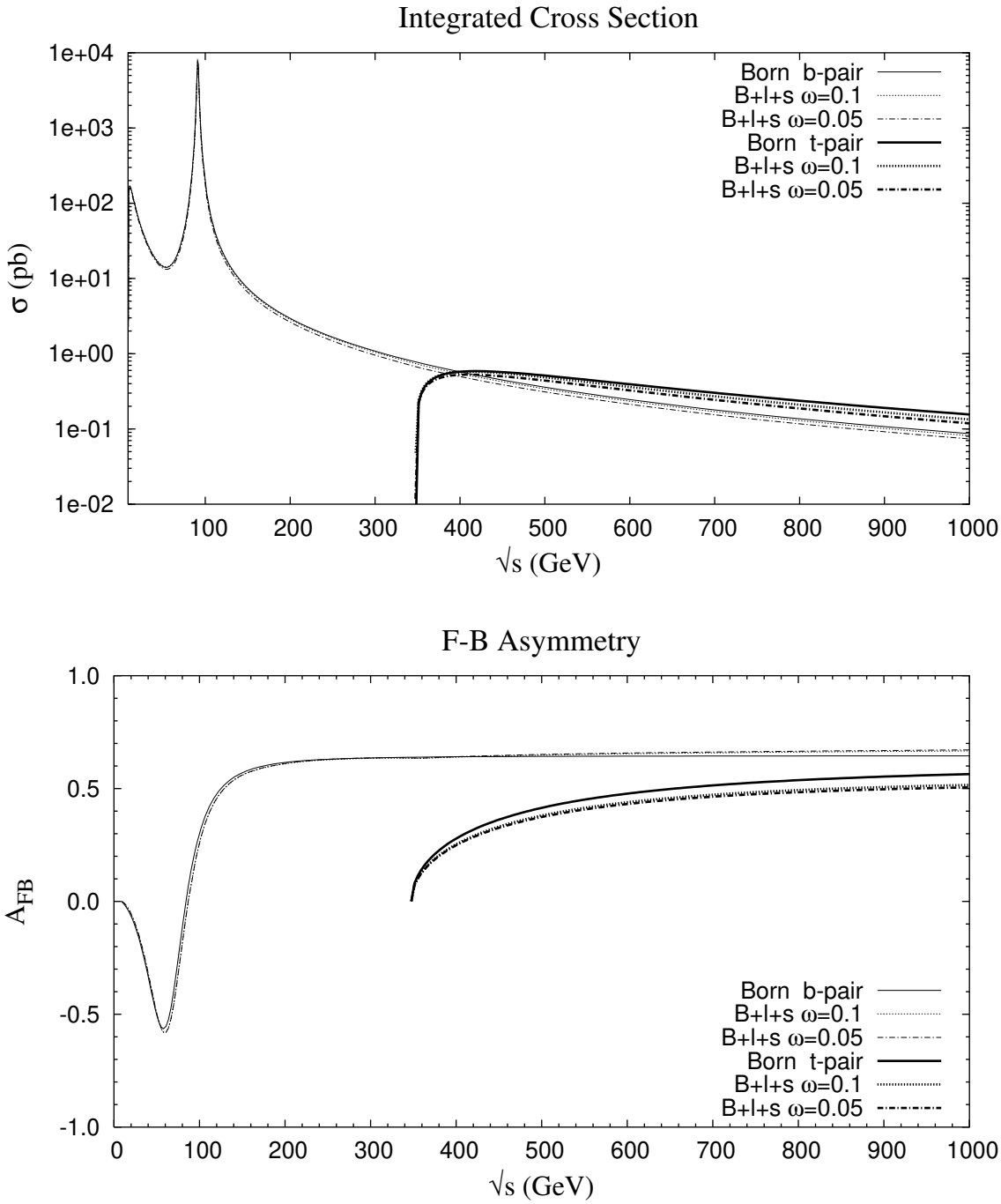

Figure 5.3: Integrated cross section (above) and Forward-backward asymmetry (below) for $b\bar{b}$ (thin lines) and $t\bar{t}$ (thick ones) production at high energies. The corrected results (B+I+s) are computed with two alternatives soft-photon maximum energy fraction, ω= 0.1 and 0.05 (`setfracomega` in Table E.5).

5.2 Bhabha scattering

In an e^+e^- collider, Bhabha scattering

$$e^+e^- \to e^+e^- \tag{5.20}$$

will surely be one of the favourite processes for calibration purposes [87, 88]. This is due to the fact that large bunch of particles in the beam is slightly deflected mainly due to electromagnetic interaction resulting in high statistics within a well understood theoretical model. The precision expectations of the measurements are around the per mill level, what could lead, for instance, to a reconstruction of the top or W masses up to few MeV.

At LEP the small angle Bhabha scattering (SABH) was approximately ranged $1^\circ \lesssim \theta \lesssim 6^\circ$. Moreover, not only high energy accelerators use this calibration technique but also B-factories as Babar or Belle. This aspect makes Bhabha scattering very important from an experimental point of view. Besides, it also shows the interesting property of interference between different production channels (pure S, T and mixed contributions), which allows to test new physics beyond the standard model already at the Born level of the theory. Even extra dimensions or new contact-interaction models might be quite sensitive to polarized configurations of Bhabha as well as Møller scattering [89].

Quantum corrections in the EWSM were calculated in [90] and followed by many studies [91,92,93], extending the complexity of analysis. Therefore, theoretical calculations have to keep up with the required level of precision requested from the experimental side, and consistently test the collinear limit.

5.2.1 In QED

Tree-level

The phenomenological implications that make Bhabha scattering so different from fermion-pair production are the possibility of production via virtual exchange of a photon in the T-channel (see (b) in Fig. 5.4), i.e. due to elastic scattering between the electron and positron, similar to Thomson scattering.

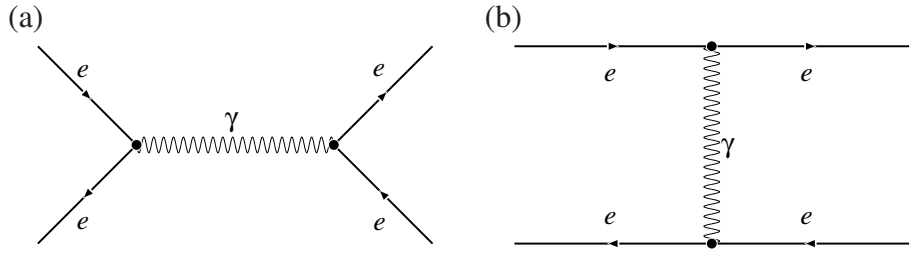

Figure 5.4: Feynman diagrams for the tree-level in QED.

The calculation of the tree-level Bhabha scattering yields the following differential cross section

$$\frac{\mathrm{d}\sigma^{(0)}}{\mathrm{d}\cos\theta} = \frac{\pi\alpha^2}{s}\left(\frac{t^2+u^2+8m_e^2(s-m_e^2)}{s^2} + \frac{2(s+t)^2-8m_e^4}{st} + \frac{s^2+u^2+8m_e^2(t-m_e^2)}{t^2}\right). \tag{5.21}$$

The three terms are respectively the product of pure S-channel contribution, S-T mixing and pure T-channel contribution.

In the massless electron limit, one obtains the well known result firstly given in [94] and in the same representation as [95], it reads

$$\lim_{m_e^2\to 0}\frac{\mathrm{d}\sigma^{(0)}}{\mathrm{d}\cos\theta} = \frac{\pi\alpha^2}{s}\left(\frac{t^2}{s^2} + u^2\left(\frac{1}{s}+\frac{1}{t}\right)^2 + \frac{s^2}{t^2}\right). \tag{5.22}$$

The last formula, is particularly handy when treating low energy (well below the electroweak scale) scattering, or at small angles (where the T-channel peaks).

Loop-level

It is a cumbersome task to present the full massive result for Bhabha scattering at one-loop order due to inverse Gram determinants showing up in the reduction of scalar to master integrals [96]. Based on shifted dimension reduction [97], the approach to Bhabha scattering in generic D-dimensions appropriately accounts for the relevant one-loop contributions to $O(\alpha^2)$ corrections [98] and in this connection a compact presentation was elaborated taking into account a finite electron mass [13]. In the limit of vanishing electron mass, however, the expressions become quite short and will be presented below for individual contributions for the interference $\mathcal{M}^{S,(0)^*}\mathcal{M}^{(1)}$.

The following notation for the *vector* fermion field counterterm,

$$\delta Z_e^V = \frac{1}{2}\left(\delta Z_{ee}^R + \delta Z_{ee}^L\right), \tag{5.23}$$

is related to the explicit counterterm definitions in Eqs. (2.81−2.93). We also introduce convenient dimensionless definitions for the loop integrals

$$B_e \equiv B_0(m_e^2;0,m_e^2), \tag{5.24}$$
$$B_s^e \equiv B_0(s;m_e^2,m_e^2), \tag{5.25}$$
$$B_s^\gamma \equiv B_0(s;0,0), \tag{5.26}$$
$$\tilde{C}_s^\gamma \equiv sC_0(m_e^2,m_e^2,s;0,m_e^2,0), \tag{5.27}$$
$$\tilde{C}_s^e \equiv sC_0(m_e^2,s,m_e^2;0,m_e^2,m_e^2), \tag{5.28}$$
$$\tilde{D}_{st} \equiv stD_0(m_e^2,m_e^2,m_e^2,m_e^2,s,t;0,m_e^2,0,m_e^2), \tag{5.29}$$

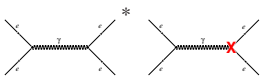

$$= e^4 \frac{t^2+u^2}{s^2}\left(2\delta Z_e + \delta Z_{AA} + 2\delta Z_e^{f,V}\right), \tag{5.30}$$

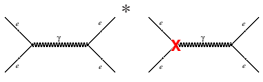

$$= e^4 \frac{t^2+u^2}{s^2}\left(2\delta Z_e + \delta Z_{AA} + 2\delta Z_e^{f,V}\right), \tag{5.31}$$

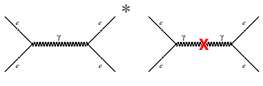

$$= e^4 \frac{t^2+u^2}{s^2}\left(-2\delta Z_{AA}\right), \tag{5.32}$$

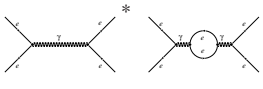

$$= \frac{e^6}{\pi^2}\frac{t^2+u^2}{s^2}\left(+\frac{1}{18} - \frac{1}{6}B_s^e\right), \tag{5.33}$$

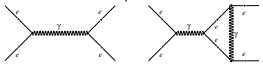

$$= \frac{e^6}{\pi^2}\frac{t^2+u^2}{s^2}\left(-\frac{1}{4} + \frac{1}{2}B_e - \frac{3}{8}B_s^e - \frac{1}{4}\tilde{C}_s^e\right), \tag{5.34}$$

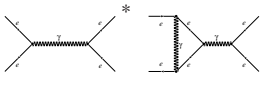

$$= \frac{e^6}{\pi^2}\frac{t^2+u^2}{s^2}\left(-\frac{1}{4} + \frac{1}{2}B_e - \frac{3}{8}B_s^e - \frac{1}{4}\tilde{C}_s^e\right), \tag{5.35}$$

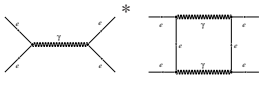

$$= \frac{e^6}{\pi^2}\left(-\frac{1}{4}\frac{u}{s}\left(B_s^\gamma - B_t^e\right) - \frac{1}{4}\frac{t-u}{s}\tilde{C}_t^e + \frac{1}{4}\frac{3t^2+u^2}{s^2}\tilde{C}_s^\gamma - \frac{1}{8}\frac{s^2+u^2}{st}\tilde{D}_{ts}\right), \tag{5.36}$$

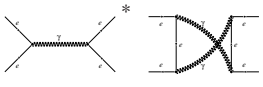

$$= \frac{e^6}{\pi^2}\left(\frac{1}{4}\frac{t}{s}\left(B_s^\gamma - B_u^e\right) - \frac{1}{4}\frac{t-u}{s}\tilde{C}_u^\gamma - \frac{1}{8}\frac{t^2+3u^2}{s^2}\left(2\tilde{C}_s^\gamma - \tilde{D}_{su}\right)\right), \tag{5.37}$$

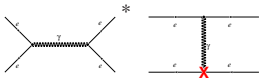

$$= e^4 \frac{u^2}{st}\left(2\delta Z_e + \delta Z_{AA} + 2\delta Z_e^{f,V}\right), \tag{5.38}$$

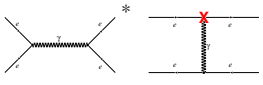

$$= e^4 \frac{u^2}{st}\left(2\delta Z_e + \delta Z_{AA} + 2\delta Z_e^{f,V}\right), \tag{5.39}$$

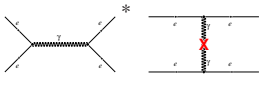

$$= e^4 \frac{u^2}{st}\left(-2\delta Z_{AA}\right), \tag{5.40}$$

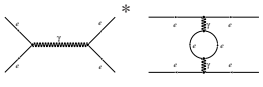

$$= \frac{e^6}{\pi^2}\frac{u^2}{st}\left(+\frac{1}{18} - \frac{1}{6}B_t^e\right), \tag{5.41}$$

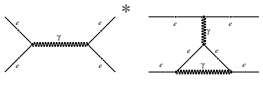

$$= \frac{e^6}{\pi^2}\frac{u^2}{st}\left(-\frac{1}{4} + \frac{1}{2}B_e - \frac{3}{8}B_t^e - \frac{1}{4}\tilde{C}_t^e\right), \tag{5.42}$$

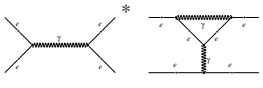

$$= \frac{e^6}{\pi^2}\frac{u^2}{st}\left(-\frac{1}{4} + \frac{1}{2}B_e - \frac{3}{8}B_t^e - \frac{1}{4}\tilde{C}_t^e\right), \tag{5.43}$$

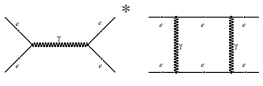

$$= \frac{e^6}{\pi^2}\left(-\frac{1}{4}\frac{u}{s}\left(B_t^\gamma - B_s^e\right) - \frac{1}{4}\frac{s-u}{s}\tilde{C}_s^e + \frac{1}{4}\frac{s^2+u^2}{st}\tilde{C}_t^\gamma - \frac{1}{8}\frac{3t^2+u^2}{st}\tilde{D}_{st}\right), \tag{5.44}$$

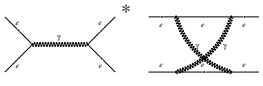

$$= \frac{e^6}{\pi^2}\frac{u^2}{st}\left(-\frac{1}{2}\tilde{C}_t^\gamma + \frac{1}{4}\tilde{D}_{tu}\right). \tag{5.45}$$

Due to crossing symmetry it is not necessary to evaluate further diagrams. For instance, any $\mathcal{M}^{T,(0)^*}\mathcal{M}^{(1)}$ is immediately obtained by performing the following substitutions in the homonymous diagram

$$\mathcal{M}^{T,(0)^*}\mathcal{M}^{S,(1)} = \mathcal{M}^{S,(0)^*}\mathcal{M}^{T,(1)}\Big|_{s\leftrightarrow t}, \tag{5.46}$$

$$\mathcal{M}^{T,(0)^*}\mathcal{M}^{T,(1)} = \mathcal{M}^{S,(0)^*}\mathcal{M}^{S,(1)}\Big|_{s\leftrightarrow t}. \tag{5.47}$$

5.2.2 Within the EWSM

Including the weak effects leads to a doubling (quadrupling if masses are considered) of the diagrams already shown in Fig. 5.4 for the tree-level. Therefore we get the eight diagrams in Fig. 5.5.

To some extent, the inclusion of the Higgs-like diagrams is physically irrelevant, but they have been kept for two reasons: on the one hand it is required from an academic point of view to take into account the complete set of contributions within the working model and include the correct description of the longitudinal modes of the Z-boson via χ. On the other hand it allows to test the numerical precision of the code since inappropriate cancellations of $\mathcal{O}(m_e^2/s)$ and smaller will lead to evident disagreement after the ~11th digit[2], see Table 5.12. We could denote such an activity as technical precision implementation.

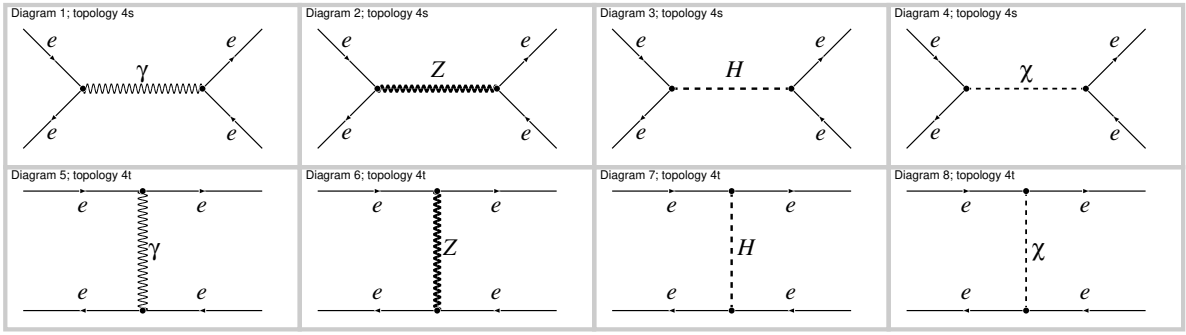

Figure 5.5: Set of graphs when considering the full massive case.

The evaluation of the form factors at tree-level gives for the different channels ($C_i = S, T$ and $c_i = s, t$ being the corresponding Mandelstam variables)

$$F_{1,1}^{C_i} = +\mathrm{i}e^2\left(\frac{m_e^2}{4s_W^2 m_W^2}\frac{1}{c_i - m_H^2}\right), \tag{5.48}$$

$$F_{1,4}^{C_i} = -\mathrm{i}e^2\left(\frac{m_e^2}{4s_W^2 m_W^2}\frac{1}{c_i - m_Z^2}\right), \tag{5.49}$$

$$F_{5,1}^{C_i} = +\mathrm{i}e^2\left(V_e V_e\frac{1}{c_i - m_Z^2} + Q_e Q_e\frac{1}{c_i}\right), \tag{5.50}$$

$$F_{5,2}^{C_i} = F_{5,3}^{C_i} = -\mathrm{i}e^2\left(V_e A_e\frac{1}{c_i - m_Z^2}\right), \tag{5.51}$$

$$F_{5,4}^{C_i} = +\mathrm{i}e^2\left(A_e A_e\frac{1}{c_i - m_Z^2}\right), \tag{5.52}$$

and for the complete evaluation of the form factors at loop-level we refer, as in the fermion-pair production case, to the online address [84] where they are available in electronic form.

[2]For comparison purposes the electron mass was deliberately increased in order to perform more evident tests.

5.2.3 Results for cross sections distributions

This part will have similar structure as in Sect. 5.1.3, but this time the numerics were computed with *a*ɪTALC (therefore weak corrections will not be separated from the rest of $O(\alpha)$: electromagnetic and soft) and focusing on different issues.

$e^-e^+ \to e^-e^+(\gamma)$, $\sqrt{s} = m_Z$			
$\cos\theta$	$\left[\frac{d\sigma}{d\cos\theta}\right]_B$ /pb	$\left[\frac{d\sigma}{d\cos\theta}\right]_{B+l+s}$ /pb	error O
−0.9	$0.12201 \cdot 10^4$	$0.11767 \cdot 10^4$	$0.8 \cdot 10^2$
−0.7	$0.10099 \cdot 10^4$	$0.95012 \cdot 10^3$	$0.5 \cdot 10^2$
−0.5	$0.85685 \cdot 10^3$	$0.79246 \cdot 10^3$	$0.4 \cdot 10^2$
+0.0	$0.73164 \cdot 10^3$	$0.64561 \cdot 10^3$	$0.3 \cdot 10^2$
+0.5	$0.10701 \cdot 10^4$	$0.91360 \cdot 10^3$	$0.4 \cdot 10^2$
+0.7	$0.16162 \cdot 10^4$	$0.13917 \cdot 10^4$	$0.5 \cdot 10^2$
+0.9	$0.70112 \cdot 10^4$	$0.63472 \cdot 10^4$	$0.1 \cdot 10^3$
+0.99	$0.62198 \cdot 10^6$	$0.57186 \cdot 10^6$	$0.5 \cdot 10^4$
+0.999	$0.62612 \cdot 10^8$	$0.57540 \cdot 10^8$	$0.3 \cdot 10^6$
+0.9999	$0.62666 \cdot 10^{10}$	$0.57822 \cdot 10^{10}$	$0.3 \cdot 10^8$

Table 5.9: Numerical prediction for Bhabha scattering at $\sqrt{s} = m_Z$ for different angles in the EWSM. Born and corrected to $O(\alpha)$ differential cross sections are shown considering the effects of the Z-boson width. Maximum soft-photon energy $E^{\max}_{\gamma_{\text{soft}}} = 0.1\sqrt{s}$.

Table 5.9 contains a distribution of differential cross sections evaluated on the Z-resonance for different scattering angles. The width of the Z-boson has been included here following the algorithm presented in Sect. 3.4, rendering finite results for Born (B) and Born+loop+soft (B+l+s) corrected cross section, given by the second and third columns respectively. The last column gives the minimal expected error coming from some of the $O(\alpha^2)$ corrections, calculated by squaring the one-loop amplitudes. This is of course not a complete estimation of the theoretical error to the corrections, but just give a flavour about the order of magnitude and it is included for this purpose. Note that due to the fact of having a possible mode of elastic photon exchange, (b) diagram in Fig. 5.4, the differential cross section diverges in the collinear limit with the beam line, $\theta \to 0$. With the intention to analyze the low angle limit, several values for small θ are picked up in this limit.

The next distribution is given for 1 TeV beam energy, and shown in Table 5.10. The columns show, as in the previous case, the scattering angle, Born and corrected differential cross sections. No Z-boson width is considered any more in these values, which are shown in FORTRAN double precision. The corrections shift down the values of the Born level around 10% as on the top of the resonance, this value being dependent on our assumption of the maximum energy cut for the soft-photon, kept as $E^{\max}_{\gamma_{\text{soft}}} = 0.1\sqrt{s}$.

A dedicated model comparison is shown in Table 5.11 for a typical linear collider energy of 500 GeV. The EWSM is compared with two slightly different QED models, one with all possible interacting fermions ($N_f = 9$), and the other with the simplest QED model in which

$e^-e^+ \to e^-e^+(\gamma)$, $\sqrt{s} = 1000$ GeV			
$\cos\theta$	$\left[\frac{d\sigma}{d\cos\theta}\right]_B$ /pb	$\left[\frac{d\sigma}{d\cos\theta}\right]_{B+1+S}$ /pb	error O
−0.9	$0.54100\,60681\,64279 \cdot 10^{-1}$	$0.47777\,39921\,39206 \cdot 10^{-1}$	$0.1 \cdot 10^{-1}$
−0.7	$0.56920\,95992\,22834 \cdot 10^{-1}$	$0.50995\,25132\,81724 \cdot 10^{-1}$	$0.1 \cdot 10^{-1}$
−0.5	$0.64161\,39356\,97570 \cdot 10^{-1}$	$0.57691\,07222\,77231 \cdot 10^{-1}$	$0.1 \cdot 10^{-1}$
+0.0	$0.14599\,89803\,30281 \cdot 10^{0}$	$0.12983\,16513\,84542 \cdot 10^{0}$	$0.2 \cdot 10^{-1}$
+0.5	$0.10505\,15972\,95452 \cdot 10^{1}$	$0.91292\,16161\,79924 \cdot 10^{0}$	$0.1 \cdot 10^{0}$
+0.7	$0.40040\,74544\,01839 \cdot 10^{1}$	$0.34831\,93169\,52564 \cdot 10^{1}$	$0.5 \cdot 10^{0}$
+0.9	$0.49148\,80960\,11362 \cdot 10^{2}$	$0.43570\,63678\,46291 \cdot 10^{2}$	$0.4 \cdot 10^{1}$
+0.99	$0.52546\,99743\,47099 \cdot 10^{4}$	$0.48234\,34869\,96972 \cdot 10^{4}$	$0.2 \cdot 10^{3}$
+0.999	$0.52099\,37736\,86769 \cdot 10^{6}$	$0.48032\,99865\,85226 \cdot 10^{6}$	$0.9 \cdot 10^{4}$
+0.9999	$0.52109\,69210\,29068 \cdot 10^{8}$	$0.47889\,96899\,36299 \cdot 10^{8}$	$0.4 \cdot 10^{6}$

Table 5.10: Numerical prediction for Bhabha scattering at $\sqrt{s} = 1$TeV for different angles in the EWSM. Born and corrected to $O(\alpha)$ differential cross sections are shown. Maximum soft-photon energy $E^{\max}_{\gamma_{\text{soft}}} = 0.1\sqrt{s}$.

only electrons and positrons are present ($N_f = 1$). The scattering angle θ is set in the first and second columns, in terms of radians and its cosine. The third column gives the Born result in the EWSM, which is going to be the reference. Later the fourth and fifth columns show the expected Born result in QED and the percent difference with the third column. In a similar way, the one-loop EWSM corrected cross section is shown in the sixth and seventh columns. The one-loop QED corrected distributions are given in the rest of the table as for the EWSM case.

It is particularly interesting to observe that even if the EWSM corrections reduce the Born result by approximately 8%, from which a sizeable amount of them (in the small angle limit) can be accounted by the full flavoured QED model. This means indeed that a difference of only 4‰ is due to pure weak effects. Moreover, the simple QED model with $N_f = 1$ does not get close enough to the weak corrections in the limit of small angle, because the running of the electromagnetic coupling is not accomplished with the full family of fermion loops. An immediate interpretation of this feature is that for a very precise determination (below per mill level) of the theoretical uncertainties in the luminosity, at least the complete two-loop QED corrections (see [99, 100, 101] and references therein) with all families (or improved treatment of the α running) plus one-loop EWSM corrections are required.

Finally Table 5.12 provides a test of numerical comparisons between our *a*ĭTALC package (first row and in quadruple precision) and an independent package composed out of FeynArts + FormCalc + LoopTools(second row in double precision). To share the same input values, Table A.1 was used with an extra restriction: treating the CKM matrix as the identity. For three angles, the vanishing electron mass result is also given, showing that the agreement after the 10th digit is forced by finite electron mass effects, testing therefore the contributions from the Higgs sector. The outstanding agreement is limited only by the possibilities of the compiler since double presicion is saturated (∼15 digits) in both, Born and full electroweak corrections.

rad	$\cos\theta$	Born EWSM	Born QED		$O(\alpha)$ EWSM		$O(\alpha)$ QED $N_f = 9$		$O(\alpha)$ QED $N_f = 1$	
2.691	−0.9000	$2.16999 \cdot 10^{-1}$	$5.23874 \cdot 10^{-1}$	141.4177%	$1.93445 \cdot 10^{-1}$	−10.85%	$4.69800 \cdot 10^{-1}$	116.50%	$4.09075 \cdot 10^{-1}$	88.51%
2.346	−0.7000	$2.30098 \cdot 10^{-1}$	$5.49082 \cdot 10^{-1}$	138.6290%	$2.08843 \cdot 10^{-1}$	−9.24%	$5.03879 \cdot 10^{-1}$	118.98%	$4.40481 \cdot 10^{-1}$	91.43%
2.094	−0.5000	$2.61360 \cdot 10^{-1}$	$6.11601 \cdot 10^{-1}$	134.0066%	$2.38707 \cdot 10^{-1}$	−8.67%	$5.66238 \cdot 10^{-1}$	116.65%	$4.96107 \cdot 10^{-1}$	89.82%
1.571	+0.0000	$5.98142 \cdot 10^{-1}$	$1.17254 \cdot 10^{0}$	96.0296%	$5.46677 \cdot 10^{-1}$	−8.60%	$1.09322 \cdot 10^{0}$	82.77%	$9.63358 \cdot 10^{-1}$	61.06%
1.047	+0.5000	$4.21273 \cdot 10^{0}$	$5.50441 \cdot 10^{0}$	30.6613%	$3.81301 \cdot 10^{0}$	−9.49%	$5.13530 \cdot 10^{0}$	21.90%	$4.56641 \cdot 10^{0}$	8.40%
0.795	+0.7000	$1.58240 \cdot 10^{1}$	$1.76316 \cdot 10^{1}$	11.4235%	$1.43357 \cdot 10^{1}$	−9.41%	$1.64548 \cdot 10^{1}$	3.99%	$1.47180 \cdot 10^{1}$	−6.99%
0.451	+0.9000	$1.89160 \cdot 10^{2}$	$1.89118 \cdot 10^{2}$	−0.0222%	$1.72928 \cdot 10^{2}$	−8.58%	$1.76464 \cdot 10^{2}$	−6.71%	$1.59652 \cdot 10^{2}$	−15.60%
0.142	+0.9900	$2.06556 \cdot 10^{4}$	$2.06382 \cdot 10^{4}$	−0.0840%	$1.90607 \cdot 10^{4}$	−7.72%	$1.91774 \cdot 10^{4}$	−7.16%	$1.77511 \cdot 10^{4}$	−14.06%
0.045	+0.9990	$2.08236 \cdot 10^{6}$	$2.08243 \cdot 10^{6}$	0.0031%	$1.91624 \cdot 10^{6}$	−7.98%	$1.92546 \cdot 10^{6}$	−7.53%	$1.82205 \cdot 10^{6}$	−12.50%
0.014	+0.9999	$2.08429 \cdot 10^{8}$	$2.08430 \cdot 10^{8}$	0.0005%	$1.91402 \cdot 10^{8}$	−8.17%	$1.92270 \cdot 10^{8}$	−7.75%	$1.85456 \cdot 10^{8}$	−11.02%

Table 5.11: Numerical prediction for Bhabha scattering at $\sqrt{s} = 500\text{GeV}$ for different angles. Born and $O(\alpha)$ corrections are shown in different columns for the EWSM, the QED model with all fermion species ($N_f = 9$)and with only one electron ($N_f = 1$).

$\cos\theta$	$\left[\frac{d\sigma}{d\cos\theta}\right]_{\text{Born}}$ (pb)	$\left[\frac{d\sigma}{d\cos\theta}\right]_{O(\alpha^3)=\text{Born+QED+weak+soft}}$	Group
−0.9999	0.21482 70434 05632 80532 92137 22041 522	0.14889 12189 28380 81306 77293 15050 269	*a*ĩTALC
−0.9999	0.21482 70434 05633	0.14889 12189 28404	*FA* + *FC*
−0.9	0.21699 88288 10920 47030 98714 36154 378	0.19344 50785 26862 70315 89749 62997 896	*a*ĩTALC
−0.9	0.21699 88288 10920	0.19344 50785 26862	*FA* + *FC*
−0.9	0.21699 88288 41513	0.19344 50785 62638	$m_e = 0$
+0.0	0.59814 23072 50330 72189 85566 54984 067	0.54667 71794 69423 03528 77433 99277 261	*a*ĩTALC
+0.0	0.59814 23072 50329	0.54667 71794 69422	*FA* + *FC*
+0.0	0.59814 23072 88584	0.54667 71794 99961	$m_e = 0$
+0.9	$0.18916\,03223\,32270\,65918\,47771\,84443\,698 \cdot 10^{3}$	$0.17292\,83490\,66508\,29307\,47453\,57027\,839 \cdot 10^{3}$	*a*ĩTALC
+0.9	$0.18916\,03223\,32271 \cdot 10^{3}$	$0.17292\,83490\,66508 \cdot 10^{3}$	*FA* + *FC*
+0.9	$0.18916\,03223\,31849 \cdot 10^{3}$	$0.17292\,83490\,61347\,4 \cdot 10^{3}$	$m_e = 0$
+0.9999	$0.20842\,90676\,46390\,74378\,73935\,63676\,670 \cdot 10^{9}$	$0.19140\,17861\,11883\,04292\,09879\,74774\,038 \cdot 10^{9}$	*a*ĩTALC
+0.9999	$0.20842\,90676\,46436 \cdot 10^{9}$	$0.19140\,17861\,11979 \cdot 10^{9}$	*FA* + *FC*

Table 5.12: Numerical comparison of Bhabha scattering at $\sqrt{s} = 500$ GeV against the package FeynArts+FormCalc and against the massless electron case. Numbers for *a*ĩTALC are shown in quadruple precision.

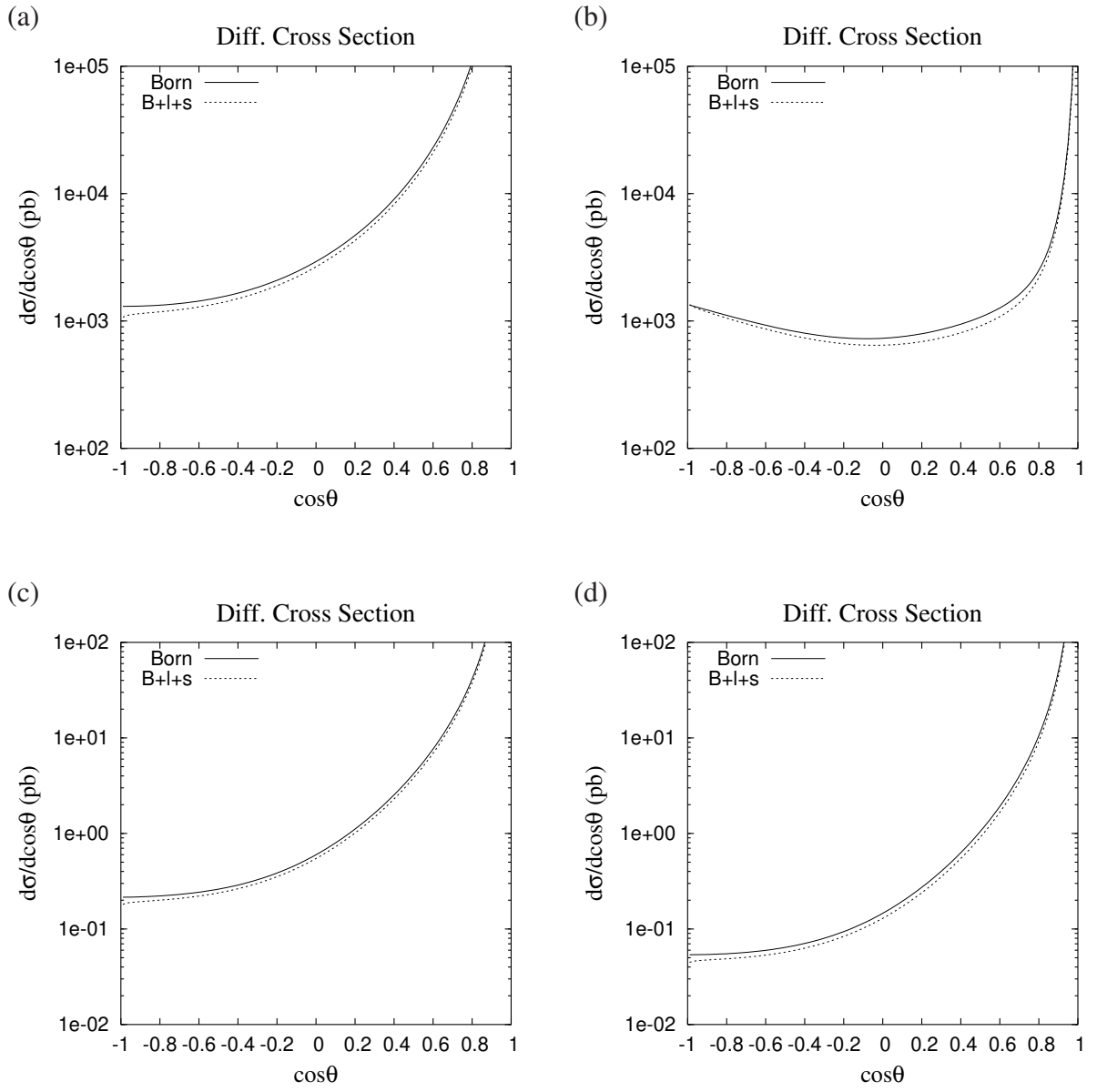

Figure 5.6: Differential cross sections at different energies for Bhabha scattering: (a) $\sqrt{s} = 10\,\text{GeV}$, (b) $\sqrt{s} = m_Z$, (c) $\sqrt{s} = 500\,\text{GeV}$, (d) $\sqrt{s} = 1000\,\text{GeV}$. Corrected cross sections are identified in the legend by B+I+s.

We switch now to the description of the plots. In Fig. 5.6 we can find the extension of Tables 5.9–5.10, given by the frames (b) and (d), respectively, with some other samples for differential cross sections at (a) 10 GeV and (c) 500 GeV (as in Table 5.11 for EWSM). The sequence shows how the shape of the differential cross section changes and gets reduced with increasing energy, as well as emphasizes the effect of the corrections on the Z-resonance. As for the case of fermion-pair production, the corrected cross section is generally smaller than the Born result.

Fig. 5.7 compiles the results for the predicted integrated cross sections with an angular region limited by $|cos\theta| \leq 0.9$. The graph (a) shows energies between 10 GeV and 1 TeV, in a logarithmic scale for both σ and energy, representing the negative linear tendency a clear fall off in the cross section proportional to $1/s$ before and beyond the Z-resonance. The behaviour on and around the resonance is plotted in (b), stating the clear difference between a calculation with Z-width (thick lines), and no width (thin lines). In both cases the corrected results within the EWSM are also shown with discontinuous lines.

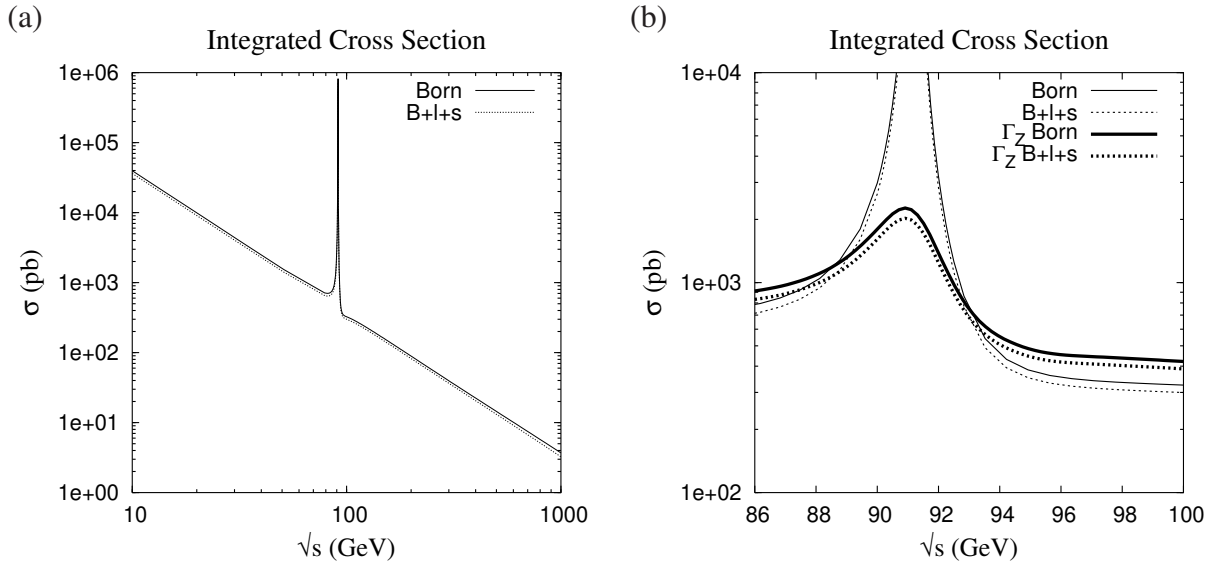

Figure 5.7: Integrated cross sections at different energies for Bhabha scattering with angular cut $|\cos\theta| < 0.9$, at (a) range of high energies, (b) Zoom for the Z-peak in which thick lines represent the calculation with finite Z width and thin lines without. Corrected cross sections are identified in the legend by B+I+s.

5.3 Other $2 \to 2$ processes

5.3.1 Møller scattering

Being a very similar process to Bhabha, the possibility to scatter not exclusively particle-anti-particle, but also particle-particle, offers new perspectives in the study of electroweak interactions. Møller scattering considers electrons both in the initial and final state

$$e^- e^- \to e^- e^- (\gamma). \tag{5.53}$$

During the last few years it has been the trailing probe for studying the weak mixing angle θ_W at low Q^2 with a precision of 3‰ (experiment E158 at SLAC), complementing our knowledge of the electroweak interactions at another energy scale than the Z-mass and beyond at LEP. The left-right asymmetry A_{LR}, has been measured with a 48 GeV polarized fixed-target beam. Particularly important are here the higher order corrections, since it was shown that the one-loop corrections reduce the A_{LR} tree-level asymmetry by $\approx 40\%$ [102], thus emphasizing the role of quantum corrections in precision tests, as it has been also realized when considering transverse polarization beams [103].

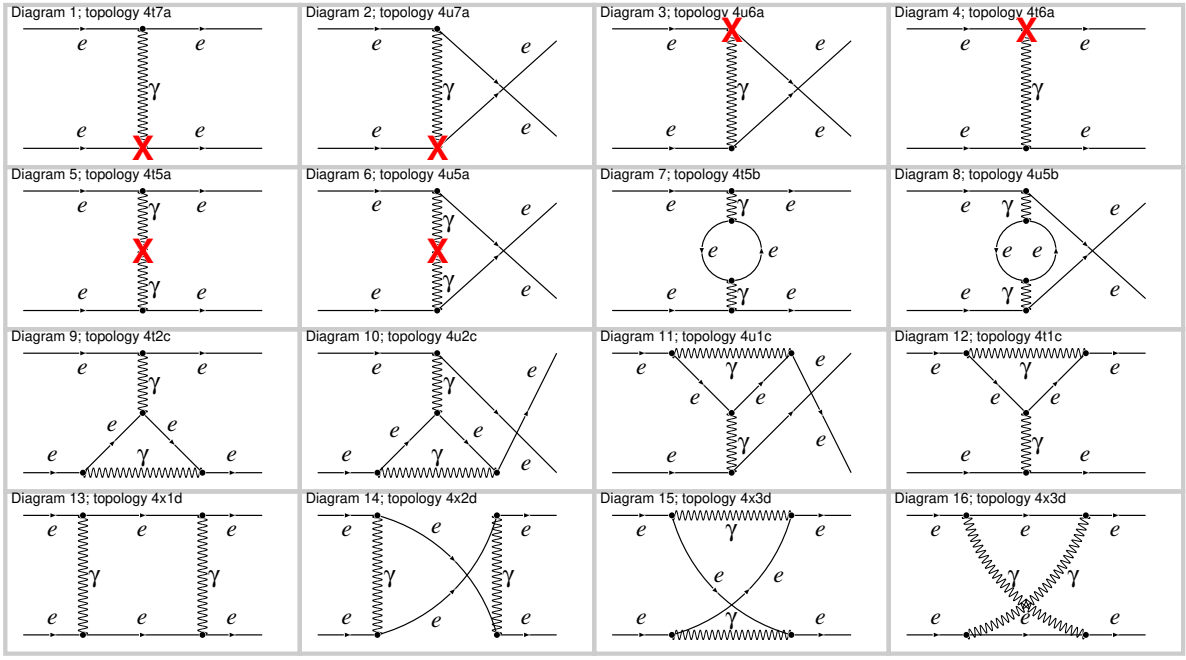

Figure 5.8: Set of graphs when considering Møller scattering in QED at one-loop.

The Feynman graphs for the Møller scattering are very similar to those of Bhabha scattering and can be obtained by interchange of the S and U channels. The one-loop diagrams in QED are shown in Fig. 5.8.

What is especially different in Møller scattering in comparison to the other processes studied is the composition of the final state by two identical particles, and from their interchange arises the $T \leftrightarrow U$ symmetry in this process. This feature implies a symmetric distribution for the differential cross section in terms of $\cos\theta$ for negative and positive values. An experimentalist will however choose the smallest of the two θ angles provided by the two electrons and count a double amount of events. So we understand that our results have to be considered in only half of the θ region and multiplied by 2 to match experimental measurements.

Numerics and plots

For the process of Møller scattering we present Table 5.13, evaluated within the EWSM[3]. In this particular case, negative and positive values for $\cos\theta$ are shown to internally check the results produced by *a*ĭTALC. Even if only 15 digits appear, the code has run with quadruple precision to avoid round-off errors for the limit of $\cos\theta = \pm 0.9999$. At the energy of 50 GeV, corrections turn out to vary between -10% at 90° and -4% in the collinear limit.

In a dedicated evaluation at 100 GeV, 500 GeV and 2 TeV we found complete agreement with the values calculated and showed in Tab. 1 of [104]. There the corrections amount between -20% and -35% according to a smaller value of $E^{\max}_{\gamma_{\text{soft}}} = 0.05\,\sqrt{s}$.

$e^-e^- \to e^-e^-(\gamma)$, $\sqrt{s} = 50\text{GeV}$			
$\cos\theta$	$\left[\frac{d\sigma}{d\cos\theta}\right]_B$ /pb	$\left[\frac{d\sigma}{d\cos\theta}\right]_{B+l+s}$ /pb	error O
−0.9999	$0.10422\,59057\,45810 \cdot 10^{11}$	$0.964912707122546 \cdot 10^{10}$	$0.8 \cdot 10^9$
−0.9	$0.10535\,00871\,43583 \cdot 10^{5}$	$0.968579279996572 \cdot 10^{4}$	$1.0 \cdot 10^3$
−0.5	$0.51058\,95481\,18313 \cdot 10^{3}$	$0.470253313121933 \cdot 10^{3}$	$0.5 \cdot 10^2$
0.0	$0.25262\,80188\,59744 \cdot 10^{3}$	$0.232631409948480 \cdot 10^{3}$	$0.2 \cdot 10^2$
+0.5	$0.51058\,95481\,18313 \cdot 10^{3}$	$0.470253313121933 \cdot 10^{3}$	$0.5 \cdot 10^2$
+0.9	$0.10535\,00871\,43583 \cdot 10^{5}$	$0.968579279996572 \cdot 10^{4}$	$1.0 \cdot 10^4$
+0.9999	$0.10422\,59057\,45810 \cdot 10^{11}$	$0.964912707122546 \cdot 10^{10}$	$0.8 \cdot 10^9$

Table 5.13: Numerical prediction for Møller scattering at $\sqrt{s} = 50$ GeV for different angles in the EWSM. Born and corrected to $O(\alpha)$ with a maximum soft-photon energy $E^{\max}_{\gamma_{\text{soft}}} = 0.1\,\sqrt{s}$ are given.

With Fig. 5.9 we close the short discussion for this process. Here we plot the Born and the corrected differential cross section for an energy (50 GeV) similar to the E158 experiment. The corrections also lower the leading order result like in the other processes analyzed. Because we explicitly enlarge the $\cos\theta$-axis to whole phase space of 'one' final electron, the expected experimental cross section will be double for a single-sided subregion $0° < \theta \leq 90°$.

[3]Note that the Feynman diagrams shown include only those with photons and electrons.

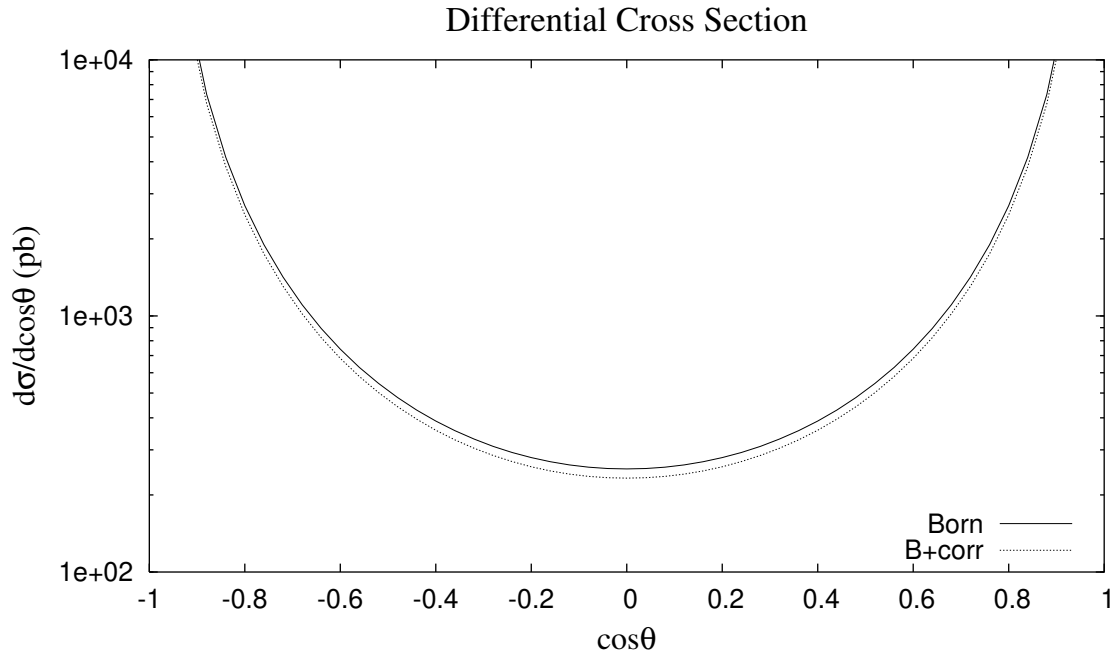

Figure 5.9: Differential cross section for Møller scattering at $\sqrt{s} = 50$ GeV within the EWSM. Born and corrected lines (B+corr) are shown. Note the even parity of the distribution around $\cos\theta = 0$ due to $U \leftrightarrow T$ crossing symmetry.

5.3.2 $e^+e^- \to t\bar{c}, b\bar{s}$

Moving into more exotic physics, where the processes involved are not measured with high precision, we could pay special attention to the flavour changing neutral current processes (FCNC),

$$e^+e^- \to f_i\bar{f}_j, \tag{5.54}$$

where the subscripts i, j denote indeed different fermion species with the same quantum numbers.

On the leptonic sector, the model is strictly flavour conserving and this process cannot occur. Only when introducing some non-zero non-degenerate masses for the neutrinos, mixing happens and it is possible to account for neutrino oscillations and double beta decay phenomena. Somehow this is still far from collider physics unless new scenarios reveal alternative mechanisms for neutrino masses [105] or supersymmetric theories show up [106].

Regarding the quarks, the non-diagonal quark-mixing matrix allows for a simple mechanism to induce the reaction 5.54 through higher-loop effects [107, 108, 109], since the coupling is absent at the tree-level.

In the following we will focus mainly on the two possibilities involving the heaviest quarks:

$$e^-e^+ \to t\bar{c}, \qquad e^-e^+ \to b\bar{s}, \tag{5.55}$$

which were investigated in [110, 111].

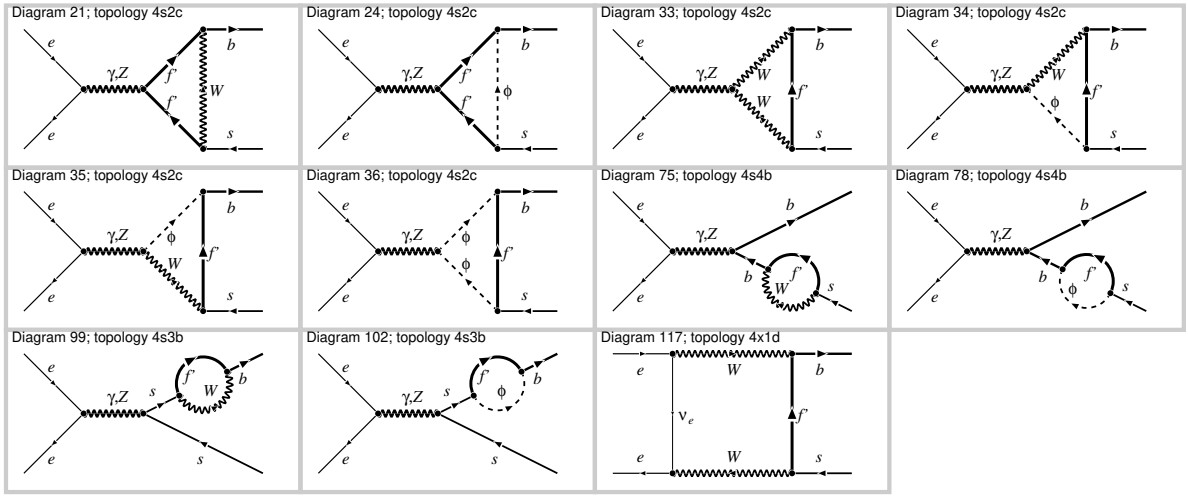

Figure 5.10: Group of relevant Feynman diagrams at leading order for $b\bar{s}$ production.

The related reactions can be depicted through loop diagrams as shown for the $b\bar{s}$ production in Fig. 5.10.

It is worth to clarify the role of the loops in the external legs: the perturbative calculations carried out in this thesis until now have always considered the loops in the external legs in terms of the fermion wave-function renormalization δZ_{f_i}. The field counterterms are evaluated with the help of self-energies and their derivatives as shown in Sect. 2.3.2. Since flavour changing neutral currents do not exist at tree-level, the one-loop amplitudes need no counterterms to yield finite contributions.

To avoid automated tools such as *a*ĩTALC from assuming that the wave function renormalization is used, we comment out the default flag `options=onshell` in the driver file `process.ini`, and the calculation proceeds with the whole set of possible diagrams, as given in Fig. 5.10, where the new diagrams are due to the mixing propagator in an external final fermion line (diagrams 75, 78, 99 and 102). The ultraviolet finiteness of the process is ensured by the unitarity condition of the CKM matrix

$$V_{ub}V_{us}^{*} + V_{cb}V_{cs}^{*} + V_{tb}V_{ts}^{*} = 0. \tag{5.56}$$

As discussed we do not need to consider the renormalization of the CKM matrix elements given by Eq. (2.64) and Eq. (2.94).

Numerical results

In the following we present the results for the leading order calculation of the processes. The results are obtained from the last column of the standard output file `main.log` in *a*ĩTALC.

In Table 5.14, the differential cross sections are shown. According to our specific input data in Table A.1, the δ_{13} parameter in the standard parametrization of the CKM matrix [112] is set here to zero. This fixes the slight difference for the $b\bar{s}$ case in comparison with the example

$e^-e^+ \to f_i\bar{f}_j(\gamma)$, $\sqrt{s} = 500$GeV		
$\cos\theta$	$\left[\frac{d\sigma}{d\cos\theta}\right]$ /pb for $b\bar{s}$	$\left[\frac{d\sigma}{d\cos\theta}\right]_{t\bar{c}}$ /pb for $t\bar{c}$
−0.9	$0.6639652 \cdot 10^{-8}$	$0.7796913 \cdot 10^{-13}$
−0.5	$0.7210026 \cdot 10^{-8}$	$0.1552342 \cdot 10^{-12}$
0.0	$0.1065626 \cdot 10^{-7}$	$0.2756448 \cdot 10^{-12}$
+0.5	$0.2118604 \cdot 10^{-7}$	$0.4142350 \cdot 10^{-12}$
+0.9	$0.4718966 \cdot 10^{-6}$	$0.5380807 \cdot 10^{-12}$

Table 5.14: Numerical prediction for flavour changing neutral current processes at $\sqrt{s} = 500$ GeV for different angles in the EWSM. The $b\bar{s}$ and $t\bar{c}$ production results are shown.

$e^-e^+ \to f_i\bar{f}_j(\gamma)$		
$\sqrt{\sigma}$ (GeV)	$b\bar{s}$ (pb)	$t\bar{c}$ (pb)
91.187	$0.1136 \pm 0.0001 \cdot 10^{-2}$	
200	$0.2032 \pm 0.0002 \cdot 10^{-5}$	$0.1846 \pm 0.0001 \cdot 10^{-11}$
500	$0.2536 \pm 0.0003 \cdot 10^{-6}$	$0.5722 \pm 0.0006 \cdot 10^{-12}$

Table 5.15: Numerical prediction for flavour changing neutral current processes. Integrated cross sections are shown for leading order with an error estimation coming from integration. Here the data are taken as in [110].

provided in Tab. 3 in [6]. In addition, comparisons were performed to make a cross-check of the results already published in [110]. There, for $t\bar{c}$-production total cross sections of $0.184 \cdot 10^{-11}$ pb at $\sqrt{s} = 200$ GeV and $0.572 \cdot 10^{-9}$ pb at $\sqrt{s} = 500$ GeV were reported. This result is in full agreement with our integrated cross section given in Table 5.15. Moreover we reaffirm those values published in [14] with apparently disagreement of a factor $\approx 3/2$ bigger than in [111].

The numbers are nevertheless too small to be seen in the planned linear colliders. The ultimate answer about new physics could eventually arise from some non-expected signals of FCNC processes, not fitting in with our understanding of the standard model.

Even if not experimentally accesible, the quantum nature of these processes is enhanced because the one-loop level represent the leading contribution to the cross section. Then, instead of a single well-understood Z-resonance as for some of the other fermion-pair production processes, two extra threshold energies appear for the $b\bar{s}$ case, one at $2m_W$ and other at $2m_t$, as illustrated in Fig. 5.11 (b). The large numerical difference between both processes is manifest in their differential distributions at 500 GeV (a), separated by several orders of magnitude.

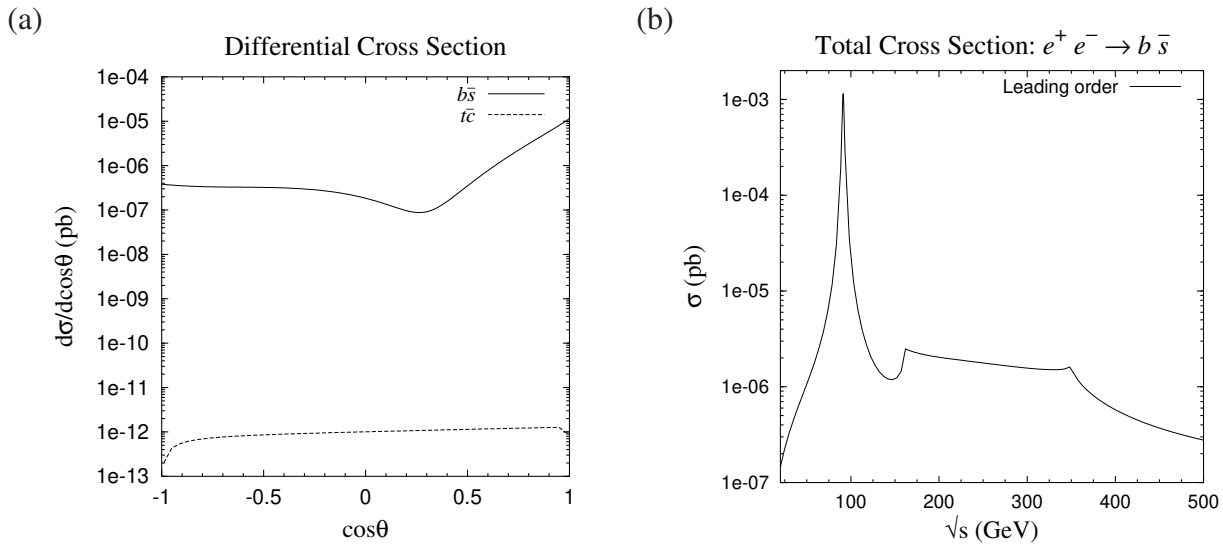

Figure 5.11: (a) Differential cross sections at 500 GeV, compared for $b\bar{s}$ and $t\bar{c}$-production. (b) Integrated cross sections at different energies for $b\bar{s}$-production. Note the threshold energies of m_Z, $2m_W$ and $2m_t$ in (b).

Chapter 6

Conclusions and Outlook

The work of many scientists in 'loops & legs' over several decades has boosted the field of perturbative calculations providing an excellent approach to the precise description of particle interactions.

In this thesis we have focussed on the development and immediate applicability of computer algebra and numerical tools to the scattering of two by two fermions. The result is twofold. On the computational side, the experience collected while working through the static code TOPFIT led to a major initiative for automated calculations, *a*i̊TALC, involving the feasibility of integrating the work performed by others and to adapt it to some specific needs. On the other hand, the possibility of testing equivalent results provided by independent groups and tools, represents one of the strongest tests for the correctness of the codes. In this sense *a*i̊TALCs results for Bhabha scattering have pushed the comparisons with the FEYNARTS+FORMCALC packages to at least the level of *double precision* agreement, which is indeed a very healthy improvement given the severe cancellations usually occurring in quantum corrections.

We would like to stress that it seems quite difficult to understand the evolution of science without the acquisition of ideas, abilities and methodology already established. Likewise, starting a diagram generator or a set of routines to calculate the loop integrals from the very beginning would be against this philosophy if we feel that there are already good packages with such intention. In addition, efficient interaction at this level is much promoted if we set our codes and our developing environments to be free-based and open source. We believe that, in this sense, *a*i̊TALC is a good example of integration and opening.

The application of our tools led to the calculation of practically all $2 \to 2$ fermion processes of present interest to $O(\alpha^3)$, showing that the corrections are of the order of a few percent. For the most heavy quark, the top, its mass plays a decisive role in the numerics. The isospin partner of the top, the b-quark, does only reflect some mass effects if very precise measurements are performed and, in principle, this could only be achieved in an operational mode like the *GigaZ* option, designed for the TESLA collider, where millions of events are available by running on top of the Z-resonance.

Nevertheless, there are other features which have to be mentioned regarding the precision and the limitation of the predictions. The method and corrections here presented have to be understood as an important part within the whole set of contributions for the determination of a

realistic observable. There are still missing ingredients which we did not treat because they obey other models or analysis techniques, becoming an independent subject by themselves. We would like to draw the attention to very important issues:

1. Inclusion of real bremsstrahlung. The soft-photon approximation assumed in the thesis deals with a maximum for the soft photon energy of 1/10 of the available beam energy. This is too optimistic since such an energetic photon will visibly modify the final state distribution. Then the three-particle phase space has to be treated properly and for this issue we recall the techniques listed in Sect. 3.3.

2. Multi-particle final states and uncorrelated distributions. Because we cannot see the track of a single quark in the detector and also the massive particles decay fast into lighter ones, a reconstruction of the events has always to be performed before we can associate the case to a definite fermion-pair production[1]. Conversely, if we can predict corrections to the processes, it might help to understand the final output if we add an appropriate tool for simulating the final distribution of particles which are going to be detected, and provide an efficient and low-correlated event generator to extract statistics.

As part of a more extensive project [113], we have shown how much Bhabha scattering is dominated at low angles by QED corrections. Nevertheless, electroweak one-loop corrections contribute with a tiny amount (around 4‰), not possible to be explained in terms of fully flavoured QED, as shown in Table 5.11 and even larger than the expected precision for luminosity calibration. This study states clearly that further work has to be performed in the direction of 2-loop QED Bhabha scattering and hadronic effects.

For the flavour changing neutral current processes, we demonstrated the possibility to recreate more exotic physics, not of phenomenological interest at present since it is sadly predicted to be out of reach of the possibilities of the next linear collider. Occasionally, a signal of these processes could bring back the interest, trailing the measurements and calculations in order to fit a consistent explanation maybe outside the standard model.

In our other considered process, Møller scattering, a first approach to the radiative corrections has been undertaken serving as example for the flexibility of our computing tool. However, a realistic implementation of the electroweak corrections is beyond the scope of the present work since we did not include so far the possibility of dealing with polarized particles and the fixed-beam particularities of the SLAC experiment.

This subject of polarized particles causes us to the think about the future of *a*ĩTALC. Though this is not a difficult issue to be considered and implemented, we did not talk about or study the possibility of having polarized fermions in the initial state. Apparently, a future linear collider will also allow different longitudinal and transverse modes of polarization because it provides a sensitive access to parameters which otherwise would be overlooked. Another possibility is to extend the operational abilities of the tool to generic $2 \to 2$ processes, with also boson or scalar particles in the final states, which would bring access to test and recreate many more dominating

[1] Remarkable exceptions are Bhabha, Møller scattering and μ-production.

processes already calculated such as ZH [40] or WW [114, 115] production. Even more realistic seems the attempt to include one more external leg for specific cases like radiative Bhabha scattering $e^+e^- \to e^+e^-\gamma$ and seek an analytical massive treatment or study the limit to low photonic energy. Additional models or extensions for supersymmetric theories [116] or QCD interactions [117] fit very well in the framework of the tool and could be covered. To this end, interesting tests such as gauge invariance at tree-level or at loop-level through the background-field formalism [118] would equally well be considered for the queue of next possibilities. They would complete the internal tests of finiteness which have been successfully performed by varying an ultraviolet or infrared parameter.

Finally a personal impression is that all the work undertaken by the world community for a global accelerator should be accompanied by a similar project on loop calculations. Up to now, the development of calculational tools is attributed to individuals or small groups, which in the best of the cases, can afford keeping the same project for several years. However, it seems feasible to join the personal knowledge in a project that would provide the perfect framework to achieve an effective and ambitious utility in continuous development, to the benefit of theorists and experimentalists.

Acknowledgements

Firstly I would like to thank profoundly my advisor at DESY Dr. Riemann for his capability to consider the important things during these years, for being ready to listen at any time and always motivating me. I also express my gratitude to my advisor at Bielefeld Universität Prof. Fleischer, keeping always a collaborative and friendly attitude, even when dealing with the critical proof-reading of the thesis. And by extension to the whole group at DESY (namely Theory + NIC) for the great atmosphere. I owe debt also with Dr. Werthenbach for guiding me on the first moments on loop calculations, to Prof. Jegerlehner because the enlightening discussions in his lectures, to Dr. Tentyukov for his continuous help with DIANA and to Dr. Hahn for providing the numerical support for FEYNARTS+FORMCALC.

I have to thank as well some people in the Universidad de Granada: Prof. del Águila and Prof. Cornet for motivation and support and to Prof. Illana for also reading so carefully the draft. At this point I should not forget the networks helping in this research: the European's 5th Framework under contract HPRN-CT-2000-00149 Physics at Colliders and the Deutsche Forschungsgemeinschaft under contract SFB/TR 9-03.

It was great that there were *special* post-docs: Kei-ichi, Alberto, James and Andrea, sharing so many delicate moments of *All in one* döners, *il Casorale* pizzas, *Aufsturz* beers and *Ciao ciao* football, unforgettable! To the colleagues with who I lived the unpayable camaraderie of a Ph.D. and the smallness of our successive working rooms (Axel, Silvia, Heiko, Thomas, Michael, Carsten, Nils, Damiano and Beatrix) I can only wish the best.

How to forget the *hidden sector*[2]?! with the many friends here in Berlin and there in Granada, but just let me cheer for the bunch of perfect flat-mates, coming from all around the world and teaching what is not usually in books: Lars, Andrea (again), Sri, Ichi, Prof. Liri and Amandine. Specially Arne, for building up together the life-experience of WG Stralauer Allee .

Finally I am indebted to my parents, giving unlimited support. Gracias a vosotros papá y mamá, por vuestro amor, empuje y ¡lotes de productos ibéricos! Os lo debo todo y a vosotros os dedico mi trabajo.

[2]Calaveras, Gilitrotters+asociadas, los demás del instituto, die 'Leute von Heute', las churris y mil más.

Appendix A

Parameters and constants

The production of tables and use of the codes TOPFIT and *a*ĩTALC share a common set of parameters and physical constants. Unless otherwise stated[1] they are:

Fermion Masses			Boson Masses & Widths		
$m_\nu =$	0.0	GeV			
$m_e =$	0.00051099907	GeV			
$m_\mu =$	0.105658389	GeV	$m_\gamma =$	0.0	GeV
$m_\tau =$	1.77705	GeV	$m_W =$	80.4514958	GeV
$m_u =$	0.062	GeV	$m_Z =$	91.1867	GeV
$m_c =$	1.5	GeV	$m_H =$	120.0	GeV
$m_t =$	173.8	GeV	$\Gamma_W =$	2.118	GeV
$m_d =$	0.083	GeV	$\Gamma_Z =$	2.49977	GeV
$m_s =$	0.215	GeV	$\Gamma_H =$	0.004	GeV
$m_b =$	4.7	GeV			

Other Parameters
CKM parameters: $\sin\theta_{12} = 0.22, \sin\theta_{23} = 0.039, \sin\theta_{13} = 0.0031, \delta_{13} = 0$
$\alpha = 1/137.03599976$
$E^{\max}_{\gamma_{\rm soft}} = \sqrt{s}/10$
$(\hbar c)^2 = 0.38937966 \cdot 10^9 \text{GeV}^2\text{pb}$

Table A.1: Input Parameter Set used for both codes.

[1] Note that the width of the bosons have been seldom used and explicitly reported.

Appendix B

Conventions and Dirac algebra

Through all the thesis, most of the notation used and the conventions are taken as in [29].

B.1 Metric and other tensors

Our theory is working on flat Minkowski space, i.e. without gravity, of 1 + 3 dimensions. The metric is defined as

$$g_{\mu\nu} = g^{\mu\nu} = \begin{cases} +1 & \text{for } \mu = \nu = 0 \\ -1 & \text{for } \mu = \nu = 1, 2, 3 \\ 0 & \text{otherwise} \end{cases} \tag{B.1}$$

and transforms a contravariant Lorentz vector $p^\mu = (p^0, \mathbf{p})$ into covariant $p_\mu = (p^0, -\mathbf{p})$ and vice versa:

$$g_{\mu\nu} p^\nu = p_\mu. \tag{B.2}$$

The Einstein summation convention is assumed for every repeated index. Greek letters will denote the indices for both space and time ($\mu = 0, 1, 2, 3$) while Latin letters account only for space ($i = 1, 2, 3$). Therefore we can write the scalar product of two four-vectors p, q as

$$p \cdot q = p^\mu q_\mu = g_{\mu\nu} p^\mu q^\nu = p^0 q^0 - p^i q^i. \tag{B.3}$$

We define the totally antisymmetric Levi-Civita tensorof rank 4 as

$$\epsilon^{\mu\nu\rho\sigma} = \begin{cases} +1 & \text{for an even permutation of (0123),} \\ -1 & \text{for an odd permutation of (0123),} \\ 0 & \text{if indices are repeated.} \end{cases} \tag{B.4}$$

It is a trivial exercise to lower all indices and check that $\epsilon_{\mu\nu\rho\sigma} = -\epsilon^{\mu\nu\rho\sigma}$

$$\epsilon_{0123} \equiv g_{0\mu} g_{1\nu} g_{2\rho} g_{3\sigma} \epsilon^{\mu\nu\rho\sigma} = (+1)(-1)(-1)(-1)\epsilon^{0123} = -\epsilon^{0123} = -1. \tag{B.5}$$

B.2 Dirac matrices

The Dirac matrices γ are the simplest 4×4 irreducible representation of the Lorentz group in 4-dimensional Minkowski space that obey the Clifford algebra or anticommutation relations

$$\{\gamma^\mu, \gamma^\nu\} \equiv \gamma^\mu\gamma^\nu + \gamma^\nu\gamma^\mu = 2g^{\mu\nu}\mathbb{1}. \tag{B.6}$$

All the explicit realizations of the Dirac matrices are unitarily equivalent to one another and their basic properties are independent of the specific choice.

The hermiticity condition reads

$$\gamma^{\mu\dagger} = \gamma^0\gamma^\mu\gamma^0, \tag{B.7}$$

so γ^0 is hermitian while the γ^is are antihermitian:

$$\gamma^{0\dagger} = \gamma^0, \qquad \gamma^{i\dagger} = -\gamma^i. \tag{B.8}$$

An arbitrary 4×4 matrix can be represented in terms of products of Dirac matrices. Antisymmetric combination of them leads to an interesting basis of 16 elements:

$$\left.\begin{array}{lcll} \Gamma_S{}^r & \equiv & \mathbb{1}, & \\ \Gamma_V{}^r & \equiv & \gamma^\mu, & \\ \Gamma_T{}^r & \equiv & \frac{\mathrm{i}}{2}\left[\gamma^\mu, \gamma^\nu\right], & (\mu < \nu) \\ \Gamma_A{}^r & \equiv & \mathrm{i}\gamma^\mu\gamma_5, & \\ \Gamma_P{}^r & \equiv & \gamma_5, & \end{array}\right\} \xrightarrow{\bar\psi\Gamma\psi \text{ transforms as}} \left\{\begin{array}{lll} \text{Scalar,} & r_{\max} = & 1 \\ \text{Vector,} & r_{\max} = & 4 \\ \text{Tensor } 2^{\text{nd}} \text{ rank,} & r_{\max} = & 6 \\ \text{Axial-vector,} & r_{\max} = & 4 \\ \text{Pseudo-scalar,} & r_{\max} = & 1 \end{array}\right. \tag{B.9}$$

with such transformation properties when considered between Dirac spinors (forming bilinears), and the γ_5 defined as

$$\gamma_5 \equiv \mathrm{i}\gamma^0\gamma^1\gamma^2\gamma^3 = -\frac{\mathrm{i}}{4!}\epsilon_{\mu\nu\rho\sigma}\gamma^\mu\gamma^\nu\gamma^\rho\gamma^\sigma. \tag{B.10}$$

The elements of the basis (B.9) hold an orthogonality condition via tracing

$$\mathrm{Tr}(\Gamma_I{}^r\Gamma_{J\,s}) = 4\delta_{IJ}\delta^r_s, \tag{B.11}$$

and therefore a closure relation

$$\frac{1}{4}\sum_J (\Gamma_J{}^r)_{ad}(\Gamma_{J\,r})_{cb} = \delta_{ab}\delta_{cd}. \tag{B.12}$$

The γ_5 matrix is, as in the case of $\mathbb{1}$ and γ^0, hermitian and with square unity

$$\gamma_5{}^\dagger = \gamma_5, \qquad \gamma_5\gamma_5 = \mathbb{1}, \tag{B.13}$$

but it has a very special property

$$\{\gamma_5, \gamma^\mu\} = 0. \tag{B.14}$$

Specific realizations

Common realizations are

- Chiral or Weyl realization

$$\gamma^0 = \begin{pmatrix} 0 & \mathbb{1} \\ \mathbb{1} & 0 \end{pmatrix}, \qquad \gamma^i = \begin{pmatrix} 0 & \tau^i \\ -\tau^i & 0 \end{pmatrix}. \tag{B.15}$$

- Non relativistic or Pauli-Dirac

$$\gamma^0 = \begin{pmatrix} \mathbb{1} & 0 \\ 0 & -\mathbb{1} \end{pmatrix}, \qquad \gamma^i = \begin{pmatrix} 0 & \tau^i \\ -\tau^i & 0 \end{pmatrix}. \tag{B.16}$$

- Majorana, satisfying $\gamma^{\mu *} = -\gamma^\mu$.

The τ^i are the standard Pauli matrices

$$\tau^1 = \begin{pmatrix} 0 & 1 \\ 1 & 0 \end{pmatrix}, \qquad \tau^2 = \begin{pmatrix} 0 & -\mathrm{i} \\ \mathrm{i} & 0 \end{pmatrix}, \qquad \tau^3 = \begin{pmatrix} 1 & 0 \\ 0 & -1 \end{pmatrix}, \tag{B.17}$$

and $\mathbb{1}$ is the identity in 2×2 dimensions.

B.3 Dirac equation and spinors

Being ψ a four-component spinor, the Dirac equation reads

$$\mathrm{i}\gamma^\mu \frac{\partial \psi(x)}{\partial x^\mu} = m\psi(x). \tag{B.18}$$

The Lagrangian is built together with the definition of the adjoint spinor

$$\bar{\psi} = \psi^\dagger \gamma^0. \tag{B.19}$$

Free particle solutions of the Dirac field also validate the Klein–Gordon equation, so they can be written in terms of plane waves

$$\psi(x) = u(p)e^{-ip\cdot x} + v(p)e^{+ip\cdot x}, \qquad \text{with} \quad p^2 = m^2 \tag{B.20}$$

and the momentum-space spinors obey equivalent Dirac equations. They are specially useful in calculations

$$(\not{p} - m)u(p) = 0, \qquad \bar{u}(p)(\not{p} - m) = 0, \tag{B.21}$$

$$(\not{p} + m)v(p) = 0, \qquad \bar{v}(p)(\not{p} + m) = 0, \tag{B.22}$$

where $\not{p} \equiv \gamma^\mu p_\mu$. They are orthogonal under different spin configuration and normalized in the following way

$$\bar{u}^r(p)u^s(p) = 2m\delta^{rs}, \qquad \bar{v}^r(p)v^s(p) = -2m\delta^{rs}, \tag{B.23}$$

$$\bar{u}^r(p)v^s(p) = 0, \qquad \bar{v}^r(p)u^s(p) = 0, \tag{B.24}$$

and the completeness relation over spin reads

$$\sum_{s=1,2} u^s(p)\bar{u}^s(p) = \not{p} + m\mathbb{1}, \tag{B.25}$$

$$\sum_{s=1,2} v^s(p)\bar{v}^s(p) = \not{p} - m\mathbb{1}. \tag{B.26}$$

During the calculations, the Dirac equation can be used to simplify the structure of the matrix elements. In a general form, for all the possible structures appearing in the basis, they are called Gordon identities.

B.4 Traces and contractions

Despite that our theory works in 4 space-time dimensions, the dimensional regularization of the loop integrals, invoked by the renormalization of the EWSM, requires some formal steps in which one switches to generic D-dimensions and evaluate the case in the limit $D \to 4$.

Nevertheless the internal structure of matrices related with the Dirac formalism and Clifford Algebra is kept as 4-dimensional, being considered as D-dimensional only the Lorentz indices affecting the evaluation of tensor contractions.

The well-known totally symmetric metric tensor defined at Eq. (B.1) has some special properties in D-dimensions:

$$g_{\mu\alpha}g^{\mu\beta} = \delta^\beta_\alpha, \tag{B.27}$$

$$g_{\mu\nu}g^{\mu\nu} = D = 4 + [D-4]. \tag{B.28}$$

Contractions of the antisymmetric Levi–Civita from Eq. (B.4)

$$\epsilon_{\mu\nu\rho\sigma}\epsilon^{\alpha\beta\gamma\delta} = (-1)\begin{vmatrix} \delta^\alpha_\mu & \delta^\beta_\mu & \delta^\gamma_\mu & \delta^\delta_\mu \\ \delta^\alpha_\nu & \delta^\beta_\nu & \delta^\gamma_\nu & \delta^\delta_\nu \\ \delta^\alpha_\rho & \delta^\beta_\rho & \delta^\gamma_\rho & \delta^\delta_\rho \\ \delta^\alpha_\sigma & \delta^\beta_\sigma & \delta^\gamma_\sigma & \delta^\delta_\sigma, \end{vmatrix} \tag{B.29}$$

also introduce dimensional dependence and we find by successively evaluation

$$\epsilon_{\mu\nu\rho\sigma}\epsilon^{\mu\nu\rho\sigma} = -(24 + 50[D-4] + 35[D-4]^2 + 10[D-4]^3 + [D-4]^4), \tag{B.30}$$

$$\epsilon_{\mu\nu\rho\sigma}\epsilon^{\mu\nu\rho\gamma} = -(6 + 11[D-4] + 6[D-4]^2 + [D-4]^3)\,\delta^\gamma_\sigma, \tag{B.31}$$

$$\epsilon_{\mu\nu\rho\sigma}\epsilon^{\mu\nu\beta\gamma} = -(2 + 3[D-4] + [D-4]^2)(\delta^\beta_\rho\delta^\gamma_\sigma - \delta^\beta_\sigma\delta^\gamma_\rho), \tag{B.32}$$

$$\begin{aligned}\epsilon_{\mu\nu\rho\sigma}\epsilon^{\mu\alpha\beta\gamma} = -(1 + [D-4])(&+ \delta^\alpha_\nu\delta^\beta_\rho\delta^\gamma_\sigma + \delta^\alpha_\rho\delta^\beta_\sigma\delta^\gamma_\nu + \delta^\alpha_\sigma\delta^\beta_\nu\delta^\gamma_\rho \\ &- \delta^\alpha_\nu\delta^\beta_\sigma\delta^\gamma_\rho - \delta^\alpha_\rho\delta^\beta_\nu\delta^\gamma_\sigma - \delta^\alpha_\sigma\delta^\beta_\rho\delta^\gamma_\nu).\end{aligned} \tag{B.33}$$

Interesting contractions also affect the γ matrices

$$\begin{aligned}
\gamma_\mu\gamma^\mu &= (4+[D-4])\mathbb{1}, && \text{(B.34)}\\
\gamma_\mu\gamma^\nu\gamma^\mu &= -(2+[D-4])\gamma^\nu, && \text{(B.35)}\\
\gamma_\mu\gamma^\nu\gamma^\rho\gamma^\mu &= 4g^{\nu\rho}\mathbb{1} + [D-4]\gamma^\nu\gamma^\rho, && \text{(B.36)}\\
\gamma_\mu\gamma^\nu\gamma^\rho\gamma^\sigma\gamma^\mu &= -2\gamma^\sigma\gamma^\rho\gamma^\nu - [D-4]\gamma^\nu\gamma^\rho\gamma^\sigma,\\
&= (2-[D-4])\gamma^\nu\gamma^\rho\gamma^\sigma - 4\gamma^\nu g^{\rho\sigma} + 4\gamma^\rho g^{\nu\sigma} - 4\gamma^\sigma g^{\nu\rho}. && \text{(B.37)}
\end{aligned}$$

Some valuable traces of γ-chains are

$$\begin{aligned}
\mathrm{Tr}(\mathbb{1}) &= 4, && \text{(B.38)}\\
\mathrm{Tr}(\gamma_5) &= 0, && \text{(B.39)}\\
\mathrm{Tr}(\gamma^\mu) &= \mathrm{Tr}(\gamma^{\mu_1}\ldots\gamma^{\mu_{2n+1}}) = 0, \quad \text{(for any odd product of } \gamma\text{s)}, && \text{(B.40)}\\
\mathrm{Tr}(\gamma^\mu\gamma^\nu) &= 4g^{\mu\nu}, && \text{(B.41)}\\
\mathrm{Tr}(\gamma^\mu\gamma^\nu\gamma^\rho\gamma^\sigma) &= 4\left(g^{\mu\nu}g^{\rho\sigma} - g^{\mu\rho}g^{\nu\sigma} + g^{\mu\sigma}g^{\nu\rho}\right), && \text{(B.42)}\\
\mathrm{Tr}(\gamma^\mu\gamma^\nu\gamma^\rho\gamma^\sigma\gamma_5) &= -4\mathrm{i}\epsilon^{\mu\nu\rho\sigma}. && \text{(B.43)}
\end{aligned}$$

B.4.1 The problem with γ_5

It is impossible in D dimensions to define an anticommuting γ_5 which module square is the 4×4 unity matrix, so we adopt a naïve use of γ_5 as discussed in [119] (and references therein):

$$(\gamma_5)^2 = \mathbb{1}_{4\times4} \qquad \text{(in)compatible in } (D)\text{4-dimens. with} \qquad \{\gamma^\mu,\gamma_5\} = 0. \tag{B.44}$$

B.4.2 Form convention

In Form we find that indices normally run from 1 to 4.

$$\epsilon^{0123} = 1 \qquad \longleftrightarrow \qquad \texttt{e_}(1,2,3,4) = 1. \tag{B.45}$$

This is usually of no importance since symbolic representation is always used. The things we have into account are

- ϵ tensors introduced automatically by means of tracing chains of γ matrices with `trace4` can be contracted with the command `contract` safely.
- Whenever one introduces for convenience the ϵ tensor in order to compact γ chains, it has to be kept in mind that:

$$\epsilon_{\mu_1\ldots}\epsilon^{\nu_1\cdots} = -1 * \texttt{e_}(\texttt{mu1},\ldots) * \texttt{e_}(\texttt{nu1},\ldots). \tag{B.46}$$

Appendix C

Dimensional regularization

C.1 Wick's rotation

Facing an integral such as

$$\int_{-\infty}^{+\infty} \mathrm{d}Q^0 f(Q) = \int_{-\infty}^{+\infty} \mathrm{d}Q^0 \frac{1}{(Q^2 - M^2 + \mathrm{i}\varepsilon)^n} \tag{C.1}$$

with n integer is not so easy when the function to integrate $f(Q)$ contains some nasty poles in the sourroundings of the real path of integration. This is unfortunately our case,

$$f(Q) = \frac{1}{\left(\left(Q^0 - \sqrt{\mathbf{Q}^2 + M^2 - \mathrm{i}\varepsilon}\right)\left(Q^0 + \sqrt{\mathbf{Q}^2 + M^2 - \mathrm{i}\varepsilon}\right)\right)^n}, \tag{C.2}$$

and we do not know how to deal with arbitrarily small parameter $\mathrm{i}\varepsilon$ for the case $Q^2 = M^2$.

The idea of integrating in the complex Q^0 plane is quite useful. Since the location of the propagator's poles is known, we can choose a closed integration way for Q^0 where we do not enclose any pole:

- $-R \to +R$ along the Real axis.
- C_R^+: from $+R$ to $+\mathrm{i}R$ anti-clock wise along the complex numbers with $|Q^0| = R$.
- $+\mathrm{i}R \to -\mathrm{i}R$ down the Imaginary axis.
- C_R^-: from $-\mathrm{i}R$ to $-R$ again with $|Q^0| = R$ but clock wise.

Due to the analyticity over and inside the closed region, the Cauchy-Goursat theorem gives us the trivial result:

$$0 = \int_{-R}^{+R} \mathrm{d}Q^0 f(Q) + \int_{C_R^+} \mathrm{d}Q^0 f(Q) + \int_{+\mathrm{i}R}^{-\mathrm{i}R} \mathrm{d}Q^0 f(Q) + \int_{C_R^-} \mathrm{d}Q^0 f(Q). \tag{C.3}$$

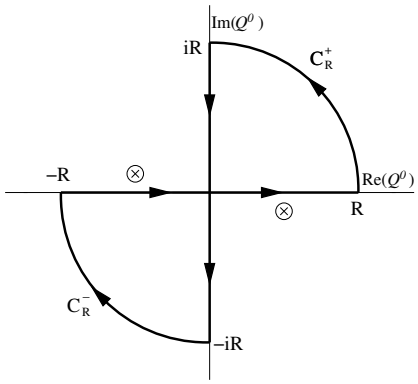

Figure C.1: "2 quarters of cheese" integration path in the complex Q^0 plane.

By taking the limit of R going to ∞ the zero result of the sum of the integrals remains, so our part reads

$$\begin{aligned}\int_{-\infty}^{+\infty} \mathrm{d}Q^0 f(Q) &= +\lim_{R\to\infty} \int_{-R}^{+R} \mathrm{d}Q^0 f(Q) \\ &= -\lim_{R\to\infty} \left(\int_{C_R^+} + \int_{+\mathrm{i}R}^{-\mathrm{i}R} + \int_{C_R^-} \right) \mathrm{d}Q^0 f(Q).\end{aligned} \tag{C.4}$$

Let us have a look to the $\int_{C_R^+}$. In polar coordinates, with $Q^0 = Re^{\mathrm{i}\theta}$, it is very easy to parametrize the path in terms of θ integration variable. Moreover, realizing that the integrand goes like $1/R^{2n-1}$ in the limit, we can neglect higher order terms and deduce

$$\begin{aligned}\lim_{R\to\infty} \int_{C_R^+} \mathrm{d}Q^0 f(Q) &= \lim_{R\to\infty} \int_0^{\frac{\pi}{2}} \mathrm{d}\theta \, \frac{\mathrm{i}Re^{\mathrm{i}\theta}}{(R^2 e^{\mathrm{i}2\theta} - \mathbf{Q}^2 - M^2 + \mathrm{i}\varepsilon)^n} \\ &= \lim_{R\to\infty} \int_0^{\frac{\pi}{2}} \mathrm{d}\theta \, \frac{\mathrm{i}e^{-\mathrm{i}\theta}}{R^{2n-1}} \left(1 - \frac{-\vec{Q}^2 - M^2 + \mathrm{i}\varepsilon}{R^2 e^{\mathrm{i}2\theta} - \mathbf{Q}^2 - M^2 + \mathrm{i}\varepsilon} \right)^n \\ &= \lim_{R\to\infty} -\frac{1}{R^{2n-1}} \int_0^{\frac{\pi}{2}} \mathrm{d}\theta \, (-\mathrm{i}) e^{-\mathrm{i}\theta} \\ &= \lim_{R\to\infty} -\frac{e^{-\mathrm{i}\frac{\pi}{2}} - e^{-\mathrm{i}0}}{R^{2n-1}} \overbrace{=}^{n>\frac{1}{2}} 0.\end{aligned} \tag{C.5}$$

This is an important and intuitive result. With it $\int_{C_R^-}$ also vanishes and the following result is established

$$\int_{-\infty}^{+\infty} \mathrm{d}Q^0 f(Q) = -\int_{+\mathrm{i}\infty}^{-\mathrm{i}\infty} \mathrm{d}Q^0 f(Q). \tag{C.6}$$

Here, we wouldn't need to worry any more. The integration is clean and we can do it without further manipulation. But it is useful to redefine the energy-momentum Q in terms of the

Euclidean energy-momentum[1] Q_e. This change of variable leaves the structure

$$\left.\begin{array}{lll} Q^0 & \to Q_e^0 & \equiv -\mathrm{i}Q^0 \\ \mathrm{d}Q^0 & \to \mathrm{d}Q_e^0 & \equiv -\mathrm{i}\mathrm{d}Q^0 \\ \mathbf{Q} & \to \mathbf{Q}_e & \equiv \mathbf{Q} \\ Q^2 & \to Q_e^2 & \equiv -Q^2 \end{array}\right\} \Rightarrow \int_a^b \mathrm{d}Q^0\, f(Q^2) = \mathrm{i}\int_{-\mathrm{i}a}^{-\mathrm{i}b} \mathrm{d}Q_e^0\, f(-Q_e^2) \tag{C.7}$$

which relates the equality between integrals.

This redefinition together with the integration strategy is the so called Wick's rotation and by plugging (C.6) into (C.7) we finally obtain the desired result

$$\int_{-\infty}^{+\infty} \mathrm{d}Q^0 \frac{1}{(Q^2 - M^2 + \mathrm{i}\varepsilon)^n} = \frac{\mathrm{i}}{(-1)^n} \int_{-\infty}^{+\infty} \mathrm{d}Q_e^0 \frac{1}{(Q_e^2 + M^2)^n}. \tag{C.8}$$

C.2 The D-dimensional space

Some of the integrals become convergent in

$$D = 4 - 2\epsilon \tag{C.9}$$

dimensions. Looking at the problem of one isolated integral, we can write down an ϵ–expansion near the 4-dimensional limit. When summing up different diagram amplitudes and incoherent contributions, it will become clear that the ϵ terms either safely cancel in the denominator ($\frac{1}{\epsilon}$) or can be neglected in the limit $\epsilon \to 0$.

Anyhow, it is important to manage some properties for D-dimensional integration:

- angular integration

$$\begin{aligned} &\int_0^\pi \mathrm{d}\theta_{D-1} \sin^{D-2}\theta_{D-1} \ldots \int_0^\pi \mathrm{d}\theta_2 \sin\theta_2 \int_0^{2\pi} \mathrm{d}\theta_1 \frac{1}{(Q_e^2 + \tilde{M}^2)^n} = \\ &= 2\,\frac{\pi^{\frac{D}{2}}}{\Gamma(\frac{D}{2})} \frac{1}{(Q_e^2 + \tilde{M}^2)^n}, \end{aligned} \tag{C.10}$$

- modulus integration

$$\int_0^\infty \mathrm{d}|Q_e||Q_e|^{D-1} \frac{1}{(Q_e^2 + \tilde{M}^2)^n} = \frac{1}{2} \frac{\Gamma(\frac{D}{2})\Gamma(n - \frac{D}{2})}{\Gamma(n)} \frac{1}{(\tilde{M}^2)^{n-\frac{D}{2}}}, \tag{C.11}$$

- ϵ prescription

$$\frac{\mu^{4-D}}{\mathrm{i}\pi^2} \int_{-\infty}^{+\infty} \mathrm{d}^D Q \frac{1}{(Q^2 - \tilde{M}^2)^n} = \frac{1}{(-1)^n} \frac{\Gamma(n - 2 + \epsilon)}{\Gamma(n)} \left(\pi \frac{\tilde{M}^2}{\mu^2}\right)^{-\epsilon} \frac{1}{(\tilde{M}^2)^{n-2}}. \tag{C.12}$$

[1] For an euclidean 4-vector, ${Q_e}^2 = (Q_e^0)^2 + \mathbf{Q}_e^2$.

Appendix D

A_0, B_0, C_0, D_0 scalar integrals

D.1 Working with A_0, B_0, C_0, D_0 integrals

D.1.1 Definition

We want to calculate D-dimensional one-loop scalar integrals. For the sake of clarity, the following momenta flow diagrams are presented:

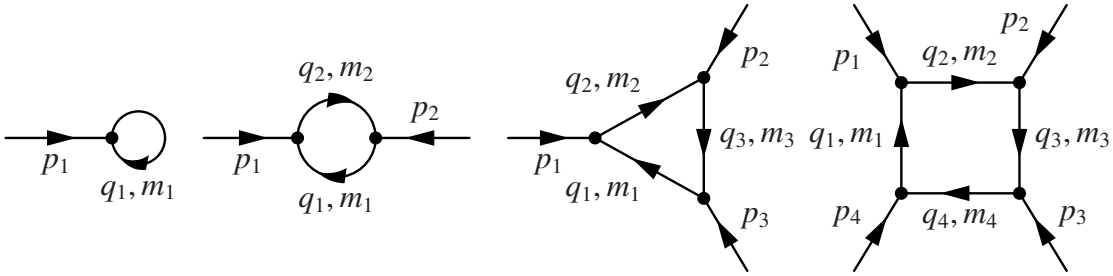

Figure D.1: Schematic representation of the 1-, 2- and 3-point functions.

The scalar one-loop master functions are defined as

$$A_0(m_1) = \frac{\mu^{4-D}}{i\pi^2}\int \mathrm{d}^D q_1 \frac{1}{N_1}, \tag{D.1}$$

$$B_0(p_1; m_1, m_2) = \frac{\mu^{4-D}}{i\pi^2}\int \mathrm{d}^D q_1 \frac{1}{N_1 N_2}, \tag{D.2}$$

$$C_0(p_1, p_2; m_1, m_2, m_3) = \frac{\mu^{4-D}}{i\pi^2}\int \mathrm{d}^D q_1 \frac{1}{N_1 N_2 N_3}, \tag{D.3}$$

$$D_0(p_1, p_2, p_3; m_1, m_2, m_3, m_4) = \frac{\mu^{4-D}}{i\pi^2}\int \mathrm{d}^D q_1 \frac{1}{N_1 N_2 N_3 N_4}, \tag{D.4}$$

N_i being an inverse scalar propagator

$$N_i = q_i^2 - m_i^2 + \mathrm{i}\varepsilon_i. \tag{D.5}$$

Of course, conservation of energy-momentum at each vertex holds, allowing a reduction of independent variables[1]:

Function	Integration var.	Parameters	Constraints
1-point	q_1	p_1 m_1	
2-point	q_1	p_1 m_1, m_2	$p_2 = -p_1$ $q_2 = q_1 + p_1$
3-point	q_1	p_1, p_2 m_1, m_2, m_3	$p_3 = -p_1 - p_2$ $q_2 = q_1 + p_1$ $q_3 = q_1 + p_1 + p_2$
4-point	q_1	p_1, p_2, p_3 m_1, m_2, m_3, m_4	$p_4 = -p_1 - p_2 - p_3$ $q_2 = q_1 + p_1$ $q_3 = q_1 + p_1 + p_2$ $q_4 = q_1 + p_1 + p_2 + p_3$

These integrals are representative since all the other integrals appearing in the course of the one-loop calculation in $2 \to 2$ processes can be reduced to these four functions.

D.1.2 Feynman parameters up to three-point function

In order to calculate it will be useful to rewrite the integrands with the help of the so-called *Feynman parameters* [10]:

$$\frac{1}{N_1} = \frac{1}{N_A}, \tag{D.6}$$

$$\frac{1}{N_1 N_2} = \int_0^1 \mathrm{d}x \frac{1}{N_B^2}, \tag{D.7}$$

$$\frac{1}{N_1 N_2 N_3} = \int_0^1 \mathrm{d}x \int_0^x \mathrm{d}y \frac{1}{N_C^3}, \tag{D.8}$$

where

$$N_A = N_1 = Q_A^2 - M_A^2 + \mathrm{i}\varepsilon, \tag{D.9}$$

$$N_B = N_1(1-x) + N_2 x = Q_B^2 - M_B^2 + \mathrm{i}\varepsilon, \tag{D.10}$$

$$N_C = N_1(1-x) + N_2 y + N_3(x-y) = Q_C^2 - M_C^2 + \mathrm{i}\varepsilon, \tag{D.11}$$

[1]For this reason the integral functions in Eqs. (D.1–D.4) do not depend on all external momenta.

with

$$\begin{aligned} Q_A^2 &= q_1^2, \\ M_A^2 &= m_1^2, \end{aligned} \tag{D.12}$$

$$\begin{aligned} Q_B^2 &= (q_1 + p_1 x)^2, \\ M_B^2 &= p_1^2 x^2 + (m_2^2 - m_1^2 - p_1^2)x + m_1^2, \end{aligned} \tag{D.13}$$

$$\begin{aligned} Q_C^2 &= (q_1 + p_3 x - p_2 y)^2, \\ M_C^2 &= p_3^2 x^2 + p_2^2 y^2 + 2p_3 p_2 xy + (-p_3^2 - m_1^2 + m_3^2)x + (-p_1^2 + p_3^2 + m_2^2 - m_3^2)y + m_1^2. \end{aligned} \tag{D.14}$$

Useful alternatives transformations are

$$\begin{aligned} \frac{1}{ABC} &= \Gamma(3) \int_0^1 \mathrm{d}x \int_0^1 \mathrm{d}y \int_0^1 \mathrm{d}z \frac{\delta(1-x-y-z)}{[Ax+By+Cz]^3}, \\ &= 2 \int_0^1 \mathrm{d}x \int_0^{1-x} \mathrm{d}y \frac{1}{[Ax+By+C(1-x-y)]^3}, \\ &= 2 \int_0^1 \mathrm{d}x \int_0^1 \mathrm{d}y \frac{x}{[A(1-x)+Bxy+Cx(1-y)]^3}, \end{aligned} \tag{D.15}$$

but all these replacements are special cases of

$$\frac{1}{A^m B} = \int_0^1 \mathrm{d}y \frac{m y^{m-1}}{[Ay + B(1-y)]^{m+1}}, \tag{D.16}$$

$$\begin{aligned} \frac{1}{A_1 A_2 \ldots A_m} &= (m-1)! \int_0^1 \mathrm{d}x_1 \int_0^{x_1} \mathrm{d}x_2 \ldots \int_0^{x_{m-2}} \mathrm{d}x_{m-1} \times \\ &\quad \frac{1}{[A_1 x_{m-1} + A_2(x_{m-2} - x_{m-1}) + \ldots + A_m(1-x_1)]^m}. \end{aligned} \tag{D.17}$$

D.1.3 Compact expressions

Now we are ready to write A_0, B_0 and C_0, in a compact notation. We just use a handy definition

$$\mathrm{I}_n(M^2) \equiv \frac{\mu^{4-D}}{i\pi^2} \int \mathrm{d}^D Q \frac{1}{(Q^2 - M^2 + \mathrm{i}\varepsilon)^n} \tag{D.18}$$

so the scalar one-loop integrals read

$$A_0 = \mathrm{I}_1\left(M_A^2\right), \tag{D.19}$$

$$B_0 = \int_0^1 \mathrm{d}x \, \mathrm{I}_2\left(M_B^2\right), \tag{D.20}$$

$$C_0 = 2 \int_0^1 \mathrm{d}x \int_0^x \mathrm{d}y \, \mathrm{I}_3\left(M_C^2\right). \tag{D.21}$$

D.2 Calculation of A_0, B_0 and C_0

Before getting deep into the technical calculation we will place a tilde to M^2 to get reminded about its infinitesimal imaginary part

$$\tilde{M}^2 \equiv M^2 - \mathrm{i}\varepsilon. \tag{D.22}$$

D.2.1 1-point function

We solve in this section the A_0 function, defined at eq. (D.1).

$$A_0(\tilde{M}_A^2) = \frac{\mu^{4-D}}{i\pi^2} \int \mathrm{d}^D Q \frac{1}{Q^2 - \tilde{M}_A^2}. \tag{D.23}$$

By using the Wick's rotation, the integration over Q^0 is done not in the real plane where the poles lay but in the imaginary axis. We thus deal with an equivalent Euclidean propagator Q_e with nice behaviour. Then using Eq. (C.8)

$$A_0(\tilde{M}_A^2) = -\frac{\mu^{4-D}}{\pi^2} \int_{-\infty}^{+\infty} \mathrm{d}^D Q_e \frac{1}{Q_e^2 + \tilde{M}_A^2}. \tag{D.24}$$

The strategy is to write Q_e in modulus and argument in D-dimensions. Using the tricks of section (C.2) we are able to separate the integral in modulus and polar angles and compute it

$$\begin{aligned} A_0(\tilde{M}_A^2) &= -\frac{\mu^{4-D}}{\pi^2} \int_0^{\infty} \mathrm{d}|Q_e| |Q_e|^{n-1} \int_0^{\pi} \mathrm{d}\theta_{n-1} \sin^{n-2}\theta_{n-1} \dots \\ &\quad \dots \int_0^{\pi} \mathrm{d}\theta_2 \sin\theta_2 \int_0^{2\pi} \mathrm{d}\theta_1 \frac{1}{Q_e^2 + \tilde{M}_A^2} \qquad \text{(D.25)} \\ &= -\frac{\mu^{4-D}}{\pi^2} \frac{\pi^{\frac{D}{2}}}{\Gamma(\frac{D}{2})} \left(\frac{\Gamma(\frac{D}{2})\Gamma(1-\frac{D}{2})}{\Gamma(1)} \frac{1}{(\tilde{M}_A^2)^{1-\frac{D}{2}}} \right). \qquad \text{(D.26)} \end{aligned}$$

A direct substitution of $D = 4$ will cause a divergence of the Γ-functions. On the contrary, we are interested into keeping track of the dimensional divergence and therefore we will carry out series expansion in ϵ, defined previously at Eq. (C.9),

$$\begin{aligned} A_0(\tilde{M}_A^2) &= \tilde{M}_A^2 \left(\frac{\mu^2}{\pi \tilde{M}_A^2} \right)^{\epsilon} \frac{\Gamma(\epsilon)}{1-\epsilon} \qquad \text{(D.27)} \\ &= \tilde{M}_A^2 \left[1 + \epsilon \,\mathrm{Log}(\dots) + \epsilon^2 \frac{\mathrm{Log}(\dots)^2}{2} + \dots \right] \times \\ &\quad \left[\frac{1}{\epsilon} - \gamma + \epsilon \frac{\frac{\pi^2}{6} + \gamma^2}{2} + \dots \right] \times \qquad \text{(D.28)} \\ &\quad \left[1 + \epsilon + \epsilon^2 + \dots \right] \\ &= \tilde{M}_A^2 \left[\frac{1}{\epsilon} + 1 - \mathrm{Log}_\mu(\tilde{M}_A^2) + \epsilon \frac{(1 - \mathrm{Log}_\mu(\tilde{M}_A^2))^2 + \frac{\pi^2}{6} + 1}{2} + O(\epsilon^2) \right] \qquad \text{(D.29)} \end{aligned}$$

with Log_μ being the function defined as

$$\mathrm{Log}_\mu(\tilde{M}_A^2) \equiv \gamma + \mathrm{Log}\left(\frac{\pi\tilde{M}_A^2}{\mu^2}\right) = \mathrm{Log}\left(\pi e^\gamma \frac{\tilde{M}_A^2}{\mu^2}\right), \tag{D.30}$$

and in case that any principal Log () has a second argument, it contains the sign of the imaginary part if needed:

$$\mathrm{Log}\,(a, b) \equiv \mathrm{Log}\,(a + bi\varepsilon)\,. \tag{D.31}$$

D.2.2 2-point function

Once computed A_0, we will see that it will help in order to obtain B_0.

$$B_0(\tilde{M}_B^2) = \int_0^1 \mathrm{d}x\, \frac{\mu^{4-D}}{i\pi^2} \int_{-\infty}^{+\infty} \mathrm{d}^D Q \frac{1}{(Q^2 - \tilde{M}_B^2)^2}, \tag{D.32}$$

and as before, we perform the Wick's rotation and angular integration in D-dimensions so it reads

$$B_0(\tilde{M}_B^2) = \int_0^1 \mathrm{d}x \left(\frac{\mu^2}{\pi\tilde{M}_B^2}\right)^\epsilon \Gamma(\epsilon), \tag{D.33}$$

which can be related with the expression found for A_0 in Eq. (D.27). In this case, again a series expansion in ϵ leads to

$$\begin{aligned} B_0(\tilde{M}_B^2) &= \int_0^1 \mathrm{d}x \frac{(1-\epsilon)}{\tilde{M}_B^2} A_0(\tilde{M}_B^2) && \text{(D.34)}\\ &= \int_0^1 \mathrm{d}x \left(-1 + \frac{1}{\epsilon} + 1 - \mathrm{Log}_\mu(\tilde{M}_B^2) + O(\epsilon)\right) && \text{(D.35)}\\ &= \frac{1}{\epsilon} - \int_0^1 \mathrm{d}x\, \mathrm{Log}_\mu(\tilde{M}_B^2). && \text{(D.36)} \end{aligned}$$

The final solution comes after integrating the logarithm of a polynomial of second order. The most convenient way is to extract the solutions to the polynomial and employ of the useful property of logarithms

$$\begin{aligned} B_0 &= \frac{1}{\epsilon} - \int_0^1 \mathrm{d}x\, \mathrm{Log}_\mu(p_1^2 x^2 - (p_1^2 + m_1^2 - m_2^2)x + m_1^2 - i\varepsilon) && \text{(D.37)}\\ &= \frac{1}{\epsilon} - \mathrm{Log}_\mu(p_1^2 + s(p_1^2)i\varepsilon) - \int_0^1 \mathrm{d}x\, \mathrm{Log}\left((x - z_-)(x - z_+) - s(p_1^2)i\varepsilon\right) && \text{(D.38)}\\ &= \frac{1}{\epsilon} - \mathrm{Log}_\mu(p_1^2 + s(p_1^2)i\varepsilon) + 2 - (\eta(1 - z_-, 1 - z_+) - \eta(-z_-, -z_+))\\ &\quad - \sum_{j=-,+} \left((1 - z_j)\mathrm{Log}\left(1 - z_j - js(p_1^2)i\varepsilon\right) + z_j \mathrm{Log}\left(-z_j - js(p_1^2)i\varepsilon\right)\right) && \text{(D.39)}\\ &= \frac{1}{\epsilon} + 2 - \mathrm{Log}_\mu(m_2^2) + \sum_{j=-,+} z_j \mathrm{Log}\left(\frac{1 - z_j}{-z_j} + js(p_1^2)i\varepsilon\right), && \text{(D.40)} \end{aligned}$$

with s(a) being the sign function with argument a and

$$z_\pm = \frac{p_1^2 + m_1^2 - m_2^2}{2p_1^2} \pm \sqrt{\left(\frac{p_1^2 + m_1^2 - m_2^2}{2p_1^2}\right)^2 - \frac{m_1^2}{p_1^2}}. \tag{D.41}$$

Summary for the special cases

$$A_0(0) = 0, \tag{D.42}$$

$$A_0(m^2) = m^2\left(\frac{1}{\epsilon} + 1 - \mathrm{Log}_\mu(m^2)\right), \tag{D.43}$$

$$B_0(0,0,m^2) = \frac{1}{\epsilon} + 1 - \mathrm{Log}_\mu(m^2), \tag{D.44}$$

$$B_0(0,m^2,m^2) = \frac{1}{\epsilon} - \mathrm{Log}_\mu(m^2), \tag{D.45}$$

$$B_0(0,m_1^2,m_2^2) = \frac{1}{\epsilon} + 1 - \frac{m_2^2\mathrm{Log}_\mu(m_2^2) - m_1^2\mathrm{Log}_\mu(m_1^2)}{m_2^2 - m_1^2}, \tag{D.46}$$

$$B_0(p_1^2,0,0) = \frac{1}{\epsilon} + 2 - \mathrm{Log}_\mu(-p_1^2,-1), \tag{D.47}$$

$$B_0(m^2,0,m^2) = \frac{1}{\epsilon} + 2 - \mathrm{Log}_\mu(m^2), \tag{D.48}$$

$$B_0(\pm|p_1^2|,0,m^2) = \frac{1}{\epsilon} + 2 - \mathrm{Log}_\mu(m^2) + \frac{p_1^2 - m^2}{p_1^2}\mathrm{Log}\left(\frac{-m^2}{p_1^2 - m^2}, \pm 1\right), \tag{D.49}$$

$$B_0(\pm|p_1^2|,m_1^2,m_2^2) = \frac{1}{\epsilon} + 2 - \mathrm{Log}_\mu(m_2^2) + \sum_{j=-,+} z_j\mathrm{Log}\left(\frac{1-z_j}{-z_j}, \pm j\right). \tag{D.50}$$

D.2.3 3-point function

Similarly to B_0 and its relation with A_0, with C_0 we proceed as

$$C_0 = -\int_0^1 \mathrm{d}x \int_0^x \mathrm{d}y \frac{1}{M_C^2 - \mathrm{i}\varepsilon} \tag{D.51}$$

$$= -\int_0^1 \mathrm{d}x \int_0^x \mathrm{d}y \frac{1}{ax^2 + by^2 + cxy + dx + ey + f - \mathrm{i}\varepsilon} \tag{D.52}$$

where by definition, the coefficients are given in Table D.1.

Solving this integral analytically in the most general case is a more elaborated task than for the previous A_0 and B_0 cases, because of the complex component and the non-positive definition of the partial coefficients. We will consider only an interesting case.

Complex Boson mass

On the reduction of the tensor integrals related to D_i functions to master integrals, C_0 functions naturally appear. If we pretend to keep trace of a complex mass for an internal line, it is absolutely necessary to provide the same mass in all the rest of the derivation, i.e. the external

Coefficient	Value
a	p_3^2
b	p_2^2
c	$2p_3p_2$
d	$m_3^2 - m_1^2 - p_3^2$
e	$m_2^2 - m_3^2 - p_1^2 + p_3^2$
f	m_1^2

Table D.1: Coefficient for the parametrization of the C_0 function.

coefficients and virtual lines in the lower order functions appearing from shrinking internal lines in the reduction.

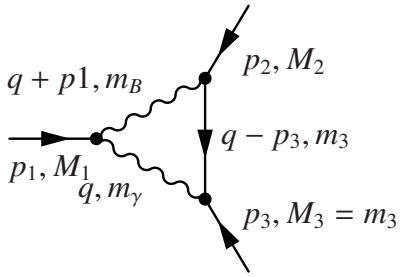

Figure D.2: Schematic representation of the 3-point function appearing in the reduction of scalar D functions with complex boson mass.

A particularly useful Feynman parametrization is

$$\frac{1}{ABC} = \int_0^1 \mathrm{d}y \int_0^1 \mathrm{d}x \, \frac{2x}{[A(1-x) + Bxy + Cx(1-y)]^3}, \tag{D.53}$$

where

$$\begin{aligned} A &= q^2 + \mathrm{i}\varepsilon, \\ B &= (q + p_1)^2 - m_2^2 + \mathrm{i}\varepsilon \;\; = q^2 + 2qp_1 + p_1^2 - m_2^2 + \mathrm{i}\varepsilon, \\ C &= (q - p_3)^2 - m_3^2 + \mathrm{i}\varepsilon \;\; = q^2 - 2qp_3 + p_3^2 - m_3^2 + \mathrm{i}\varepsilon. \end{aligned} \tag{D.54}$$

The full denominator may be redefined as:

$$ABC = (Q^2 - \tilde{M}^2)^3 \equiv \left([q - p_y x]^2 - [p_y^2 x^2 - s_y x - \mathrm{i}\varepsilon]\right)^3, \tag{D.55}$$

with p_y and s_y linear functions on y defined by

$$p_y = p_3 + p_2 y = p_2^2(y - y_-)(y - y_+), \qquad \text{and roots} \tag{D.56}$$

$$y_\pm = -\frac{p_1^2 - p_2^2 - p_3^2}{2p_2^2} \pm \sqrt{\left(\frac{p_1^2 - p_2^2 - p_3^2}{2p_2^2}\right)^2 - \frac{p_3^2}{p_2^2}}, \tag{D.57}$$

$$s_y = (p_1^2 - p_3^2 - m_2^2 + m_3^2)y + (p_3^2 - m_3^2). \tag{D.58}$$

Then, following the strategy presented in the previous section, our C_0 function can be simplified

$$C_0 = \int_0^1 \mathrm{d}y \int_0^1 \mathrm{d}x \, \frac{\mu^{4-D}}{i\pi^2} \int_{-\infty}^{\infty} \mathrm{d}^D Q \frac{2x}{[Q^2 - \tilde{M}^2]^3} \tag{D.59}$$

$$= \int_0^1 \mathrm{d}y \int_0^1 \mathrm{d}x \, \frac{1}{p_y^2 x - s_y - \mathrm{i}\varepsilon} \tag{D.60}$$

$$= \int_0^1 \mathrm{d}y \frac{1}{p_y^2 + \mathrm{s}(p_y^2)\mathrm{i}\varepsilon} \left[\mathrm{Log}\left(1 - \frac{s_y}{p_y^2}, -\mathrm{s}(p_y^2)\right) - \mathrm{Log}\left(-\frac{s_y}{p_y^2}, -\mathrm{s}(p_y^2)\right) \right], \tag{D.61}$$

and outside of the threshold (see below) can be further manipulated with partial fraction decomposition on the roots of y:

$$C_0 = -\frac{1}{p_2^2(y_+ - y_-)} \int_0^1 \mathrm{d}y \left(\frac{1}{y - y_+ + \mathrm{s}(p_y^2 p_2^2)\mathrm{i}\varepsilon} - \frac{1}{y - y_- - \mathrm{s}(p_y^2 p_2^2)\mathrm{i}\varepsilon} \right) \times$$
$$\left[\mathrm{Log}\left((y - s_-)(y - s_+), -\mathrm{s}(p_2^2)\right) - \mathrm{Log}\left(\frac{-s_y}{p_2^2}, -\mathrm{s}(p_2^2)\right) \right], \tag{D.62}$$

with $s_\pm$ being the roots of $p_y^2 - s_y$. They are the same than $y_\pm$ with the changes $p_1^2 \to m_2^2$ and $p_3^2 \to m_3^2$. The final answer can be expressed in terms of complex logarithms and dilogarithms.

$$C_0 = \frac{1}{p_2^2(y_+ - y_-)} \sum_{k=\{-,+\}} (k) \Bigg[\mathrm{Log}\left(-\tfrac{p_1^2 - m_B^2}{p_2^2}, -1\right) \mathrm{Log}\left(\tfrac{y_k - 1}{y_k}, k\right) + \mathrm{Li}_2\left(\tfrac{1}{y_k}, -k\right)$$
$$- \sum_{j=-,+} \left\{ \mathrm{Log}\left(\tfrac{y_k - 1}{y_k}, k\right) \mathrm{Log}\left(y_k - z_j, j\right) + \mathrm{Li}_2\left(\tfrac{y_k}{y_k - z_j}, j\right) - \mathrm{Li}_2\left(\tfrac{y_k - 1}{y_k - z_j}, j\right) \right\} \Bigg]. \tag{D.63}$$

In the unphysical limits of threshold production

$$p_1^2 = (M_2 + M_3)^2 \quad \text{or} \quad p_1^2 = (M_2 - M_3)^2, \tag{D.64}$$

there is only a unique root ($y_+ = y_-$) and the partial fraction decomposition is not well defined. The value on this points can be inferred by analytical continuation:

$$C_0|_{\text{threshold}} = \lim_{p_1^2 \to \text{thresholds}^+} C_0 = \lim_{p_1^2 \to \text{threshold}^-} C_0. \tag{D.65}$$

In Fig. D.3 we present an implementation of the C_0 function with a complex argument equivalent to the unstable Z-boson and the corresponding result for real arguments. It is observed the smooth transition through the resonance.

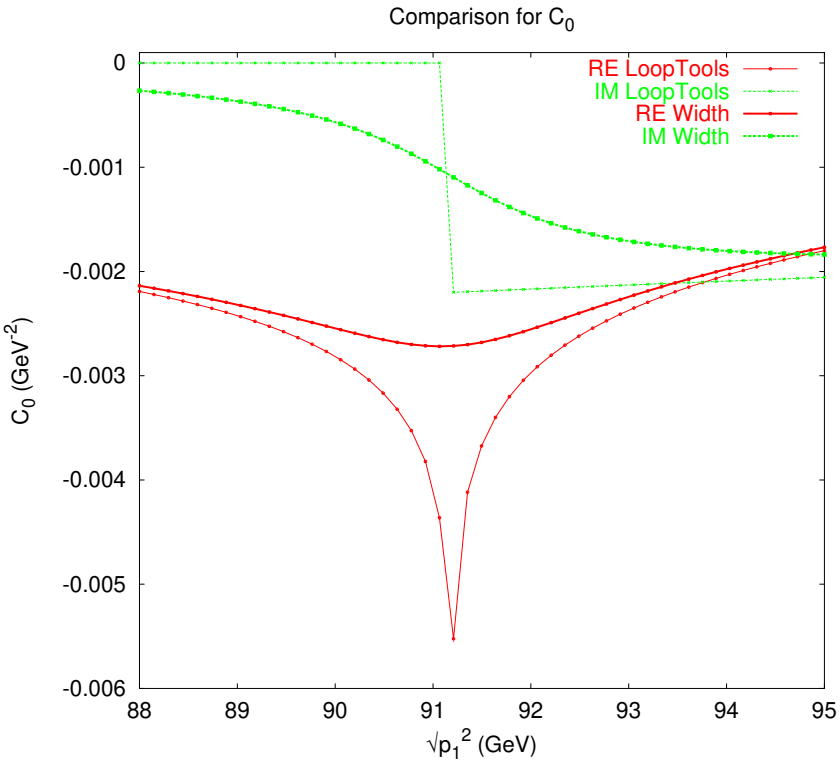

Figure D.3: Real and Imaginary part of C_0 at the peak. The values for the real argument are given by LoopTools, where $M_1 = 1$ GeV, and $M_2 = 5$ GeV. The function `c0wcc0.F` was used for the finite width and it is distributed inside of the directory `fortran/src/` of *aleTALC*.

D.2.4 The 4-point function with complex mass

In this section we will include the implementation of the infrared D_0 integral for the case of one complex argument. It was calculated in [70] and we reproduce here the result for a massive unstable particle m_0.

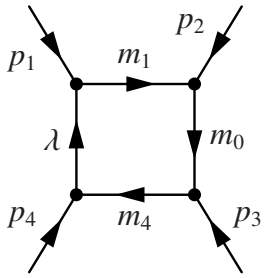

Figure D.4: Schematic representation of 4-point function with complex mass m_0 and photon mass regulator λ.

$$
\begin{aligned}
D_0 \;=\; & \frac{x_s}{m_1 m_4 (t-m_0^2)(1-x_s^2)} \Bigg\{ \\
& +2\log(x_s)\left(\log(1-x_s^2) - \log\frac{m_0\lambda}{m_0^2 - t - \mathrm{i}\varepsilon}\right) \\
& +\frac{\pi^2}{2} + \mathrm{Li}_2(x_s^2) + \log^2(x_2) + \log^2(x_3) \\
& -\sum_{\sigma,\rho=\pm 1}\left(\mathrm{Li}_2(x_s x_2^\rho x_3^\sigma) + \left(\log x_s + \log x_2^\rho + \log x_3^\sigma\right)\log(1 - x_s x_3^\sigma x_2^\rho)\right)\Bigg\}
\end{aligned}
\tag{D.66}
$$

with the following definitions for the x variables

$$x_s \equiv -K(s+\mathrm{i}\varepsilon, m_1, m_4), \tag{D.67}$$

$$x_2 \equiv -K(m_2^2+\mathrm{i}\varepsilon, m_1, m_0), \tag{D.68}$$

$$x_3 \equiv -K(m_3^2+\mathrm{i}\varepsilon, m_4, m_0), \tag{D.69}$$

and the definition of the K function (with z complex and m, m' real)

$$K(z,m,m') \equiv \begin{cases} \dfrac{1-\sqrt{1-\frac{4mm'}{z-(m-m')^2}}}{1+\sqrt{1-\frac{4mm'}{z-(m-m')^2}}} & z \neq (m-m')^2, \\ -1 & z \neq (m-m')^2. \end{cases} \tag{D.70}$$

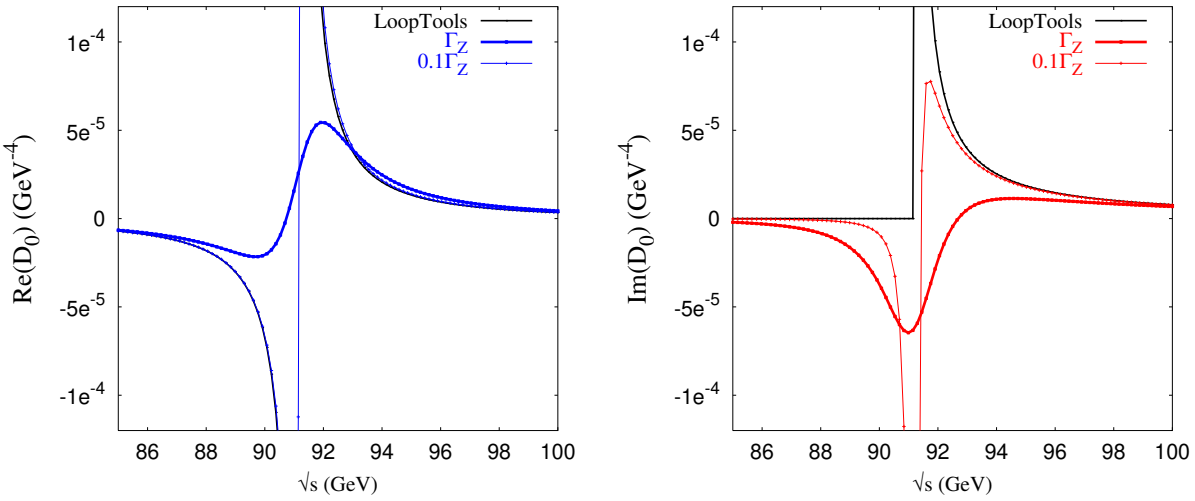

Figure D.5: Real and imaginary parts of D_0 for different values of the Z-width argument.

The implementation of this formula is done in the `fortran/src/d0wdd0.F` file of *a*ℓTALC. Analytical behaviour is shown in Fig. D.5, separately for the real and imaginary part of a D_0 function with different Z-boson width values and other arbitrary arguments. The zero-width result is provided by LoopTools.

Appendix E

List of tables for aitalc

E.1 Directory listing for any level

```
alorca@linux:~AITALCHOME/examples/muon_production/tree> ls -XFl
total 183
drwxr-xr-x    2 alorca   users     2048 Oct 14 15:02 EPS/
drwxr-xr-x    2 alorca   users     2048 Oct 14 15:02 FFmuon_production/
drwxr-xr-x    2 alorca   users     2048 Oct 14 15:02 InfoEPS/
-rw-r--r--    1 alorca   users     3291 Oct 14 15:02 Makefile
-rw-r--r--    1 alorca   users     3710 Oct 14 15:02 muon_production.cnf
-rw-r--r--    1 alorca   users       20 Oct 14 15:02 fermioncurrentsnames.in
-rw-r--r--    1 alorca   users     3870 Oct 14 15:02 muon_production.in
-rw-r--r--    1 alorca   users     4531 Oct 14 15:02 Make_kit.log
-rw-r--r--    1 alorca   users      149 Oct 14 15:02 Makefile.log
-rw-r--r--    1 alorca   users     1088 Oct 14 15:02 do_amplitude.log
-rw-r--r--    1 alorca   users      245 Oct 14 15:02 joinff.1.log
-rw-r--r--    1 alorca   users     1059 Oct 14 15:02 joinff.log
-rw-r--r--    1 alorca   users      629 Oct 14 15:02 joinkinematics.log
-rw-r--r--    1 alorca   users   121102 Oct 14 15:02 joinmm.log
-rw-r--r--    1 alorca   users    14779 Oct 14 15:02 muon_production.ps
-rw-r--r--    1 alorca   users    18277 Oct 14 15:02 muon_productionInfo.ps
```

Table E.1: Listing for the `tree` directory inside our muon production example.

E.2 Implemented models

Code	Arguments	Particle	Name	Lorentz type
Lepton				
`le`, `Le`	`(;`p_i`)`	e^-, e^+	electron, positron	fermion
Gauge boson				
`A`	`(`μ_i`;`p_i`)`	γ	photon	boson

Table E.2: Particle content for the QED model (`QED.model`)

Code	Arguments	Particle	Name	Lorentz type
Leptons				
`ne` , `Ne`		ν_e, $\bar{\nu}_e$	neutrino-e, antineut-e	
`nm` , `Nm`	$(;p_i)$	ν_μ, $\bar{\nu}_\mu$	neutrino-μ, antineut-μ	fermion
`nt` , `Nt`		ν_τ, $\bar{\nu}_\tau$	neutrino-τ, antineut-τ	
`le` , `Le`		e^-, e^+	electron, positron	
`lm` , `Lt`	$(;p_i)$	μ^-, μ^+	muon, antimuon	fermion
`lt` , `Lt`		τ^-, τ^+	tau, antitau	
Quarks				
`u` , `U`		u, $\bar{u}$	up, antiup	
`c` , `C`	$(;p_i)$	c, $\bar{c}$	charm, anticharm	fermion
`t` , `T`		t, $\bar{t}$	top, antitop	
`d` , `D`		d, $\bar{d}$	down, antidown	
`s` , `S`	$(;p_i)$	s, $\bar{s}$	strange, antistrange	fermion
`b` , `B`		b, $\bar{b}$	bottom, antibottom	
Gauge bosons				
`A`		γ	photon	
`Z`	$(\mu_i;p_i)$	Z	Z-boson	vector
`Wm` , `Wp`		W^-, W^+	W-boson	
Higgs sector				
`H`		H	Higgs	
`G0`	$(;p_i)$	χ	"the would-be	scalar
`Gm` , `Gp`		ϕ^-, ϕ^+	Goldstone bosons"	
Faddeev-Popov ghosts				
`ghA`, `GhA`		η_γ, $\bar{\eta}_\gamma$	photon ghosts	
`ghZ`, `GhZ`	$(;p_i)$	η_Z, $\bar{\eta}_Z$	Z-ghosts	scalar
`ghm`, `Ghm`		η_{W^-},$\bar{\eta}_{W^-}$	W^--ghosts	(with fermion statistics)
`ghp`, `Ghp`		η_{W^+}, $\bar{\eta}_{W^+}$	W^+-ghosts	

Table E.3: Particle content for the electroweak sector in the Standard Model (`EWSM.model`)

E.3 List of form procedures

Name	Args.	Description
`LTtoPV`		Translates the indexing of loop integrals from [44] into [52] convention.
`aitalcnotation`	N	Translates the FORM code into FORTRAN readable. The argument $N = 1$ allows for complex masses while $N = 0$ does not
`analyzeterms`		Part of `simplifygrams`
`argsymmetries`		Applies symmetry properties on arguments for loop functions and Gram determinants
`canceldens`		To cancel composition of `den(a,b)*(a-b)=1`
`chisholm`		Applies Chisholm identities by converting all chains of γ matrices that are contracted by their dimensional value
`contgammas`		Simplifies contractions in products of gamma matrices
`contractepsilon`		It contracts the product of two ϵ tensors
`ctfeynmanrules`		Insertion of Feynman rules with counterterms
`definegrams`		Defines a FORM global variable with the explicit expression of a Gram determinant
`derivateself`		Derivates self energies functions
`dimensionfour`		To reach the limit $D \to 4$ taking care of the UV-behaviour of scalar integrals
`diracequation`		Applies Dirac equation to available spinors
`dummytovar`	N	Part of `simplifygrams`. N stands for the amount of arguments in `dummyN` function
`equalindex`		Gives the same index to potentially different contractions keeping them ordered by number
`externalmomenta`		To substitute the internal momenta in loops with external ones
`gamma3to1`		Introduces an ϵ tensor and γ_5 to remove the product of three γ's
`gammaalgebra`		Prepares γ chain structures for `diracequation`
`gammamunu`		Introduces indices in the vector structures
`gramback`	N	Part of `simplifygrams`. Returns the Gram determinant of order N if no simplification was found
`gramsubstitution`	N, w	It substitutes the w-element to match possible order N Gram determinants

continued on next page

continued from previous page

Name	Args.	Description
`identifyintegrals`		Picks up the different loop integrals and provides a set of FORM `$`-variables with the right substitutions, inserting the function `LoopIntegral=LI(n)`
`integrationde93`		Procedure to integrate 4,3,2,1-point functions with internal momenta decomposition like in [44]
`invgammamunu`		Undoes the `gammamunu` effects
`keepUVloops`		Keeps only integrals actually UV divergent
`loopsymmetries`		Minimize loop integrals in boxes by symmetrizing arguments
`lorentzinvariants`		Adapts scalar product of vectors to Lorentz invariant squared masses
`massconvention`		To use single variables with M instead of MM outside arguments
`massivefofa`	j, c, N	Calculates and saves the form factors as in Eq. (3.19) basis. `j` stands for topology, `c` for left-right or $\mathbb{1}$-γ_5 and `N=1(0)` do (not) print the form factors
`movepslash`		Places the desired $\not{p}_i$ to the side of fermion chain to apply `diracequation`
`neglectmass`	`zero`	Neglects positive powers of terms as indicated in the file `Neglectedmasses.inc`. `zero` is the substituted value
`nosymboliccouplings`		To put explicit values of charges and weak couplings
`onshell`		Substitutes external momenta for external particle masses and Mandelstam variables
`pslashaway`		Reorder away the non desired position of $\not{p}_i$
`pushgamma5`		Pushes γ_5 to the right in fermion chains
`pushomegas`		Orders and pushes Left or Right projectors ($\omega_{L,R}$) to the right in fermion chains
`recoverargumentsde93`		Catches back the arguments of loop integrals in combination with `integrationde93`
`reductionDD02`	N	Reduction algorithm from scalar tensor integrals to master integrals given in [96]. $N = 1$ sorts after each integral type, $N = 0$ does not sort at all
`reductionLT`		`reductionDD02(1)` with LOOPTOOLS notation
`simplifygrams`		Tries to remove inverse Gram determinants by looking to the numerator (time and memory consuming!)
`simplihelp`	N, r	It helps `simplifygrams` to run sequentially r times from the highest power of one variable for N order Gram determinants

continued on next page

continued from previous page		
Name	Args.	Description
`storeself`	j, c, N	Stores self energies, `j` stands for topology, `c` for left-right or $\mathbb{1}$-γ_5 and `N=1(0)` do (not) print the form factors
`threegammastoepsilon`		Introduces and removes the ϵ tensor simplifying chains of 3 γ matrices that naturally don't dissappear after `diracequation`
`tracefermiloops`		Traces possible fermion loops in self-energies
`transvorlongit`	x	Sets the longitudinal and transverse part of self energies, keeping off-shell but with mass^2 argument x
`unityCKM`		Makes $\mathrm{CKM}_{ij} = \delta_{ij}$
`usegamma5`		Uses γ_5, instead of $\omega_{L,R}$ projectors
`useomegas`		The opposite to `usegamma5`
`vartodummy`		Part of `gramback`, opposite as `dummytovar`

Table E.4: Different procedures used.

E.4 Settings for main.f

Variable	Type	Default Value	Meaning
Kinematical			
`icostloop`	integer	`5`	Dimension of `setcostarray`
`isqrtsloop`	integer	`5`	Dimension of `setsqrtsmanarray`
`setcostarray`	double prec.	`data //`	Set of default values for the `setcost` ($\cos\theta$) do loop in the `dcs` evaluation
`setsqrtsmanarray`	double prec.	`data //`	Set of default values for the `setsqrtsman` ($\sqrt{s}$) do loop in the `ICS` evaluation
`setfracomega`	double prec.	`0.1d0`	Limit for the maximum soft photon energy fraction of `sqrtsman`
`setlimcost`	double prec.	`0.9999d0`	Limit of integration for `ics` and `fba`
Process flags			
`lrenorm`	logical	`.true.`	Call the renormalization subroutine to calculate the counterterms parameters
`lwidth`	logical	`.false.`	Call the loop integrals with complex values for boson masses. For the 4-point integrals, only the case with one massless boson (photon) is considered.
`lidentCKM`	logical	`.false.`	Brings the CKM mixing matrix in a diagonal form, so no mixing occurs
Checking flags			
`luvcheck`	logical	`.false.`	Perform a shift in the `mudim` and `delta` parameters in LoopTools
`lircheck`	logical	`.false.`	Perform a shift in the `lambda` parameter in LoopTools
Output flags			
`lcostloop`	logical	`.true.`	Performs a do-loop over `setcost`
`lprintics`	logical	`.false.`	Performs a do-loop over `setsqrtsman` and prints the `ics`
`lprintfba`	logical	`.false.`	Performs a do-loop over `setsqrtsman` and prints the `fba`
`llongoutput`	logical	`.false.`	Prints cross sections in double prec.

Table E.5: Kinematical and variables and logical flags for different settings in `main.f`.

Bibliography

[1] J. Fleischer, A. Leike, A. Lorca, T. Riemann, and A. Werthenbach, "Fortran program TOPFIT version 0.92 (01.07.2003)." Web address at `http://www.ifh.de/~riemann/doc/topfit/topfit.html`.

[2] T. Hahn, "Generating Feynman diagrams and amplitudes with FeynArts 3," *Comput. Phys. Commun.* **140** (2001) 418–431, `hep-ph/0012260`. Available at `http://www.feynarts.de`.

[3] T. Hahn, W. Hollik, A. Lorca, T. Riemann, and A. Werthenbach, "$\mathcal{O}(\alpha)$ electroweak corrections to the processes $e^+e^- \to \tau^-\tau^+, c\bar{c}, b\bar{b}, t\bar{t}$: A comparison," `hep-ph/0307132`.

[4] E. W. N. Glover *et al.*, "Top quark physics," *Acta Phys. Polon.* **B35** (2004) 2671–2694, `hep-ph/0410110`.

[5] A. Biernacik, K. Kołodziej, A. Lorca, and T. Riemann, "Towards high precision predictions for top quark pair production and decay at a linear collider," *Acta Phys. Polon.* **B34** (2003) 5487–5496, `hep-ph/0311097`.

[6] A. Lorca and T. Riemann, "An integrated tool for loop calculations: *a*i̊TALC," *Submitted to Comput. Phys. Commun.* (2004) `hep-ph/0412047`. Web address `http://www-zeuthen.desy.de/theory/aitalc`.

[7] M. Tentyukov and J. Fleischer, "A Feynman diagram analyser DIANA," *Comput. Phys. Commun.* **132** (2000) 124–141, `hep-ph/9904258`. Available at `http://www.physik.uni-bielefeld.de/~tentukov/diana.html`.

[8] J. Fleischer, A. Lorca, and M. Tentyukov, "DIANA and applications to fermion production in electron positron annihilation," *Nucl. Instrum. Meth.* **A534** (2004) 284–288.

[9] J. A. M. Vermaseren, "New features of FORM," `math-ph/0010025`. Available at `http://www.nikhef.nl/~form`.

[10] T. Hahn and M. Perez-Victoria, "Automatized one-loop calculations in four and D dimensions," *Comput. Phys. Commun.* **118** (1999) 153–165, `hep-ph/9807565`. LoopTools available at `http://www.feynarts.de/looptools`.

[11] J. Fleischer, A. Lorca, and T. Riemann, "Automatized calculation of 2-fermion production with DIANA and *a*ℶTALC," *To appear in the proceedings of International Conference on Linear Colliders (LCWS 04), Paris, France, 19-24 Apr* (2004) hep-ph/0409034.

[12] J. Gluza, A. Lorca, and T. Riemann, "Automated use of DIANA for two-fermion production at colliders," *Nucl. Instrum. Meth.* **A534** (2004) 289–292, hep-ph/0409011.

[13] J. Fleischer, A. Lorca, and T. Riemann, "First order radiative corrections to massive Bhabha scattering in *D*-dimensions." To be submitted to Eur. Phys. J.

[14] A. Lorca and T. Riemann, "Automated calculations for massive fermion production with *a*ℶTALC," *Nucl. Phys. Proc. Suppl.* **135** (2004) 328–332, hep-ph/0407149.

[15] "Extended joint ECFA/DESY study on physics and detector for a linear e^+e^- collider," in *Workshops at Krakow, St.Malo, Prague, Amsterdam, September 2001 to April 2003*, R. Settles, ed. March, 2004. ISSN 1435-8077, ISBN 3-935702-13-2.

[16] The LEP Collaborations: ALEPH, DELPHI, L3 and OPAL, the LEP Electroweak Working Group, the SLD Electroweak and the Heavy Flavour Groups, "A combination of preliminary electroweak measurements and constraints on the standard model," hep-ex/0412015. Online address http://lepewwg.web.cern.ch/LEPEWWG/.

[17] G. Altarelli and M. W. Grunewald, "Precision electroweak tests of the standard model," *Phys. Rept.* **403-404** (2004) 189–201, hep-ph/0404165.

[18] **NuTeV** Collaboration, G. P. Zeller *et al.*, "A precise determination of electroweak parameters in neutrino nucleon scattering," *Phys. Rev. Lett.* **88** (2002) 091802, hep-ex/0110059.

[19] M. Y. Kuchiev and V. V. Flambaum, "Radiative corrections to parity non-conservation in atoms," hep-ph/0305053.

[20] **ECFA/DESY LC Physics Working Group** Collaboration, J. A. Aguilar-Saavedra *et al.*, "TESLA technical design report part iii: Physics at an e^+e^- linear collider," hep-ph/0106315.

[21] R. P. Feynman, "Space-time approach to nonrelativistic quantum mechanics," *Rev. Mod. Phys.* **20** (1948) 367–387.

[22] G. Passarino and M. J. G. Veltman, "One loop corrections for e^+e^- annihilation into $\mu^+\mu^-$ in the Weinberg model," *Nucl. Phys.* **B160** (1979) 151.

[23] H. Eck, *FeynArts 2.0. Development of a generic Feynman diagram generator*. PhD thesis, Julius-Maximilians Universität Würzburg, 1995. Available at http://www.feynarts.de/hagendiss.ps.gz.

[24] S. L. Glashow, "Partial symmetries of weak interactions," *Nucl. Phys.* **22** (1961) 579–588.

[25] S. Weinberg, "A model of leptons," *Phys. Rev. Lett.* **19** (1967) 1264–1266.

[26] A. Salam, *Elementary Particle Theory*. Svartholm, N. and Amquist and Wiksells, Stockholm, 1969.

[27] N. Cabibbo, "Unitary symmetry and leptonic decays," *Phys. Rev. Lett.* **10** (1963) 531–532.

[28] M. Kobayashi and T. Maskawa, "CP violation in the renormalizable theory of weak interaction," *Prog. Theor. Phys.* **49** (1973) 652–657.

[29] M. Böhm, A. Denner, and H. Joos, *Gauge Theories of the Strong and Electroweak Interaction*. B.G. Teubner Stuttgart/Leipzig/Wiesbaden, 2001.

[30] L. D. Faddeev and V. N. Popov, "Feynman diagrams for the Yang-Mills field," *Phys. Lett.* **B25** (1967) 29–30.

[31] B. W. Lee and J. Zinn-Justin, "Spontaneously broken gauge symmetries. i. preliminaries," *Phys. Rev.* **D5** (1972) 3121–3137.

[32] B. W. Lee and J. Zinn-Justin, "Spontaneously broken gauge symmetries ii. perturbation theory and renormalization," *Phys. Rev.* **D5** (1972) 3137–3155.

[33] G. 't Hooft and M. J. G. Veltman, "Regularization and renormalization of gauge fields," *Nucl. Phys.* **B44** (1972) 189–213.

[34] G. 't Hooft, "Renormalization of massless Yang-Mills fields," *Nucl. Phys.* **B33** (1971) 173–199.

[35] G. 't Hooft, "Renormalizable Lagrangians for massive Yang-Mills fields," *Nucl. Phys.* **B35** (1971) 167–188.

[36] G. 't Hooft, "Dimensional regularization and the renormalization group," *Nucl. Phys.* **B61** (1973) 455–468.

[37] W. A. Bardeen, A. J. Buras, D. W. Duke, and T. Muta, "Deep inelastic scattering beyond the leading order in asymptotically free gauge theories," *Phys. Rev.* **D18** (1978) 3998.

[38] D. C. Kennedy and B. W. Lynn, "Electroweak radiative corrections with an effective Lagrangian: Four fermion processes," *Nucl. Phys.* **B322** (1989) 1.

[39] D. A. Ross and J. C. Taylor, "Renormalization of a unified theory of weak and electromagnetic interactions," *Nucl. Phys.* **B51** (1973) 125–144.

[40] J. Fleischer and F. Jegerlehner, "Radiative corrections to higgs decays in the extended Weinberg-Salam model," *Phys. Rev.* **D23** (1981) 2001–2026.

[41] K.-i. Aoki, Z. Hioki, R. Kawabe, M. Konuma, and T. Muta, "One loop corrections to neutrino *e* scattering in Weinberg- Salam theory: Neutral current processes," *Prog. Theor. Phys.* **64** (1980) 707.

[42] D. Y. Bardin, P. K. Khristova, and O. M. Fedorenko, "On the lowest order electroweak corrections to spin 1/2 fermion scattering. 2. the one loop amplitudes," *Nucl. Phys.* **B197** (1982) 1.

[43] M. Böhm, H. Spiesberger, and W. Hollik, "On the 1-loop renormalization of the electroweak standard model and its application to leptonic processes," *Fortsch. Phys.* **34** (1986) 687–751.

[44] A. Denner, "Techniques for calculation of electroweak radiative corrections at the one loop level and results for W physics at LEP-200," *Fortschr. Phys.* **41** (1993) 307–420.

[45] W. J. Marciano and A. Sirlin, "On the renormalization of the charm quartet model," *Nucl. Phys.* **B93** (1975) 303.

[46] P. Gambino, P. A. Grassi, and F. Madricardo, "Fermion mixing renormalization and gauge invariance," *Phys. Lett.* **B454** (1999) 98–104, `hep-ph/9811470`.

[47] D. Espriu, J. Manzano, and P. Talavera, "Flavor mixing, gauge invariance and wave-function renormalisation," *Phys. Rev.* **D66** (2002) 076002, `hep-ph/0204085`.

[48] A. Denner, E. Kraus, and M. Roth, "Physical renormalization condition for the quark-mixing matrix," *Phys. Rev.* **D70** (2004) 033002, `hep-ph/0402130`.

[49] F. J. Dyson, "The S matrix in quantum electrodynamics," *Phys. Rev.* **75** (1949) 1736–1755.

[50] G. Passarino and M. Veltman, "One loop corrections for e^+e^- annihilation into $\mu^+\mu^-$ in the Weinberg model," *Nucl. Phys.* **B160** (1979) 151.

[51] G. J. van Oldenborgh, "FF: A package to evaluate one loop Feynman diagrams," *Comput. Phys. Commun.* **66** (1991) 1–15. Available at `http://www.xs4all.nl/~gjvo/FF.html`.

[52] G. 't Hooft and M. J. G. Veltman, "Scalar one loop integrals," *Nucl. Phys.* **B153** (1979) 365–401.

[53] F. Bloch and A. Nordsieck, "Note on the radiation field of the electron," *Phys. Rev.* **52** (1937) 54–59.

[54] A. A. Akhundov, D. Y. Bardin, O. M. Fedorenko, and T. Riemann, "Some integrals for exact calculation of QED bremsstrahlung,". JINR-E2-84-777.

[55] D. Y. Bardin, O. M. Fedorenko, and T. Riemann, "Some integrals for analytic bremsstrahlung calculation. Photon and Z^0 boson exchange in the ultrarelativistic limit,". JINR-E2-87-664.

[56] E. . Altarelli, G., E. . Kleiss, R., and E. . Verzegnassi, C., "Z physics at LEP-1. proceedings, workshop, Geneva, Switzerland, september 4-5, 1989. vol. 3: Event generators and software,". CERN (1989) 340 p. CERN Geneva - CERN 89-08 (89,rec.Dec.) 340 p.

[57] F. A. Berends, R. Kleiss, and W. Hollik, "Radiative corrections to Bhabha scattering at high- energies. 2: Hard photon corrections and monte carlo treatment," *Nucl. Phys.* **B304** (1988) 712.

[58] S. Jadach, E. Richter-Was, B. F. L. Ward, and Z. Was, "Monte Carlo program BHLUMI-2.01 for Bhabha scattering at low angles with Yennie-Frautschi-Suura exponentiation," *Comput. Phys. Commun.* **70** (1992) 305–344.

[59] W. T. Giele and E. W. N. Glover, "Higher order corrections to jet cross-sections in e^+e^- annihilation," *Phys. Rev.* **D46** (1992) 1980–2010.

[60] S. Weinberg, "Infrared photons and gravitons," *Phys. Rev.* **140** (1965) B516–B524.

[61] S. Catani, S. Dittmaier, and Z. Trocsanyi, "One-loop singular behaviour of QCD and SUSY QCD amplitudes with massive partons," *Phys. Lett.* **B500** (2001) 149–160, hep-ph/0011222.

[62] M. J. G. Veltman, "Unitarity and causality in a renormalizable field theory with unstable particles," *Physica* **29** (1963) 186–207.

[63] D. Y. Bardin, A. Leike, T. Riemann, and M. Sachwitz, "Energy dependent width effects in e^+e^- annihilation near the Z pole," *Phys. Lett.* **B206** (1988) 539–542.

[64] D. Y. Bardin *et al.*, "A realistic approach to the standard Z peak," *Z. Phys.* **C44** (1989) 493.

[65] R. G. Stuart, "Gauge invariance, analyticity and physical observables at the Z^0 resonance," *Phys. Lett.* **B262** (1991) 113–119.

[66] A. Aeppli, G. J. van Oldenborgh, and D. Wyler, "Unstable particles in one loop calculations," *Nucl. Phys.* **B428** (1994) 126–146, hep-ph/9312212.

[67] D. Bardin, W. Hollik, and G. Passarino, "Reports of the working group on precision calculation for the Z resonance," *CERN* **95-03** (1995). Genève.

[68] E. N. Argyres *et al.*, "Stable calculations for unstable particles: Restoring gauge invariance," *Phys. Lett.* **B358** (1995) 339–346, hep-ph/9507216.

[69] W. Beenakker *et al.*, "The fermion-loop scheme for finite-width effects in e^+e^- annihilation into four fermions," *Nucl. Phys.* **B500** (1997) 255–298, hep-ph/9612260.

[70] W. Beenakker and A. Denner, "Infrared divergent scalar box integrals with applications in the electroweak standard model," *Nucl. Phys.* **B338** (1990) 349–370.

[71] H. Strubbe, "Manual for SCHOONSCHIP: a cdc-6000/7000 program for symbolic evaluation of algebraic expressions," *Comp. Phys. Commun.* **8** (1974) 1. CERN-DD/74/5.

[72] A. Pukhov *et al.*, "CompHEP: A package for evaluation of Feynman diagrams and integration over multi-particle phase space. user's manual for version 33," hep-ph/9908288. Available at http://theory.sinp.msu.ru/comphep.

[73] D. Y. Bardin *et al.*, "ZFITTER v.6.21: A semi-analytical program for fermion pair production in e^+e^- annihilation," *Comput. Phys. Commun.* **133** (2001) 229–395, hep-ph/9908433.

[74] F. Yuasa *et al.*, "Automatic computation of cross sections in HEP: Status of GRACE system," *Prog. Theor. Phys. Suppl.* **138** (2000) 18–23, hep-ph/0007053. Project web site at http://minami-home.kek.jp.

[75] T. Stelzer and W. F. Long, "Automatic generation of tree level helicity amplitudes," *Comput. Phys. Commun.* **81** (1994) 357–371, hep-ph/9401258. Available at http://madgraph.hep.uiuc.edu.

[76] A. Andonov *et al.*, "Project SANC (former CalcPHEP): Support of analytic and numeric calculations for experiments at colliders," hep-ph/0209297. Project page at http://brg.jinr.ru/sanc/intro/index.php.

[77] J. Fleischer *et al.*, "One-loop corrections to the process $e^+e^- \to t\bar{t}$ including hard bremsstrahlung," hep-ph/0203220.

[78] J. Fleischer, T. Hahn, W. Hollik, T. Riemann, C. Schappacher, and A. Werthenbach, "Complete electroweak one-loop radiative corrections to top-pair production at TESLA: A comparison," 2002. hep-ph/0202109.

[79] A. Andonov *et al.*, "Update of one loop corrections for e^+e^- to f anti-f, first run of CalcPHEP system," *Phys. Part. Nucl.* **34** (2003) 577–618, hep-ph/0207156.

[80] J. Fleischer, A. Leike, T. Riemann, and A. Werthenbach, "Electroweak one-loop corrections for e^+e^- annihilation into $t\bar{t}$ including hard bremsstrahlung," *Eur. Phys. J.* **C31** (2003) 37–56, hep-ph/0302259.

[81] P. Nogueira, *An introduction to Qgraf 2.0.* Available at http://cfif.ist.utl.pt/~paulo/qgraf.html.

[82] W. H. Press, B. P. Flannery, S. A. Teukolsky, and W. T. Vetterling, *Numerical Recipes in FORTRAN: The Art of Scientific Computing, 2nd ed.*, ch. 4.3 Romberg integration, and 16.4 Richardson Extrapolation and the Bulirsch-Stoer Method, pp. 134–135 and 718–725. Cambridge University Press, Cambridge, U.K., 1992.

[83] G. Montagna, F. Piccinini, O. Nicrosini, G. Passarino, and R. Pittau, "Topaz0: A program for computing observables and for fitting cross-sections and forward - backward asymmetries around the Z^0 peak," *Comput. Phys. Commun.* **76** (1993) 328–360. Available at `http://www.to.infn.it/~giampier/topaz0.html`.

[84] A. Lorca, "Physics." `http://www-zeuthen.desy.de/~alorca/physics.html`.

[85] K. Kołodziej, "Top quark pair production and decay into 6 fermions at linear colliders," *Eur. Phys. J.* **C23** (2002) 471–477, `hep-ph/0110063`.

[86] S. Dittmaier and M. Roth, "LUSIFER: A lucid approach to six fermion production," *Nucl. Phys.* **B642** (2002) 307–343, `hep-ph/0206070`.

[87] S. T. Boogert and D. J. Miller, "Questions about the measurement of the e^+e^- luminosity spectrum," `hep-ex/0211021`.

[88] K. Mönig, "Measurement of the differential luminosity using Bhabha events in the forward tracking region at TESLA,". LC-PHSM-2000-060.

[89] A. A. Pankov and N. Paver, "Bhabha vs. Møller scattering as a contact-interaction analyzer at a polarized linear collider," *Eur. Phys. J.* **C29** (2003) 313–323, `hep-ph/0209058`.

[90] M. Consoli, "One loop corrections to $e^+e^- \to e^+e^-$ in the Weinberg model," *Nucl. Phys.* **B160** (1979) 208.

[91] M. Bohm, A. Denner, W. Hollik, and R. Sommer, "Radiative corrections to Bhabha scattering in su(2) x u(1)," *Phys. Lett.* **B144** (1984) 414.

[92] M. Bohm, A. Denner, and W. Hollik, "Radiative corrections to bhabha scattering at high-energies. 1. virtual and soft photon corrections," *Nucl. Phys.* **B304** (1988) 687.

[93] D. Y. Bardin, W. Hollik, and T. Riemann, "Bhabha scattering with higher order weak loop corrections," *Z. Phys.* **C49** (1991) 485–490.

[94] H. J. Bhabha *Proc. Roy. Soc. Lond.* **A154** (1935) 159.

[95] M. E. Peskin and D. V. Schroeder, *An introduction to Quantum Field Theory*. Addison Wesley, 1995. Resolution of differential cross section for Bhabha scattering in problem 5.3.

[96] A. Denner and S. Dittmaier, "Reduction of one-loop tensor 5-point integrals," *Nucl. Phys.* **B658** (2003) 175–202, `hep-ph/0212259`.

[97] J. Fleischer, F. Jegerlehner, and O. V. Tarasov, "Algebraic reduction of one-loop feynman graph amplitudes," *Nucl. Phys.* **B566** (2000) 423–440, hep-ph/9907327.

[98] J. Fleischer, O. V. Tarasov, T. Riemann, and A. Werthenbach, "Factorizing one-loop contributions to two-loop Bhabha scattering and automatization of Feynman diagram calculations," *Nucl. Instrum. Meth.* **A502** (2003) 567–569, hep-ph/0210180. Talk available at http://acat02.sinp.msu.ru/presentations/fleischer/ACAT.ps.

[99] R. Bonciani, A. Ferroglia, P. Mastrolia, E. Remiddi, and J. J. van der Bij, "Two-loop n(f) = 1 QED Bhabha scattering differential cross section," *Nucl. Phys.* **B701** (2004) 121–179, hep-ph/0405275.

[100] M. Czakon, J. Gluza, and T. Riemann, "Master integrals for massive two-loop Bhabha scattering in QED," hep-ph/0412164. To appear in Phys. Rev. D.

[101] A. A. Penin, "Two-loop corrections to Bhabha scattering," hep-ph/0501120.

[102] A. Czarnecki and W. J. Marciano, "Electroweak radiative corrections to polarized Møller scattering asymmetries," *Phys. Rev.* **D53** (1996) 1066–1072, hep-ph/9507420.

[103] L. Dixon and M. Schreiber, "Radiative corrections to the azimuthal asymmetry in transversely polarized Møller scattering," *Phys. Rev.* **D69** (2004) 113001, hep-ph/0402221.

[104] A. Denner and S. Pozzorini, "Electroweak radiative corrections to polarized Møller scattering at high energies," *Eur. Phys. J.* **C7** (1999) 185–195, hep-ph/9807446.

[105] J. I. Illana and T. Riemann, "Charged lepton flavour violation from massive neutrinos in Z decays," *Phys. Rev.* **D63** (2001) 053004, hep-ph/0010193.

[106] J. I. Illana and M. Masip, "Lepton flavor violation in Z and lepton decays in supersymmetric models," *Phys. Rev.* **D67** (2003) 035004, hep-ph/0207328.

[107] E. Ma and A. Pramudita, "Flavor changing effective neutral current couplings in the Weinberg-Salam model," *Phys. Rev.* **D22** (1980) 214.

[108] V. Ganapathi, T. J. Weiler, E. Laermann, I. Schmitt, and P. M. Zerwas, "Flavor changing Z decays: A window to ultraheavy quarks?," *Phys. Rev.* **D27** (1983) 579.

[109] G. Mann and T. Riemann, "Effective flavor changing weak neutral current in the standard theory and Z boson decay," *Annalen Phys.* **40** (1984) 334.

[110] C.-S. Huang, X.-H. Wu, and S.-H. Zhu, "Top-charm associated production at high energy e^+e^- colliders in standard model," *Phys. Lett.* **B452** (1999) 143–149, hep-ph/9901369.

[111] C.-S. Huang, X.-H. Wu, and S.-H. Zhu, "Bottom-strange associated production at high energy e^+e^- colliders in standard model," *J. Phys.* **G25** (1999) 2215–2223, hep-ph/9902474.

[112] S. Eidelman *et al.*, "Review of Particle Physics," *Physics Letters B* **592** (2004) 1+.

[113] T. Riemann *et al.*, "Bhabha homepage at Zeuthen." Web address `http://www-zeuthen.desy.de/theory/research/bhabha`.

[114] M. Lemoine and M. J. G. Veltman, "Radiative corrections to $e^+e^- \to W^+W^-$ in the Weinberg model," *Nucl. Phys.* **B164** (1980) 445.

[115] M. Bohm *et al.*, "Electroweak radiative corrections to $e^+e^- \to W^+W^-$," *Nucl. Phys.* **B304** (1988) 463.

[116] T. Hahn and C. Schappacher, "The implementation of the minimal supersymmetric standard model in FeynArts and FormCalc," *Comput. Phys. Commun.* **143** (2002) 54–68, `hep-ph/0105349`.

[117] J. Fleischer, O. V. Tarasov, F. Jegerlehner, and P. Raczka, "Two loop $O(\alpha_s G_\mu m_t^2)$ corrections to the partial decay width of the Z^0 into b anti-b final states in the large top mass limit," *Phys. Lett.* **B293** (1992) 437–444.

[118] A. Denner, G. Weiglein, and S. Dittmaier, "Application of the background field method to the electroweak standard model," *Nucl. Phys.* **B440** (1995) 95–128, `hep-ph/9410338`.

[119] F. Jegerlehner, "Facts of life with gamma(5)," *Eur. Phys. J.* **C18** (2001) 673–679, `hep-th/0005255`.